

Calculation of the effective permeability and simulation of fluid flow in naturally fractured reservoirs

Author:

Teimoori Sangani, Ahmad

Publication Date:

2005

DOI:

<https://doi.org/10.26190/unsworks/22463>

License:

<https://creativecommons.org/licenses/by-nc-nd/3.0/au/>

Link to license to see what you are allowed to do with this resource.

Downloaded from <http://hdl.handle.net/1959.4/22408> in <https://unsworks.unsw.edu.au> on 2024-05-04

**CALCULATION OF THE EFFECTIVE
PERMEABILITY AND SIMULATION OF FLUID
FLOW IN NATURALLY FRACTURED RESERVOIRS**

By

Ahmad Teimoori Sangani

Supervisor: Associate Professor Sheikh S. Rahman

A dissertation submitted to the University of New South Wales in partial fulfilment of the requirements for the Degree of Doctor of Philosophy

In

Petroleum Engineering

School of Petroleum Engineering
The University of New South Wales
Sydney, Australia

March 2005

AFFIRMATION

I hereby declare that this submission is my own work and that, to the best of my knowledge and belief, it contains no material previously published or written by another person nor material which to a substantial extent has been accepted for the award of any other degree or diploma of a university or other institute of higher learning, except where due reference is made through the text.

(Signed)

A handwritten signature in black ink, consisting of the initials 'A.T.' followed by a stylized surname, all enclosed within a large, hand-drawn oval.

.....

Ahmad Teimoori Sangani

ACKNOWLEDGMENTS

I wish to express my sincere gratitude to my supervisor A/Prof. S. S. Rahman for his support, encouragement, guidance and inspiration provided during the course of this research.

The author also wishes to express his sincere thanks for helpful contributions made by Professor V. Pinczewski, Dr. Chen Z. and Dr. T. Tran during the period of this study.

Most importantly, I would like to express my sincere thanks, as always, to my wife Parisa and my son Ali for their support and encouragement over the period of this research. Also thanks to members of my family for their patience and continuous encouragement throughout the study.

Thanks also to Mr. Nino Zajaczkowski for his technical supports and providing softwares and thanks to all staff and research students at the school of petroleum engineering for their assistance throughout the project.

ABSTRACT

This thesis is aimed to calculate the effective permeability tensor and to simulate the fluid flow in naturally fractured reservoirs. This requires an understanding of the mechanisms of fluid flow in naturally fractured reservoirs and the detailed properties of individual fractures and matrix porous media. This study has been carried out to address the issues and difficulties faced by previous methods; to establish possible answers to minimise the difficulties; and hence, to improve the efficiency of reservoir simulation through the use of properties of individual fractures.

The methodology used in this study combines several mathematical and numerical techniques like the boundary element method, periodic boundary conditions, and the control volume mixed finite element method. This study has contributed to knowledge in the calculation of the effective permeability and simulation of fluid flow in naturally fractured reservoirs through the development of two algorithms.

The first algorithm calculates the effective permeability tensor by use of properties of arbitrary oriented fractures (location, size and orientation). It includes all multi-scaled fractures and considers the appropriate method of analysis for each type of fracture (short, medium and long). In this study a characterisation module which provides the detail information for individual fractures is incorporated. The effective permeability algorithm accounts for fluid flows in the matrix, between the matrix and the fracture and disconnected fractures on effective permeability. It also accounts for the properties of individual fractures in calculation of the effective permeability tensor.

The second algorithm simulates flow of single-phase fluid in naturally fractured reservoirs by use of the effective permeability tensor. This algorithm takes full advantage of the control volume discretisation technique and the mixed finite element method in calculation of pressure and fluid flow velocity in each grid block. It accounts for the continuity of flux between the neighbouring blocks and has the advantage of calculation of fluid velocity and

pressure, directly from a system of first order equations (Darcy's law and conservation of mass's law).

The application of the effective permeability tensor in the second algorithm allows us the simulation of fluid flow in naturally fractured reservoirs with large number of multi-scale fractures. The fluid pressure and velocity distributions obtained from this study are important and can be considered for further studies in hydraulic fracturing and production optimization of NFRs.

PUBLICATIONS PRODUCED FROM THIS WORK

1. Teimoori, A., Tran, T., Chen, Z., Rahman, S.S., (2003) Calculation of permeability tensor using the boundary element method provides a unique tool to simulate naturally fractured reservoirs. SPE84545, Society of Petroleum Engineers Annual technical Conference and Exhibition held in Denver, Colorado, U.S.A., Oct. 18-20.
2. Teimoori, A., Tran, T., Chen, Z., Rahman, S.S., (2004) Effective permeability calculation using the boundary element methods in naturally fractured reservoirs. This paper has been accepted to be published by the Journal of petroleum science and engineering.
3. Teimoori, A., Tran, N. H., Chen, Z., Rahman, S.S., (2004) Simulation of production from naturally fractured reservoirs with the use of effective permeability tensor. SPE88620, Society of Petroleum Engineers Asia Pacific Oil & Gas Conference and Exhibition, Perth, Australia, Oct. 18-20.
4. Teimoori, A., Tran, N. H., Chen, Z., Rahman, S.S., (2004) Simulation of fluid flow in naturally fractured reservoirs with the use of effective permeability tensor. This paper is published in the bulletin and presented in Annual proceeding of Geothermal Resources Council (GRC), Australia.

TABLE OF CONTENTS

AFFIRMATION	ii
ACKNOWLEDGMENTS	iii
ABSTRACT	iv
PUBLICATIONS PRODUCED FROM THIS WORK	vi
TABLE OF CONTENTS	vii
LIST OF TABLES	xi
LIST OF FIGURES	xii
NOMENCLATURE	xix
CHAPTER 1 GENERAL INTRODUCTION	2
1.1 Naturally fractured reservoirs	3
1.2 Review of the previous works	4
1.2.1 Single continuum approach.....	4
1.2.2 Dual continuum (porosity/ permeability) approach.....	7
1.2.3 Discrete fracture approach	9
Deterministic discrete methods	9
Stochastic discrete methods	10
Heuristic discrete methods	11
1.2.4 Models using the effective permeability tensor	11

Methods to calculate the effective permeability tensor.....	12
Simulation of fluid flow in NFRs using the effective permeability.....	17
Control volume finite difference methods	17
Control volume mixed finite element methods.....	18
1.3 Objectives and scope of the thesis	18
1.4 Thesis outline	19
CHAPTER 2 CALCULATION OF EFFECTIVE PERMEABILITY TENSOR.....	22
2.1 Overview.....	22
2.2 Properties of natural fracture	23
2.2.1 Field data sources for this study.....	25
2.3 Theory of fluid flow in fractured reservoirs	28
2.4 Mathematical formulation.....	29
2.4.1 Boundary conditions	36
Short fractures	37
Medium to long fractures	38
Boundaries of grid block	38
2.5 Solution of the integral equation.....	40
2.5.1 Discretisation using the boundary element method	41
Short fractures and matrix porous media	42
Medium to long fractures and interconnected fractures	42
2.5.2 Boundary element solution of the system of equations	46
2.6 Comparative analysis between analytical and numerical results	51
2.7 Closure.....	56

CHAPTER 3 SIMULATION OF FLUID FLOW IN NFR USING CONTROL VOLUME MIXED FINITE ELEMENT METHOD	58
3.1 Overview.....	58
3.2 Theory of simulation of fluid flow in NFRs	59
3.3 Governing equations	60
3.3.1 Boundary conditions	62
3.4 Discretisation using the Control Volume	63
3.5 Solution to the system of linear equations	71
3.6 Comparative analysis	73
3.7 Closure	80
CHAPTER 4 RESULTS AND CASE STUDY.....	82
4.1 Overview.....	82
4.2 Evaluation of the permeability calculation algorithm.....	83
4.2.1 Example-1: Short Fractures.....	83
4.2.2 Example-2: Medium to long fractures	86
4.2.3 Example-3: Interconnected fractures	90
4.2.4 Example-4: Multiple length fractures	93
4.2.5 Sensitivity studies for the effective permeability algorithm	95
Effect of aperture.....	95
Effect of matrix permeability	97
Effect of Fracture density and orientation.....	99
Effect of the number of boundary elements.....	102
Effect of aspect ratio	103

Effect of Poisson's region.....	105
4.3 Evaluation of the production algorithm	107
Example-1: Region with no flow boundary.....	107
Example-2: Fractured region with no-flow boundaries	110
4.3.1 Sensitivity studies for production estimation algorithm	115
Effect of fluid viscosity.....	115
Effect of number and location of injectors and producers	117
4.4 Case studies.....	119
4.4.1 Otsego fault map	124
4.4.2 Discussion	129
CHAPTER 5 CONCLUSIONS AND SCOPE OF FUTURE WORK.....	131
5.1 Conclusions and perspectives.....	131
5.2 Recommendation for further studies.....	132
APPENDIX A	146
APPENDIX B.....	150

LIST OF TABLES

Table 2-1: Results of the numerically calculated diagonal and off-diagonal elements of the permeability tensor using this study.	54
Table 2-2: Results of the analytically calculated diagonal and off-diagonal elements of the permeability tensor using	55
Table 3-1: Results of the pressure and velocity in X- and Y-directions from this study.	75
Table 3-2: Results of the pressure and velocity in X- and Y-directions from Sutopo et al. (2001).	76
Table 4-1: Local permeability for shorts fractures shown in figure 4-3.....	86
Table 4-2: Coordinates of the fractures (x (feet), y (feet)) related to figure 4-5.	88
Table 4-3: Coordinates of the fractures (x (feet), y (feet)) related to figure 4-8.	91
Table 4-4: Coordinates of fractures in figure 4-20 to investigate the effect of fracture orientation and density.	100
Table 4-5: Results of the simulation for matrix permeability equal to 200 mD with different injection rate and fracture density.	124

LIST OF FIGURES

Figure 1-1: Representative elementary Volume in a rock mass (after Chen et al., 1999)...	5
Figure 1-2: Statistical representation of homogeneity and Rev. (a) Homogeneous rock (b) Fractured rock (after Kunkel et al., 1988).	6
Figure 1-3: Conceptual discrete hydraulic featured related to REV: (A) Unfractured rock, (B) Fractured rock when REV includes sufficient fracture intersections to represent the mass flow domain and (C) Fractured rock, where large-scale features mean that REV is very large or non-Exist (after Kunkel et al., 1988; Lee and Farmer, 1993).	7
Figure 1-4: (a) cubic region with 3-D real fractured rock. (b) Cubic region which shows dual-porosity concept of fractured rock (after Warren and Root, 1963).....	8
Figure 1-5: Cubic region with three-dimensional fractured network of disc-shaped orthogonal fractures (after Long et al., 1985).	10
Figure 1-6: A solid volume of dimensions W cut by parallel plane conduits (after Snow, 1969).....	13
Figure 1-7: Fluid flow simulation (after Cacas et al., 1990).....	14
Figure 1-8: A grid block containing medium size fractures of arbitrary orientation and different sizes (after Lough et al., 1998).....	16
Figure 2-1: 2D schematic for a single fracture with centre O(x,y), orientation (teta), length (L) and aperture (H) in x-y coordinate system.	24
Figure 2-2: Fractures generated in a portion of a reservoir characterised by Tran (2004). Different sizes of fractures from short to long are presented in three- dimensional disk shape format.	26
Figure 2-3: Schematic for calculation of direction cosines	27

Figure 2-4: A schematic of two-dimensional fractured reservoir used in this study. (a) Short fractures (b) Medium size fractures (c) long fractures.....	27
Figure 2-5: Differential volume element of fluid flow equilibrium.....	31
Figure 2-6: (a) Arbitrary points on domain A. (b) Points on the region around medium fractures	34
Figure 2-7: Homogeneous block with an arbitrary fracture	35
Figure 2-8: Periodic boundary condition over the grid-block.....	39
Figure 2-9: Boundary nodes on fractures and block and interior discretisation in two dimensions.....	44
Figure 2-10: Defining the Poisson's region around the medium and long fractures. 11 and 12 are the boundary elements along the length and edge of fracture.	45
Figure 2-11: Intersected line between interconnected fractures with circular shapes	45
Figure 2-12: A block containing a single fracture to show the elements of stiffness matrix.	
47	
Figure 2-13: Stiffness matrix for block in figure 2-12 containing single fracture, F is the fundamental solution and G is its derivative B and C represent the boundary conditions around fracture, surrounding part and along the block boundaries.	48
Figure 2-14: Flow chart for calculation of the effective permeability of naturally fractured reservoirs with multiple blocks and multiple fractures. Each part of the figure is connected to its related section in the text by addressing the related section number.....	50
Figure 2-15: Validation of the method against the analytical solution by rotating a single fracture inside the matrix block.....	52
Figure 2-16: Comparison of analytically and numerically calculated diagonal elements of the permeability tensor for single fracture rotating in a block.	53

Figure 2-17: Comparison of analytically and numerically calculated off-diagonal elements of the permeability tensor for single fracture rotating in a block.....	54
Figure 3-1: Describes Neumann type of boundary condition at the external boundaries of the reservoir	62
Figure 3-2: Control volume and unknowns for rectangular grid.	63
Figure 3-3: The Fluxes, pressure and velocities of block (i,j) in CVMFE method.....	67
Figure 3-4: Flow chart of production simulation from naturally fractured reservoirs using code written in the FORTRAN using the CVMFE method described in this chapter.	72
Figure 3-5: Schematic diagram of the example which shows boundary conditions and unknowns as well as the position of injector (q_{in}) and producer (q_{out}).....	74
Figure 3-6: Pressure profile for homogeneous system.	74
Figure 3-7: Velocity profile for a homogeneous system in (m/sec)	75
Figure 3-8: Comparison of the results of this study and the results calculated by Sutopo et al. (2001) for pressure and average velocity of the Grid blocks.	77
Figure 3-9: Pressure difference for a reservoir with unit thickness calculated in this study for injection rate of 100,000 bbl/day and block permeability of 50 mD.....	79
Figure 3-10: Pressure difference for a reservoir with unit thickness calculated by IMEX for injection rate of 100,000 bbl/day and block permeability of 50 mD.	79
Figure 4-1: Region containing multiple fractures to calculate permeability and to investigate its sensitivity against different parameters.....	84
Figure 4-2: Schematic of a block containing short fractures presenting the number of boundary elements around the grid block and fractures.	84
Figure 4-3: Short fractures in an array of 4×4 blocks in a region of $60(ft) \times 60(ft)$	85

Figure 4-4: Schematic of the block containing medium size fractures to show the boundary elements around the grid block, fractures and Poisson's region.	87
Figure 4-5: Arbitrary oriented fractures in an array of 4×4 blocks.....	88
Figure 4-6: The results of the effective permeability tensors for fractures in figure 4-5...	89
Figure 4-7: Elliptical form of the effective permeability tensors presented in figure 4-6.	89
Figure 4-8: Arbitrary connected fractures in an array of 4×4 blocks	91
Figure 4-9: Calculated the effective permeability tensors for interconnected fractures related to the figure 4-8.....	92
Figure 4-10: Results of the effective permeability tensors presented in figure 4-9.	92
Figure 4-11: Multiple scale length fractures in calculation of effective permeability.	93
Figure 4-12: The calculated effective permeability tensors for fractures in figure 4-11.	94
Figure 4-13: Elliptical presentation of the tensors in figure 4-12	94
Figure 4-14: Sensitivity analysis for short fractures. Effect of aperture on local permeability assuming matrix permeability of $K_m=0.1$ (mD).....	96
Figure 4-15: Normalised horizontal permeability values of the effective permeability tensor versus fracture aperture with matrix permeability of $K_m=0.1$ (mD). ..	96
Figure 4-16: Normalized permeability in y-direction from the effective permeability tensor versus fracture aperture with matrix permeability $K_m=1$ (mD).	97
Figure 4-17: Sensitivity analysis for short fracture model. Effect of Matrix permeability on the block effective permeability with fracture aperture $H=0.001$ (ft).	98
Figure 4-18: Normalized horizontal permeability values of the effective permeability tensor for different matrix permeability and constant fracture aperture $H=0.001$ (ft).....	98

Figure 4-19: Normalized vertical permeability values of the effective permeability tensor for different matrix permeability and constant fracture aperture $H=0.001$ (ft).
99

Figure 4-20: Arbitrary oriented fractures in a region containing 4 grid-blocks to show the effect of fracture density and orientation on the effective permeability tensor.101

Figure 4-21: Effective permeability tensors calculated for fractures in **figure 4-20** to show the effect of fracture density and orientation.101

Figure 4-22: The elliptical presentation of the block effective permeability tensors related to **figure 4-20** and **figure 4-21**.102

Figure 4-23: Square block with single fracture to investigate the sensitivity against the number of boundary elements along the boundaries of block, fracture and Poisson's region.103

Figure 4-24: (a) Description of aspect ratio which is defined as the ratio of distance between nodes to the width of fracture without considering boundary elements along the fracture edges. (b) Discretisation method using constant elements in this thesis with a number of boundary elements at the edges of the fractures.104

Figure 4-25: Normal to the boundary (a) constant type boundary elements (b) linear type boundary elements.105

Figure 4-26 Effect of aspect ratio on diagonal and off-diagonal terms of the effective permeability tensor.105

Figure 4-27: Definition of Poisson's ratio which is the proportion of distance between the nodes on Poisson's region from the corresponding nodes on the fracture boundary to the distance between nodes on the fracture boundary.106

Figure 4-28: Effect of Poisson's ratio on diagonal and off-diagonal terms of effective permeability.106

Figure 4-29: (a) Heterogeneous region in array of 12×15 blocks and Neumann boundary conditions. (b) no-flow Neumann boundary conditions.	108
Figure 4-30: Pressure distribution in steady state conditions in homogeneous reservoir explained in example-1, (psi).	109
Figure 4-31: Velocity field distribution in steady state conditions in heterogeneous reservoir in example-1, (ft/sec).	109
Figure 4-32: Velocity distribution in region with single fracture oriented at 45 degrees. .	111
Figure 4-33: Pressure distribution in region with single fracture oriented at 45 degrees. .	111
Figure 4-34: Velocity distribution in the region containing a single fracture with 135 degrees in.	112
Figure 4-35: Pressure distribution in the region containing a single fracture with 135 degrees in.	112
Figure 4-36: Velocity distribution in the region containing a horizontally distributed single fracture in.	113
Figure 4-37: Pressure distribution in the region containing a horizontally distributed single fracture in.	113
Figure 4-38: Velocity distribution in the region containing a single fracture oriented in y-direction.	114
Figure 4-39: Pressure distribution in the region containing a single fracture oriented in y-direction.	114
Figure 4-40: Pressure distribution for homogeneous reservoir with viscosity of 1(cp).	115
Figure 4-41: Pressure distribution for homogeneous reservoir with viscosity of 10(cp).	116
Figure 4-42: Velocity distribution for homogeneous reservoir in steady state condition. .	116
Figure 4-43: Sensitivity study for effect of fluid viscosity on pressure difference between the injector and producer.	117

Figure 4-44: Pressure distribution in the homogeneous region with one producer located in the centre and four injectors located in the corners.	118
Figure 4-45: Pressure distribution in the homogeneous region with one producer in the centre and four injectors located in grids (1, 3), (1, 14), (1, 16) and (1, 27).	119
Figure 4-46: Elliptical presentation of the effective permeability tensors calculated for the first case study. Each ellipse shows the permeability values in x- and y- directions and the orientation of fractures in each grid -block.	121
Figure 4-47: Well trajectories in case study 1.	122
Figure 4-48: Pressure distribution for the high fracture density in case study 1.	122
Figure 4-49: Pressure distribution for the low fracture density in case study 1.	123
Figure 4-50: Pressure distribution for the region with out fracture in case study 1.	123
Figure 4-51: Fault map of Otsego County and the surrounding areas (New York, USA)[http://www.nywaterfind.com/fractureotsego.JPG].....	125
Figure 4-52: Fault map of Otsego County and the surrounding areas (New York, USA).	125
Figure 4-53: Arbitrary oriented fractures in a naturally fractured region containing different types of fractures in 144 grid -blocks (case study).	127
Figure 4-54: Elliptical presentation of the effective permeability tensors calculated for the case study 2. Each ellipse shows the permeability values in x- and y- directions and the orientation of fractures in each grid -block.	127
Figure 4-55: Velocity distribution in the region (related to the case study).	128
Figure 4-56 Pressure distribution in the region (related to the case study).	128
Figure A. 5-1 Differential volume element for flow equilibrium	148

NOMENCLATURE

The following nomenclature is used in this dissertation. It is tried to assign one definition to each symbol and define each symbol when it first appear in the text.

Symbols:

A = area

[A] = matrix of coefficient

Azimuth = fracture azimuth angle

[B] = load vector

Det[K] = determinant of permeability tensor

Dip = fracture dip angle

H = fracture aperture

H_i = aperture of arbitrary fracture 'i'

K = permeability of matrix or fracture

K_i = permeability of arbitrary fracture 'i'

\bar{K} = permeability tensor

K_{xx} = diagonal element of permeability tensor in x direction

K_{yy} = diagonal element of permeability tensor in y direction

K_{xy}, K_{yx} = off-diagonal elements of permeability tensor

L = fracture length

n = normal vector to the surface

P = fluid pressure

Q = flow rate of injection or production or sink/source

q_{ff} = fluid flow between interconnected fractures

$Q_{i,j}$ = control volume

r = distance between two points in boundary element calculation

S = area of each element in the discretised domain in the boundary element method

T = transmissibility function

t = time

v = fluid velocity

$[X]$ = matrix of unknowns

Ω = area of domain under calculation in the boundary element method

m = fluid velocity

$x, y, z = 1$. Coordinates of fracture centre

2. Cartesian direction vectors

l, m, n = directional cosines of fracture

g = gravitational acceleration

\mathbf{a} = internal angle of element S in boundary element discretisation

$\mathbf{b}, \mathbf{g}, \mathbf{d}$ = arbitrary angles

\mathbf{q} = rotation angle of fracture

\mathbf{r} = density

\mathbf{f} = porosity

$\mathbf{d}(\cdot)$ = dirac delta function (finite element definition)

\mathbf{x} = arbitrary point inside the domain of the boundary element method

Γ = grid block boundary or boundary of Poisson's region

\mathbf{l} = mobility

∇ = 'change in'

Δ =laplace

Subscripts:

f = fracture

i, j = elements

m = matrix porous media

short= short fractures

Abbreviations:

BC = boundary condition

BEM = the boundary element method

CVMFE = control volume finite element method

FDM = finite difference method

FEM = finite element method

NFR = naturally fractured reservoirs

REV = representative elementary volume

CHAPTER 1

GENERAL INTRODUCTION

CHAPTER 1

GENERAL INTRODUCTION

Importance of production of oil and natural gas from naturally fractured reservoirs has been growing with decreasing conventional hydrocarbon reserves. Economic exploration of these resources primarily depends on understanding of fluid flow mechanism in fractured rocks. Majority of previous models in the simulation of Naturally Fractured Reservoirs (NFR) have been limited by considering fluid flow through interconnected fracture networks with no calculation of flow through matrix.

In this first chapter, these issues are addressed by reviewing the literature and the previously documented modelling approaches are discussed. This is followed by introducing the most efficient techniques for calculation of effective permeability tensor and simulation of production from NFR with a statement of objectives and scope of the thesis.

1.1 Naturally fractured reservoirs

Natural fractures are geologic features capable of transferring fluids through the rock over long distances. In petroleum geology, naturally-occurring fractures are described as complex-shaped openings in rocks, filled with gas, liquid or solid mineral matters and have been found in sandstone, carbonates, shales, cherts and basement rocks filled with hydrocarbons.

To some extent fractures exist in all rocks in the earth's crust and could be originated from tectonic forces, litho-static force, high fluid pressure, or thermal loading. In recent years, several permeability enhancement techniques, such as hydraulic fracturing are also used to enhance the efficiency of production from reservoirs with very dense rock, such as hot dry rock reservoirs or with very low matrix permeability, such as coal bed methane, tight gas, etc.

Presence of arbitrary oriented fractures, with variable length, spacing and orientation, makes it difficult to provide a simple methodology for simulation of NFRs. Therefore, simulation of NFRs is not governed in essence by the same equations as those with homogeneous media. It should be also considered that, although in most cases fractures are the main conduits and transformers of fluid flow inside the porous media, their effect on fluid flow becomes important only when they have sufficient spacing and length. For the above reasons and to assess the role of fractures in fluid production and permeability anisotropy, detailed study of characterisation and simulation of naturally fractured reservoirs is essential.

Due to the lack of knowledge about the properties of individual fractures and complexities involved in the calculation of permeability in NFRs, previous works in the simulation of these reservoirs either used the average properties for sets of fractures or did not consider the fluid flow in matrix porous media. However, recent advances in reservoir characterization allow construction of realistic, highly detailed models which provide properties of individual fractures. Moreover, using the techniques of the boundary element methods, periodic boundary conditions, control volume and mixed finite element methods

(used in this study) have made it possible to overcome the complexities involved in calculation of the effective permeability and simulation of fluid flow in fractured reservoirs containing large numbers of arbitrary oriented fractures.

1.2 Review of the previous works

Considerable contributions to the understanding of fluid flow and solute transport in fractured porous media have been made and a number of methods have been developed. In general, they could be divided into three main categories: single continuum, dual continuum and discrete fracture approaches.

In single continuum approach, fractured medium is represented by an equivalent porous medium and the bulk macroscopic values of the fractured medium are defined by averaging the point-to-point variations in the petrophysical properties over a representative volume. In dual continuum or double porosity approach, any unit of fractured media is considered to have a large number of fissures and matrix porous media. In this approach, two pressure values are defined to each point one for the flow in the fracture and the other for the flow in the matrix. Finally, in discrete fracture approach, fluid flow is only considered through a network of connected fractures. Discrete fracture approaches usually define an effective permeability tensor, which represents the directional permeability caused by fractures. In the following, different approaches in the simulation of fluid flow and methods to calculate effective permeability in NFR are reviewed with their benefits and drawbacks.

1.2.1 Single continuum approach

Single or equivalent continuum approach is a grid based method and requires the definition of a Representative Elementary Volume (REV), which represents the properties of fractured reservoir, see figure 1-1.

REV is usually calculated by measuring the permeability of samples with variable volumes in a statistical way to arrive at a constant value which is the volume that is representative

for the reservoir (figure 1-2 (a)). In fractured reservoirs, if the resulted volume is greater than or equal to fluctuations of the measured permeability, the values are representative (figure 1-2 (b)). It can be seen in figure 1-2(b) that the complex nature of rock discontinuity in NFR makes it difficult to define a representative volume.

Kunkel et al. (1988) showed that REV will increase in size with discontinuity spacing. As shown in figure 1-3, in fractured rock REV should be large enough to include sufficient fracture intersections to maintain constant permeability if a small volume of the rock mass is added to, or subtracted from REV (Lee and Farmer, 1993). The applicability of this approach was studied by Schwartz and Smith (1988), Long et al. (1982) and Therrien and Sudicky (1996) among others, in the context of groundwater flow under saturated conditions.

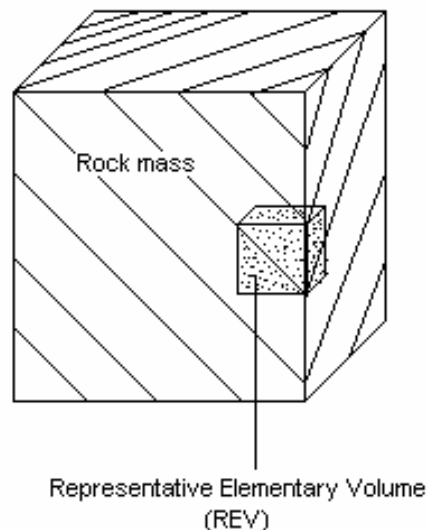


Figure 1-1: Representative elementary Volume in a rock mass (after Chen et al., 1999)

Chen et al. (1999) developed a mathematical formulation based on REV method to calculate anisotropic permeability tensor in global coordinate setting and its projection to the local coordinate system. In Chen et al.'s model, properties of fracture sets in REV, are calculated by manipulating the average parameters of natural fracture in three-dimensional coordinate system and total flux through a REV containing multiple sets of fractures. Despite the simplicity of equivalent continuum approaches, these methods are not of the interest of this study as the properties of fracture such as geometry and orientation are not being considered. In these methods, heterogeneity of fracture reservoir is represented by their averaged properties and as a result, individual fractures are not treated explicitly. Moreover, use of REV is not recommended in NFRs due to the high degree of heterogeneity.

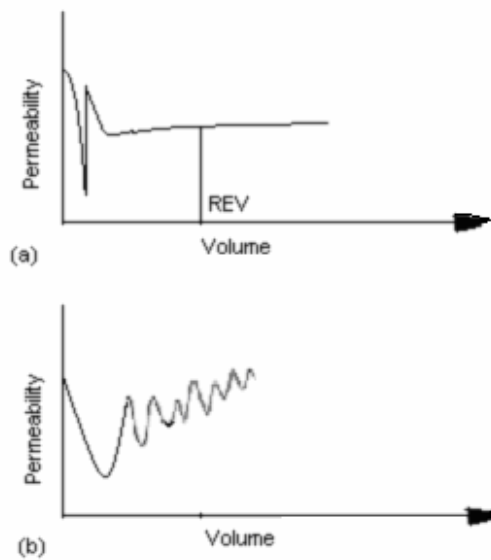


Figure 1-2: Statistical representation of homogeneity and Rev. (a) Homogeneous rock (b) Fractured rock (after Kunkel et al., 1988).

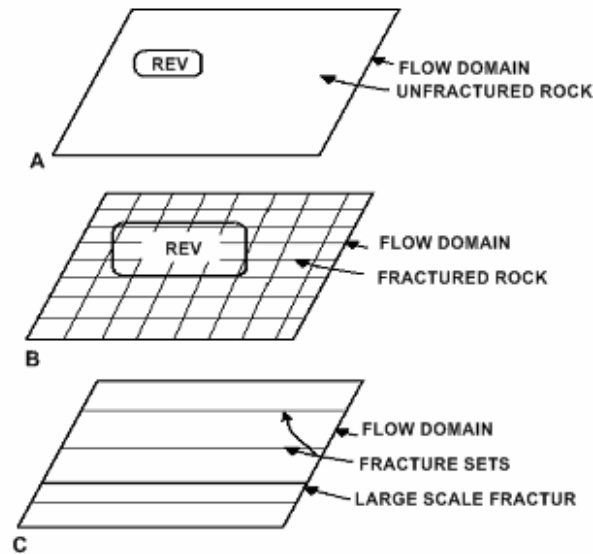


Figure 1-3: Conceptual discrete hydraulic features related to REV: (A) Unfractured rock, (B) Fractured rock when REV includes sufficient fracture intersections to represent the mass flow domain and (C) Fractured rock, where large-scale features mean that REV is very large or non-Exist (after Kunkel et al., 1988; Lee and Farmer, 1993).

1.2.2 Dual continuum (porosity/ permeability) approach

Dual porosity approach was first introduced by Barenblatt (1960) to simulate flow of multiphase fluids in a fractured reservoir assuming matrix and fracture as parallel layers with unlimited lengths. A modification of dual porosity approach which takes into account of fluid flow between matrix and fracture called dual permeability. Many researchers have applied dual porosity/ permeability (dual continuum) approach in the simulation of multiphase flow in NFRs. Sugar cube, layered and matchstick models are three different types of dual porosity approach.

In dual continuum approach, it is assumed that the fracture and the matrix are two interacting continua: the primary porosity blocks with low permeability and high storage capacity and the secondary porosity fractures of high permeability and negligible storage capacity. In both methods the greater part of the flow exists through a well-connected

fracture network (Gilman and Kazemi, 1983 and Nakashima et al., 2000). In fact, the fractures provide the pathways for flow, while the matrix provides the source of flow to a well. Dual porosity approach assumes no flow between matrix blocks whereas the dual permeability approach considers the flow between matrix blocks. The transfer of fluids between fracture and matrix is formulated as a function of saturation. The two systems are linked via a leakage term representing the exchange of fluid between them (Therrien and Sudicky, 1996). Figure 1-4 presents the dual porosity approach in the simulation of naturally-fracture reservoirs.

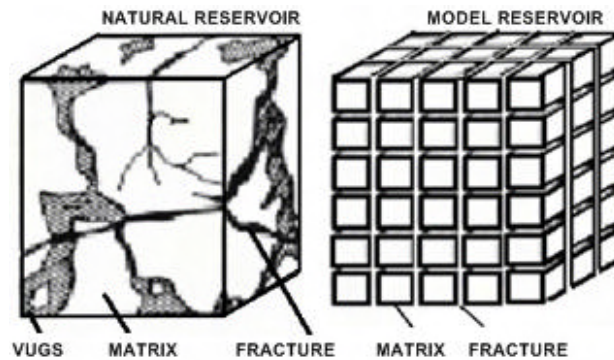


Figure 1-4: (a) cubic region with 3-D real fractured rock. (b) Cubic region which shows dual-porosity concept of fractured rock (after Warren and Root, 1963).

Chilingarian et al (1992, 1996) presented a model to simulate fluid flow in carbonate reservoirs based on dual continuum model. They claimed that the fractured grid block can be replaced with a dual system containing one matrix and one fracture. Chilingarian et al (1992, 1996) calculated the properties of fractured system using the traditional empirical equations or by direct laboratory measurement. The main drawback of the dual porosity/permeability approaches are that they are generally concerned of fluid flow and do not account for the characteristics of individual fractures and their geometry. In fact, most dual continuum approaches employ simple and uncomplicated mathematical formulation in the simulation of fluid flow by assuming matrix and fractures as parallel layers with infinite

length. However, the continuum approaches are not satisfactory for the detail modelling of NFRs.

1.2.3 Discrete fracture approach

In the last ten years, a considerable number of research projects were carried out which made effective use of discrete fracture approach. Discrete models accounts for fracture geometry and their formulations are based on the properties of fracture. However, they do not account for the effect of matrix permeability. In general, discrete fracture models are presented in three different forms: deterministic, stochastic and heuristic depending on the source and availability of information of fracture properties. Each technique is based on theoretical, numerical, exact or approximated method. Some of these methods are based on the calculation of effective permeability tensor in order to simulate fluid flow in the heterogeneous or naturally fractured porous media.

Deterministic discrete methods

In deterministic method, the geological model of reservoir is well known. This is generally true for a sufficiently simple case, where an exact analytical solution can be found. For more general cases, the theories of percolation (Berkowitz and Balberg, 1993 and Guyon et al., 1984), effective media (Dagan, 1979); Dagan, 1989 and Poley, 1988), streamline (Begg and King, 1985) and renormalization (king, 1989) are employed to make approximate calculation with varying precision. One may also find the analyses given by Durlofsky et al. (1997) and Yang and Deo (2001) from fine to coarse scale in heterogeneous and fractured porous media.

Hughes and Blunt (2000) developed a model for the simulation of fractured porous media by use of micro networks. Long et al. (1985) developed a three-dimensional deterministic discrete model which accounts for the properties of fractures as shown in figure 1-5. Unfortunately, in discrete models matrix permeability and disconnected fractures are not considered.

Stochastic discrete methods

In contrast to deterministic methods, stochastic methods assume an approximate knowledge of the model and take the probabilistic view to study variables as random functions in the space. Stochastic methods are grouped by Renard and Marsily (1997) as: spectral method, perturbation method, field theory and Monte-Carlo. Matheron et al. (1987); Dagan (1993) and Gelhar (1993), among others have worked on these models. A brief review of the different stochastic methods can be found in Kitanidis (1995).

Oda (1985) stochastically derived a simple expression for modelling of NFR with very short fractures. He employed a line source-sink to represent the randomly distributed fractures in the calculation of effective permeability. Oda (1985) assumed that the average pressure gradient inside the fracture is equal to the pressure gradient in the matrix. Because of this assumption, flow in fracture becomes independent of the matrix permeability. Cacas et al. (1990) developed a direct stochastic discrete method in modelling the flow in a fracture network. Unfortunately, they did not account for matrix permeability and properties of individual fractures. Some other stochastic methods were introduced by Matheron et al. (1987); Dagan (1993) and Gelhar (1993). Although stochastic methods have shown some great advantages over the deterministic methods as they can work even with limited number of available data, their accuracy is limited only to the well-bore area.

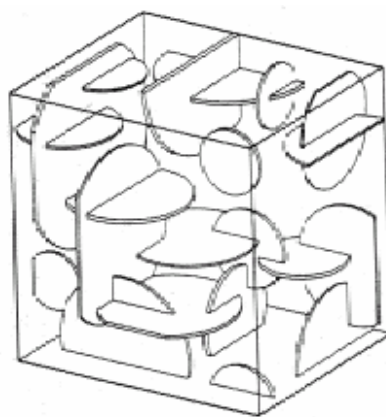


Figure 1-5: Cubic region with three-dimensional fractured network of disc-shaped orthogonal fractures (after Long et al., 1985).

Heuristic discrete methods

Finally, heuristic discrete methods propose rules for calculating reasonable equivalent permeability. The main heuristic methods are known as: sampling, averaging means, power average and flexible grid methods. These methods are widely used in the calculation of effective permeability and in the simulation of fluid flow in heterogeneous reservoirs. For detailed information and related references about the heuristic methods see Renard and Marsily (1997).

Due to the complexities involved in discrete models, these models are unable to model the flow of multi-phase flow in NFR. Moreover, discrete models consider fluid flow through a system of connected fractures ignoring the flow of isolated fractures and matrix porous media.

1.2.4 Models using the effective permeability tensor

It can be seen that modelling of NFR is a complete task which has not succeeded by previous methods. Discrete models do not consider the matrix permeability and also have difficulties in the simulation of multiple-phase flow. In a like manner, stochastic and continuum models do not consider the properties of individual fractures. A complete task can be achieved by employing the concept of block effective permeability tensor in the simulation of fluid flow in NFRs. The effective permeability calculation is to replace the fractured block with a homogeneous block taking into account the properties of individual fractures and matrix porous media in the original block. These methods are effective as they consider the fracture properties and matrix permeability, while ignoring the complexities involved in the previous works.

Recently, a number of works have been introduced in the simulation of heterogeneous and NFRs using the effective permeability tensor (Lee et al., 1998, 2002; Sutopo et al., 2001; Aavatsmark et al., 1998a; Edwards and Rogers, 1998; Lee et al., 1999; Durlofsky, 1991; Arbogast et al., 1995, 1997, 1998; Koebbe, 1993; Durlofsky, 1993, 1994; Cai et al., 1997; Russell, 2000; Jones, 1995; Naff et al., 2000). The calculated effective permeability tensor

in most cases is a diagonal tensor in two- or three-dimensions with zero off-diagonal elements. However, in NFRs it is necessary to calculate full tensor effective permeability (with none zero off-diagonal elements) to account for the effect of fracture orientation inside the block.

In the following, first the methods which calculate the effective permeability tensor and then the methods to simulate fluid flow in NFR using the effective permeability tensor are reviewed and discussed.

Methods to calculate the effective permeability tensor

The idea of using effective permeability is to replace the heterogeneous block with a homogeneous block in which the fracture properties remain the same throughout the grid block (Lough et al., 1998). For this purpose, different methods are developed with different simplifications depending on the size and density of fractures in the media.

One of the earliest models for the calculation of effective permeability in NFR was introduced by Snow (1968, 1969). His model is essentially a mathematical model based on the concept of infinite parallel plate with some statistical observation of fracture patterns with their parameters such as anisotropy, aperture, spacing and porosity (figure 1-6). However, Snow's model assumes that the fractures belong to fracture sets and have infinite length. Moreover it does not account for matrix permeability in calculation of effective permeability.

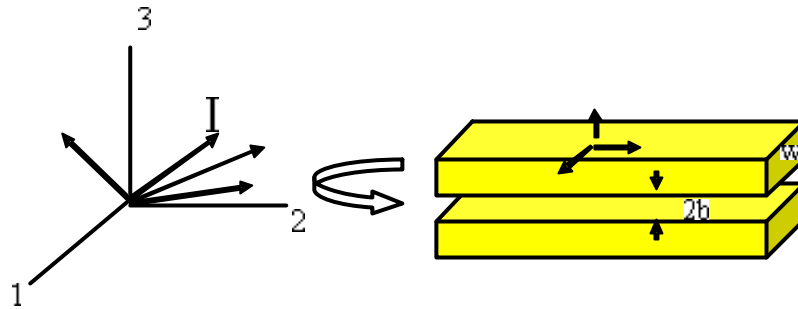


Figure 1-6: A solid volume of dimensions W cut by parallel plane conduits (after Snow, 1969).

Long et al. (1985) investigated the relationship between the degree of interconnection and its effect on permeability of fracture networks. They found that assuming degree of interconnection for dead end or isolated fractures and adding up the degree of heterogeneity in the system cause the actual permeability to be less than what Snow originally predicted. To improve the model devised by Snow (1969), Gupta et al. (2001) introduced a simple mathematical approach to calculate the permeability tensor, considering actual length of fractures. Their formula is a product of two components: a scalar permeability value which is calculated by a stochastic method and a unit permeability tensor which accounts for normal vector to fracture's plane and dip angle of fractures. However, matrix permeability was not considered and correlations were written only for sets of parallel fractures, thus ignoring the properties of individual fractures.

Oda (1985) stochastically derived a simple expression for very short fractures. He employed a line source-sink to represent the randomly distributed small fractures in the calculation of effective permeability and assumed that the average pressure gradient inside the fracture is equal to the pressure gradient in the matrix. Given this assumption, the flow in the fracture becomes independent of the matrix permeability. Other stochastic methods have been introduced by Matheron et al. (1987); Dagan (1993) and Gelhar (1993).

Cacas et al. (1990) developed a direct stochastic discrete method in modelling of flow in a fracture network which includes all types of fractures in the network. Information of

fractures is obtained in a grid base system by stochastic methods employing the seismic technology and using outcrops as source information. Cacas et al. (1990) assumed that the flow between intersected fractures occurs through bonds joining the centre of each fracture to the intersected line (figure 1-7). The bonds were one dimensional and made up of two parts, one for each fracture from the centre to the intersection of two fractures. Permeability for each bond was given by the fracture to which it belongs. Unfortunately, the stochastic model developed by these investigators did not include the matrix permeability and the properties of individual fractures.

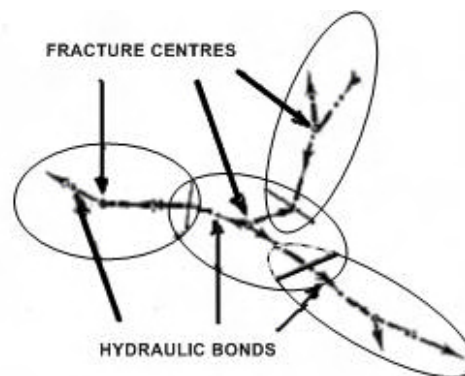


Figure 1-7: Fluid flow simulation (after Cacas et al., 1990)

Durlofsky (1991) developed a method which made use of the pressure solution in calculation of effective permeability tensor, employing Laplace's equation and periodic boundary conditions. Components of the permeability tensor are calculated in his method in a unit cell by applying a constant pressure difference in the x and y directions and solving the Laplace's equation. Periodic boundary conditions always obtain symmetric and positive definite permeability tensor and imply full correspondence between pressures and flux at opposite sides of the block. Periodic boundary conditions are taken into account by other

investigators in the calculation of effective permeability (Lough et al., 1996, 1998; Lee et al., 1999, 2001; Nakashima et al., 2000).

Apart from the above mentioned methods, numerical methods are also routinely used in the calculation of effective permeability. Methods such as Finite Difference Method (FDM), Finite Element Method (FEM) and the Boundary Element Method (BEM) are the main methods which are used by engineers. Most numerical techniques have inherent difficulties in terms of the formulation of heterogeneous media with complex geometry and generate a very complicated system of equations.

Rasmussen et al. (1987) investigated the effect of the fracture/matrix vertical permeability ratio on hydraulic conductivity in a simple fracture system. They employed BEM to model three-dimensional fluid flow by considering the matrix and the fractures as separate systems and did not account for the continuity of flux between fractures and matrix porous media. They claimed that the accuracy of their model is dependant on the aspect ratio, which is the distance between mesh points on fracture faces to the width of fracture. They drew the conclusion that aspect ratio should be less than 10 to achieve accurate results. For the type of problems in NFR, the fracture aperture is in the order of 10-100 *mm* and the length of fracture is in order of 1m. For such a problem, the original formulation would require about 1000×1000 mesh points on each surface of the fracture (Lough et al., 1998). This scheme becomes quite time consuming especially when the number of fractures becomes large and the order of elements becomes higher.

Nakashima et al. (2000) developed a model to calculate the effective permeability using the complex variable boundary element method. However, they assumed fractures are uniformly distributed systems and did not account for fluid flow in the matrix and flow between the interconnected fractures.

In a recent work, Lough et al. (1996, 1998) treated fractures as planner sources in the matrix applying the Poisson's equation to fractures and to the whole matrix inside the block (figure 1-8). By considering very small fracture aperture, they assumed that fluid flow in fracture is equivalent to the flow between a pair of parallel plates. They also assumed that the

velocity and pressure in fractures are being the average fluid velocity and pressure. Lough et al. (1998) concluded that the fracture connectivity has a less influence on the effective permeability than the fracture density because of the strong coupling of the matrix and fractures. In order to relate the fluid flow in matrix to the fluid flow in fracture they assumed that the potential gradient in the fracture is proportionate to the average potential gradient in the grid block. Lough et al. (1998) observed that their method is applicable only to medium size fractures due to complexities involve with the application of Poisson's equation for the whole matrix inside the block. Lee et al. (2001, 1999) modified Lough et al.'s model by introducing a hierarchical approach to include short and large fractures in calculation of effective permeability tensor. They approximated the effect of short fractures on matrix permeability by introducing an analytic expression derived from Oda (1985). They assumed that long fractures act as fluid conduit inside the reservoir and are explicitly implemented in a reservoir simulator using the equation of horizontal wells.

In the following, methods to simulate fluid flow using the effective permeability tensor are introduced with their benefits and drawbacks.

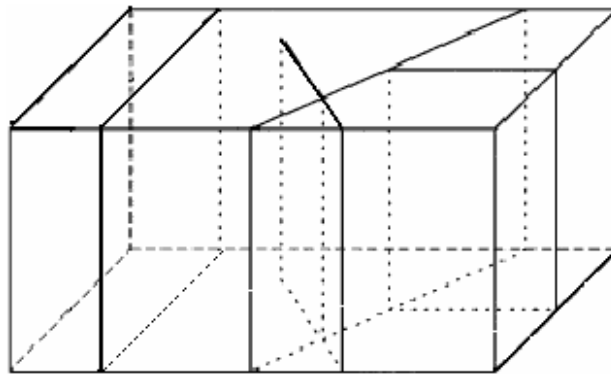


Figure 1-8: A grid block containing medium size fractures of arbitrary orientation and different sizes (after Lough et al., 1998)

Simulation of fluid flow in NFRs using the effective permeability

Recently, a number of theoretical and numerical methods have been developed using the control volume method in the calculation of fluid flow from homogeneous reservoirs. Kwak and Kim (2000) outlined the necessity of these methods in fluid flow simulation and employed them for the calculation of fluid velocity. The control volume approach for the mixed formulation of linear elliptic problem was first developed by Russell (1995). This technique has been widely used as discretisation techniques for conservation of mass by Ohlberger (1997); Feistauer et al. (1995); Durlofsky et al. (1992); Weiser and Wheeler (1988); Suli (1991); Cai et al. (1991, 1997). Control volume discretisation in finite difference and mixed finite element methods has been used by engineers in the simulation of fluid flow in petroleum reservoirs.

Control volume finite difference methods

Recently, a number of models have been developed using the block-centred finite difference method with continuity of velocity between blocks, (Thomas and Trujillo, 1995; Aavatsmark et al., 1998a, b). Lee et al. (1997, 2002) further improved the simulation of NFR using the full tensor effective permeability in a flux-continuous finite difference method. Lee et al. (1997, 1999) developed a flux-continuous finite difference model in the simulation of production from heterogeneous reservoirs by applying a full tensor effective permeability. One of the advantages of this method is the applicability of the model to simulation of fractured reservoirs where the heterogeneity is described by permeability tensor.

Combining finite difference with control volume permits the direct calculation of fluid velocity, whereas in the previous methods velocity is calculated by differentiating the pressure and is not very accurate in the simulation of NFRs.

However, finite difference formulation is valid for uniform grids and creates error in the case of fractured reservoirs with complex geometry. For heterogeneous systems and reservoirs with non-uniform grids, finite difference formulation is not effective and one

needs to use other methods such as finite element which are capable of handling the complex geometry in simulation of fluid flow.

Control volume mixed finite element methods

More recently, control volume and mixed finite element techniques are used in modelling of fluid flow in heterogeneous and fractured reservoirs (Edwards and Rogers, 1994, 1998; Naji and Kazemi, 1996; Nakashima et al., 2000; Park et al., 2002 and Cia et al., 1997). Cia et al. (1997) theoretically formulated this method for heterogeneous reservoirs with irregular geometry and outlined its technical success and applicability. They used a block-centred approach to calculate pressure at the centre and velocity at the middle of the grid block edges. They claimed that their method is more accurate than the methods utilised by Aavatsmark et al. (1998a, b) in which dual velocity grids are associated with the corners of pressure block. The use of control-volume mixed finite element method enables us to simulate fluid flow in reservoirs with irregular geometry while maintaining many of the familiar properties of block-centred finite difference methods for rectangular grids.

Chou and Kwak (2000) developed a mathematical control volume model in a same manner as Cia et al.'s and proved its first order optimal rate of convergence for the approximate velocities as well as for the approximate pressures. Sutopo et al. (2001) applied Cia et al.'s model for the simulation of NFR with two-phase flow and regular fracture pattern. In Cia et al.'s method permeability was assumed to be a scalar term whereas in the simulation of NFR permeability is usually defined in tensor form. Detailed information about this method is provided in chapter 3. However, it should be noted that in the mixed methods pressure is not a continuous function and is calculated in the block centres.

1.3 Objectives and scope of the thesis

From the review, it can be concluded that although numerous approaches have been developed for the modelling of fluid flow in NFRs, very little is known about their actual

mechanism. Many of previous methods are not able to consider the flow in fractured reservoirs with multi-scaled fractures. Others merely characterise the properties of individual fracture. A clear distinction must be made to account for fluid flow in the matrix and the fractures, using the appropriate tools that can be applied to the reservoirs with thousands of fractures of different sizes and orientations.

Review revealed that the use of effective permeability tensor is an efficient method for simulation of fluid flow in NFR due to its computational simplifications and allows use of detail properties of all types of individual fractures. Effective permeability tensor overcomes the problems such as irregular fracture patterns, flow interactions between matrix and fractures and effect of fracture characteristics (i.e. dimension, density and orientation).

This study attempts to contribute to our understanding of fluid flow mechanism in fractured reservoirs. The primary aims of the research are:

- 1) To review the previous methods for the calculation of block effective permeability tensor and simulation of fluid flow and production from NFRs.
- 2) To develop a mathematical formulation and necessary computer code for the calculation of full tensor effective permeability taking into account the effect of different types of fractures and matrix permeability.
- 3) To develop a mathematical formulation and necessary computer code for the simulation of fluid production in naturally fractured reservoirs using the effective permeability tensor.
- 4) To evaluate the computational results of these numerical tools by performing the sensitivity analysis of the reservoir parameters.

1.4 Thesis outline

This thesis is presented in five chapters according to the mathematical formulation, results and discussion. It is divided into two major parts: effective permeability calculation

(Chapter 2) and simulation of fluid flow in NFRs (Chapter 3). Examples and sensitivity analysis for both parts are presented in Chapter 4.

Chapter 2 Provides the theoretical background and mathematical formulation of the calculation of effective permeability in NFR. It defines basic concepts regarding the calculation of effective permeability and provides a detail process of derivation of boundary integral equations, discretisation using the boundary element methods and application of periodic boundary conditions. The result from effective permeability model is also compared with the results from analytical solution.

Chapter 3 Provides the theoretical background and mathematical formulation of simulation of production in NFR. Flux-continuous CVMFE model is employed using the effective permeability tensor in modelling of flow through fractured porous media.

Chapter 4 Presents examples for the effective permeability calculation and fluid flow simulation algorithms in NFRs. Sensitivity analysis is conducted through a number of examples to show the effect of size, density and orientation of fractures as well as matrix permeability.

Chapter 5 Draws the general conclusion followed by recommendations of areas for future study. It presents the findings of the research and the performance of the theoretical methods and computational tools.

CHAPTER 2

CALCULATION OF EFFECTIVE PERMEABILITY TENSOR

CHAPTER 2

CALCULATION OF EFFECTIVE PERMEABILITY TENSOR

2.1 Overview

Recent advances in reservoir characterization have allowed us the construction of realistic methods using the detailed properties of naturally fractured reservoirs. In this chapter a numerical method is developed to calculate the effective permeability tensor in naturally fractured reservoirs. The objective of the presented method is to treat small fractures as part of matrix (pores) and medium to large fractures as source/sink inside the matrix porous media. The former is formulated using the Laplace's equation and the later is formulated using the Poisson's equation for fluid flow inside matrix and fractures. Improvements have been made by introducing a new region (Poisson's region) around the medium to long fractures and in defining the most efficient type of boundary conditions at the grid block boundaries and at the matrix/fracture interface. The equations are formulated in two-dimensions and a computer program is written in FORTRAN to calculate full tensor effective permeability in each grid block. Discretisation of the problem is conducted using the boundary element method. Fractures are classified according to their relative length to the grid block dimensions into short to long fractures. Input data which is the detail information for the individual fractures (location, size and orientation) is taken from the work of Tran (2004).

This chapter begins with the properties of natural fractures, followed by a review of the input data and the theory of fluid flow in NFRs. Then, the methodology for derivation of integral equations and the procedure for calculation of effective permeability tensor are described. Finally, the method is compared with an analytical solution. The calculated effective permeability tensors are employed in the simulation of fluid flow in chapter 3 and a number of examples as well as a case study are presented in chapter 4.

2.2 Properties of natural fracture

Fracture's spatial shape, length, orientation and aperture are essential properties in the simulation of NFRs (see figure 2-1). Natural fractures usually appear in irregular shapes and occur on a variety of scales, from microscopic to continental. In addition, they might have regular or irregular distribution, closed and filled with cement, or open to flow. In this study, all fractures are grouped in the same way and are distinguished from each other by a set of properties of location, geometry, length, orientation, aperture and permeability.

- **Location and Geometry**: Two dimensional line fractures are defined by coordinate of centre (x, y) and orientation. They may also define by the coordinates of start and end points of fractures. Geometry of a fracture affects both the flow properties and the physical properties of the rock mass. Fractures are usually considered as smooth parallel plates, (Rasmussen et al., 1987; Lough et al., 1998; Gupta et al., 2001; Snow, 1965, 1968 and 1969). In numerical methods and in simulators, they are simplified by lines, rectangles or disk shapes in two or three-dimensions.
- **Length**: Fracture length is also an important parameter in the simulation of NFR. Length of fracture is depended on field geology and varies over a wide range from 10^{-4} to 10^8 cm (Chernyshev and Dearman, 1991). In this study, fractures are usually grouped as short, medium and long based on their length and different techniques are applied to different size of fractures in the simulation of fluid flow. In the examples presented throughout this study, it is assumed that short fractures have a length less than 0.05% of the grid block size and long fractures are those that have a length of higher than the grid block diagonals. Medium fractures will have a length between short and long fractures.
- **Orientation**: Fracture orientation is calculated by measuring the angle between the centre line of fracture and y axis (north direction), positively clockwise (figure 2-1).

- **Aperture**: Fracture aperture is also an important factor in the simulation of fluid flow. Many methods assume a constant aperture and some consider the aperture as a function of length (e.g. Oda, 1985). In this thesis the aperture is assumed to be very small, compared to the length of the fractures. This assumption allows the fluid flow inside the fracture to be equivalent to the flow between a pair of parallel plates, (Lough et al., 1996, 1998 and Lee et al., 2001).
- **Permeability**: Fracture permeability is very high as it connects isolated pores and acts as the main conduit for fluid flow in the reservoir. Thus, the presence of fractures can greatly increase the permeability of rocks with very low matrix permeability such as tight gas reservoirs.

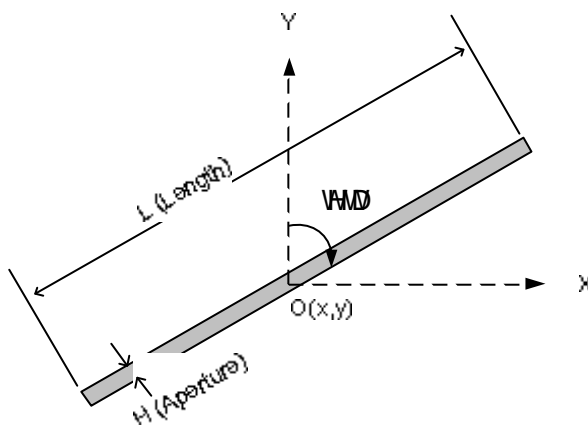


Figure 2-1: 2D schematic for a single fracture with centre O(x,y), orientation (theta), length (L) and aperture (H) in x-y coordinate system.

It is possible to estimate fracture permeability and fluid flow through the fractures by using the simplifications made by Snow (1969) which assumes fractures are parallel plates with smooth surfaces. Fluid flow through a single fracture is usually expressed by cubic law. Cubic law is deduced from Darcy's law with the assumptions of laminar flow through a channel bounded by parallel plates with permeability:

$$k_i = \frac{h_i^2}{12} \dots\dots\dots 2-1$$

where $h_i(m)$ is the aperture in the fracture “i” and k (m^2) is the permeability between the two parallel plates (Lee et al., 2001). Cubic law is valid for rough and uneven discontinuities when they are open (Witherspoon et al., 1980; Iwai, 1976; Lee and Farmer, 1993).

2.2.1 Field data sources for this study

In the previous methods such as continuum or parallel plate, fractures are considered in regular patterns or grouped as fracture sets and systems in the medium. A fracture set is usually known as a group of fractures which run more or less parallel to each other and a fracture system is grouped as a number of fracture sets which intersect at a constant angle. This simplification does not consider the properties of individual fractures by defining the mean length, aperture and orientation for set of fractures. By use of new techniques, it is now possible to characterise NFRs to generate the detail information of all types of individual fractures.

This study calculates the effective permeability tensor based on the specification of individual fractures to provide realistic results with higher accuracy. Input data for this study are taken from the work of Tran (2004) which includes coordinates of the centre, half length, dip and azimuth and considers fractures in three dimensional penny shapes, see figure 2-2.



Figure 2-2: Fractures generated in a portion of a reservoir characterised by Tran (2004). Different sizes of fractures from short to long are presented in three-dimensional disk shape format.

To calculate the coordinates of individual fractures in two-dimensions, fractures are first converted into direction cosines using their dip angle and azimuth angle. To do this, the normal to the fracture is projected to the vertical and horizontal surface to calculate the direction cosines, as shown in figure 2-3. In this figure, OX is directed horizontally east, OY is horizontally north and OZ is vertically upward and the direction cosines are assigned for fracture in vertical and horizontal directions. The directional cosines of the fracture in terms of fracture dip and azimuth can be presented as:

$$\begin{aligned}
 l &= \sin(dip) \sin(azimuth) \\
 m &= \sin(dip) \cos(azimuth) \dots\dots\dots 2-2 \\
 n &= \cos(dip)
 \end{aligned}$$

where the parameters d and g are defined as: $d = 90 - dip$ and $g = 90 - azimuth$. Using the equation 2-2 and having the fracture centre location and its length or radius from input data, it is possible to calculate the two-dimensional information for individual fractures as line fractures.

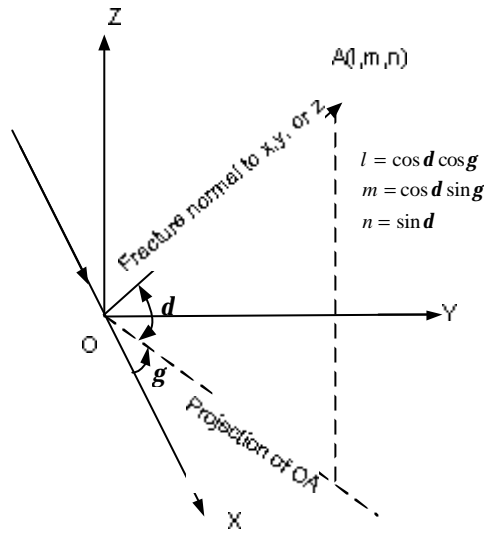


Figure 2-3: Schematic for calculation of direction cosines

Figure 2-4 shows schematic view of a fractured reservoir which is divided into a number of grids containing different types of fractures. The effective permeability algorithm developed in this study requires the fractures to be divided into three categories based on their relative length to the grid block size: short and medium size fractures. Long fractures are divided into their crossing blocks and modelled in a same manner as medium fractures.

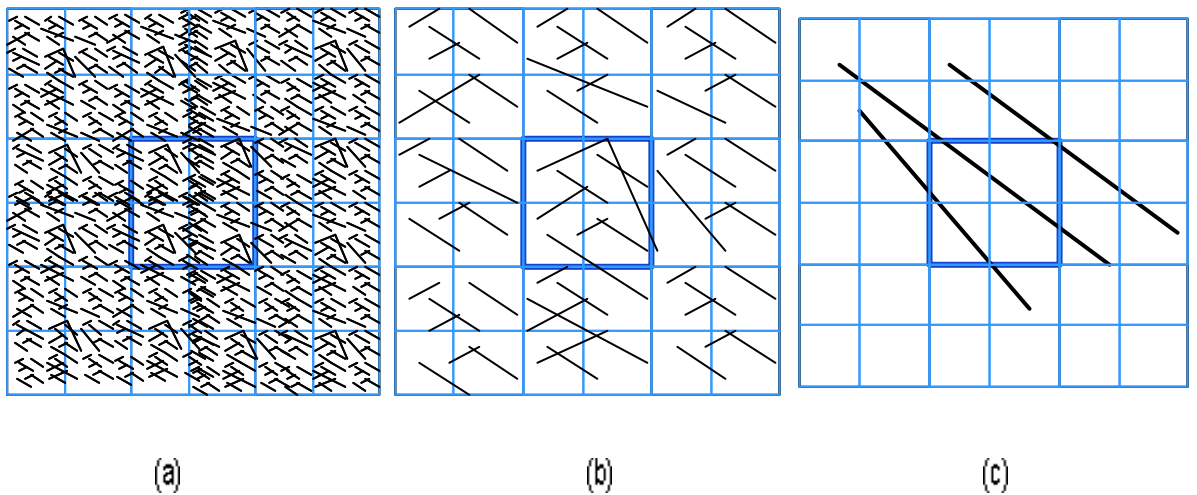


Figure 2-4: A schematic of two-dimensional fractured reservoir used in this study. (a) Short fractures (b) Medium size fractures (c) long fractures.

2.3 Theory of fluid flow in fractured reservoirs

In chapter 1, the methods to calculate the effective permeability tensor were discussed. It was mentioned that some of previous methods did not consider the fluid flow in the matrix and flow interaction between matrix and fractures (e.g., methods which use Snow's method and discrete fracture approach). Other methods did not consider the properties of individual fractures like size, aperture and orientation in the calculation of effective permeability tensor (e.g., methods which use dual porosity/ permeability approaches). It was also mentioned that the majority of methods assumed fracture to be separated from the matrix by applying the Laplace's equation. It was concluded that the recent work by Lough et al. (1996, 1998) which treats fractures as planar sources inside the matrix is one of the most efficient methods which applies Poisson's equation to the matrix and fractures. However, that method requires the discretisation of the whole matrix block and is only applicable for medium size fractures due to its complexity. Recently, further improvement was made by Lee et al. (2001, 1999) by introducing a hierarchical approach which includes short and large fractures in calculation of effective permeability tensor. Short fractures were analysed using a stochastic method and long fractures were modelled using the equation of horizontal well and were implemented explicitly to the reservoir simulator.

In this study, the previous works are improved in several ways: by introducing a new region around the medium fractures (called Poisson's region) to simplify the complexities involved with using the Poisson's equation for matrix porous media. By considering the fluid flow in the matrix, fluid flow in the fracture, flow between the matrix and the fracture and fluid flow between the interconnected fractures. By including short to long fractures and considering the properties of individual fractures in calculation of effective permeability tensor. Finally, by applying appropriate types of boundary conditions at the boundaries of grid block, fractures and Poisson's region, the integral equations are obtained. The above improvements are discussed throughout this chapter and are addressed in the mathematical formulation section.

2.4 Mathematical formulation

In this section boundary integral equations for matrix and fractures are derived and different types of boundary conditions along the grid block and fracture boundaries are presented. It is assumed that the fracture aperture is very small in comparison to the fracture lengths. In the definitions provided for matrix and fractures, it is assumed that the individual fractures and matrix are isotropic with considering a constant permeability inside the fracture and in the matrix porous media. Then the effective permeability in the three-dimensional fractured reservoir is described as permeability tensor, \bar{k} taking into account the effects of the matrix and the fracture,

$$\bar{K} = \begin{bmatrix} k_{xx} & k_{xy} & k_{xz} \\ k_{yx} & k_{yy} & k_{yz} \\ k_{zx} & k_{zy} & k_{zz} \end{bmatrix} \dots\dots\dots 2-3$$

and in two-dimensional problems it reduced to:

$$\bar{K} = \begin{bmatrix} k_{xx} & k_{xy} \\ k_{yx} & k_{yy} \end{bmatrix} \dots\dots\dots 2-4$$

where k_{xx} and k_{yy} are diagonal terms and k_{xy} and k_{yx} are off-diagonal terms of permeability tensor K . It is necessary for effective permeability tensor to be symmetric, $k_{xy} = k_{yx}$ and positive definite, $k_{xx}k_{yy} > k_{xy}^2, k_{xx} > 0, k_{yy} > 0$, in order to have a physical meaning (Durlflosky, 1991).

Effective permeability tensor in porous media is usually estimated by solving single-phase fluid flow equations subject to periodic boundary conditions (Durlflosky, 1991 and Nakashima et al., 2000). The well known Darcy's equation for fluid flow in porous media is described as,

$$v = -\frac{\bar{K}}{m} \frac{\partial P}{\partial x} \dots\dots\dots 2-5$$

and the continuity equation is written as follows:

$$\bar{\nabla} \cdot v = Q \dots\dots\dots 2-6$$

where v is the velocity, m is the fluid viscosity, Q and P are the flow rate and pressure, respectively. Then the equation describing the flow of incompressible fluid can be derived by combining Darcy's law and mass conservation as follows:

$$\bar{\nabla} \cdot \left[\frac{K}{m} (\nabla P) \right] + Q = 0 \dots\dots\dots 2-7$$

Assuming unique fluid viscosity ($m=1$), the above equation can be written in expanded form as,

$$\frac{\partial}{\partial x} \left(K \frac{\partial P}{\partial x} \right) + \frac{\partial}{\partial y} \left(K \frac{\partial P}{\partial y} \right) + \frac{\partial}{\partial z} \left(K \frac{\partial P}{\partial z} \right) + Q = 0 \dots\dots\dots 2-8$$

It is immediately apparent that in steady state condition, given the isotropic porous media, the above equation can be rewritten in the following form,

$$K_x \frac{\partial^2 P}{\partial x^2} + K_y \frac{\partial^2 P}{\partial y^2} + K_z \frac{\partial^2 P}{\partial z^2} + Q = 0 \dots\dots\dots 2-9.$$

Equation 2-9 states that the sum of flow rates in three directions and flow rate related to source/sink to the differential elementary volume is zero (see figure 2-5). Derivation for the above equations is presented in Appendix-A.

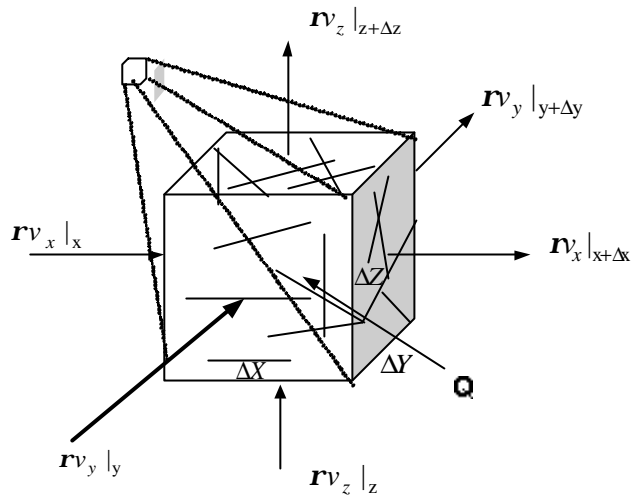


Figure 2-5: Differential volume element of fluid flow equilibrium.

One of the improvements made by this study is to consider the fluid flow in the matrix, fracture and between the matrix and fractures. This requires the formulation for equations of both matrix and fracture medias. In previous works, in the calculation of effective permeability in NFR, fracture and matrix were formulated as separated systems having a common interface. The common interface is made up of those parts of the fracture boundaries that are contained in the matrix (Lough et al., 1998). The fracture aperture is considered very small and the fluid flow in the fracture is equivalent to the flow between a pair of parallel plates. An example of the methods which consider fracture and matrix as separate systems was presented by Rasmussen et al. (1987). Fluid flow and pressure equations in the fracture and matrix can be presented as follows (Lough et al., 1998):

Fracture:

$$v_i(x) = -k_i \nabla p_i(x) \dots\dots\dots 2-10$$

$$\nabla \cdot v_i(x) = -\frac{1}{h} Q_i(x) + \sum_{j=1}^m q_j \dots\dots\dots 2-11$$

where $Q_i(x)$ represents the source strength of the fluid flow from fracture i to the matrix and q is the fluid flow from the intersected fractures to the fracture i at the intersection line. Flow of incompressible fluid in the matrix is based on Darcy's law. Assuming v_m and p_m to be fluid velocity through the matrix and pressure in the matrix, respectively.

Matrix:

$$v_m(x) = -k_m \nabla p_m(x) \dots\dots\dots 2-12$$

$$\nabla v_m(x) = 0 \dots\dots\dots 2-13$$

Equation 2-13 is modified to treat medium size fractures inside the matrix by applying the source term of the Poisson's equation to the matrix porous media around the medium size fractures. As a result, fracture system and matrix porous media are coupled from the outset part using the Poisson's equation and fluid velocity through the matrix which was previously presented by equation 2-13 becomes,

$$\nabla \cdot u_m(x) = \sum_{j=1}^N \int_{F_i} q_j(x(z)) \mathbf{d}(x_o - z) dA_z \dots\dots\dots 2-14$$

where q_j is the flow interaction between matrix and fracture in element j , $\mathbf{d}(\cdot)$ is the dirac delta function and A is the area of element j .

Finally, the governing equations for flow in the matrix and fractures in a two-dimensional reservoir are expressed as:

$$\text{Fracture: } k_f \frac{\partial^2 p_i}{\partial L^2} + Q_i + q_{ff} = 0 \dots\dots\dots 2-15$$

$$\text{Matrix: } k_m \frac{\partial^2 p_m}{\partial x^2} + k_m \frac{\partial^2 p_m}{\partial y^2} + Q_i = 0 \dots\dots\dots 2-16$$

where $k_f = 7.842 \times 10^{12} h^2$, h is fracture aperture, L is one-dimensional coordinate and subscripts m and f represent matrix and fracture, respectively.

Term Q represents the flow interaction between the fracture and matrix. q_{ff} is fluid flow from intersected fracture to the fracture i at the intersection lines (Lough et al., 1998):

$$q_{ff} = \sum_{j=1}^{m_i} \int_{L_i^j} q_i^j(x_o) \mathbf{d}(x - x_o) dl(x_o) \dots\dots\dots 2-17$$

where x and x_o represent the position vectors for points on fracture i and it is assumed that there are m_i intersections on fracture i which is located along the lines $[L_i^j, j = 1, \dots, m_i]$.

To explain the methodology of solving the above equations using the boundary element methods, let us begin with the derivation of the general form of boundary integral equation. The linear form of Poisson's equation in domain A is defined as follows Kwon (2001):

$$\nabla \cdot (k \nabla p(x)) + Q(x) = 0 \text{ in } A, \dots\dots\dots 2-18$$

where k denotes the permeability, $x = (x_1, x_2)$ for an arbitrary point in interior of A and $Q(x)$ characterises the source term associated with interior domain A , (figure 2-6(a)). In the case of medium or long fracture, the term $Q(x)$ is defined as $(Q_i + q_{ff})$, (figure 2-6 (b)).

To solve the above equation with numerical techniques, it is necessary to solve the related integral equations in a way to produce reasonable results in reservoirs with large number of fractures and high degree of heterogeneity. For this purpose, all the existing methods were examined and the related literature was reviewed. It was found that there exist basically two approaches toward solving the boundary integral formulation: direct formulation using Green's second identity and weighted residual method. The later is usually described as strong form, weak form, inverse form via integral by parts.

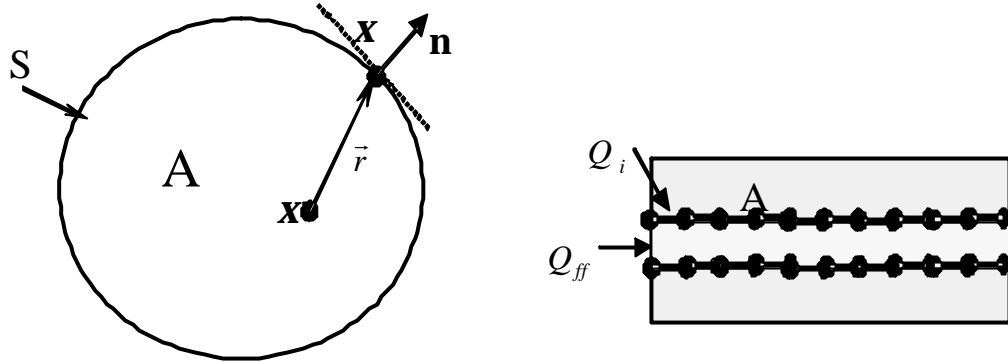


Figure 2-6: (a) Arbitrary points on domain A. (b) Points on the region around medium fractures

Green's second identity for a regular function G is the fundamental solution (or Green's solution) and defined as $\nabla^2 G = \mathbf{d}(\bar{x} - \bar{x}')$. A fundamental solution is a function that satisfies the differential equation with zero right hand side at every point of an infinite domain except at points known as the source or sink, where the right hand side is infinite, (Beer and Watson, 1992). The derivative of G is the function F which is defined in an infinite space singular at any point within the region under consideration, (see figure 2-6(a)). Function G can be found from,

$$G = \left\{ \begin{array}{l} \frac{1}{2p} \ln r \dots \text{in } 2D \\ -\frac{1}{4pr} \dots \text{in } 3D \end{array} \right\} \dots \dots \dots 2-19.$$

The fundamental solution, G is a solution satisfying the following equation

$$\int_{\Omega} (P \nabla^2 G - G \nabla^2 P) d\Omega = \int_{\partial\Omega} \left(P \frac{\partial G}{\partial n} - G \frac{\partial P}{\partial n} \right) ds \dots \dots \dots 2-20.$$

where $r = |\bar{x}' - \bar{x}|$, (Beer and Watson, 1992).

In the boundary element method the arbitrary points are moved to the surface of domain such that the nodes are defined at the boundaries. In view of this, the boundary integral equation form of equation 2-19 for an arbitrary point $\mathbf{x} = (\mathbf{x}_1, \mathbf{x}_2)$ in domain A is written as, (Beer and Watson, 1992):

$$c(\mathbf{x})p(\mathbf{x}) = \int_S G(x, \mathbf{x})v(x)ds(x) - \int_S F(x, \mathbf{x})p(x)ds(x) + \int_A Q(x)G(x, \mathbf{x})dA(x) \quad \dots\dots\dots 2-21$$

where $v = k\nabla p \cdot \vec{n}$ and \vec{n} is the exterior normal vector of S at \mathbf{x} . S is the boundary of domain A in figure 2-6(a) and also the boundary of block A2 in figure 2-7. For a single fracture inside the block, G is the fundamental solution, F which is the flux corresponding to the fundamental solution, is equal to $k \partial G / \partial n$ and $Q(x)$ is equal to the Dirac delta function $\delta(x - \mathbf{x})$. The coefficient $c(\mathbf{x})$, which is a function of the internal angle of the boundary S at point \mathbf{x} , equals 1 if $\mathbf{x} \in A$, 0 if $\mathbf{x} \notin A \cup S$ and $\mathbf{a}/2\mathbf{p}$ if $\mathbf{x} \in S$, where \mathbf{a} denotes the internal angle of S at \mathbf{x} (\mathbf{a} equals \mathbf{p} at a smooth point on S). In the above formulations, k is permeability and is defined for matrix or fractures individually.

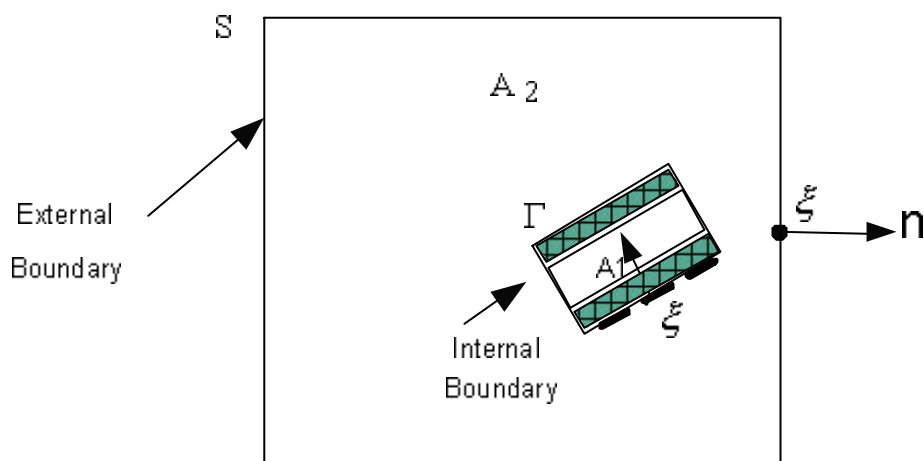


Figure 2-7: Homogeneous block with an arbitrary fracture

Short fractures are considered as large matrix pores and hence the source term ($\int_A QGdA$) is not considered. The equation 2-21 is rewritten for short fractures as:

$$c(\mathbf{x})P(\mathbf{x}) = \int_S G(x, \mathbf{x})v(x)ds(x) - \int_S F(x, \mathbf{x})pds(x). \dots\dots\dots 2-22$$

The effective permeability tensors calculated for short fractures using the equation 2-22 have the following form,

$$K_{short} = \begin{bmatrix} K_{xx} & K_{xy} \\ K_{yx} & K_{yy} \end{bmatrix} \dots\dots\dots 2-23$$

To find the local permeability, the result from the short fractures are averaged inside the grid block as,

$$K = \sqrt{\frac{1}{2}(K_{xx}^2 + K_{yy}^2)} \dots\dots\dots 2-24$$

This technique enhanced our ability to predict the local permeability. The calculated local permeability from short fractures is then used to calculate the full tensor effective permeability considering the effect of medium and long fractures.

2.4.1 Boundary conditions

In order to define the boundary conditions along the fracture boundaries three parallel surfaces are assumed for fracture: front, back and centre where the front and back surfaces are considered as the common interface with the matrix (porous media). In the previous works, fractures in the matrix are assumed as separate systems having a common interface. As a result, the type of boundary condition around the matrix/fracture interface is called interface boundary conditions where the boundary nodes are defined as having equal pressures with no flow at the interface of two regions.

In this study, the following conditions are considered at the interface of matrix and fractures:

$$n_i \cdot v_i(x) = 0 \dots\dots\dots 2-25$$

$$p_i(x) = p_i \dots\dots\dots 2-26$$

where n_i is the unit normal to the fracture, x is position vector on the fracture and “ i ” represents i 'th fracture.

In this thesis, improvements are made by applying different types of boundary conditions at the boundaries of grid block, fractures and Poisson's region around the fractures. Interface boundary conditions are applied to the boundaries of short fractures assuming them as belonging to matrix (pores) which are included in the local permeability. Other fractures are considered as source/sink in the matrix and Poisson's equation is applied to the portion of matrix which is located around medium and long fractures and is termed as Poisson's region. It is assumed that medium and long fractures contribute to the fluid flow inside the fractured porous media. Finally, periodic boundary conditions are applied to the block boundaries to calculate the effective permeability in tensor form. Below are the boundary conditions for each type of fractures and the grid block boundaries:

Short fractures

The boundary conditions for short fractures are expressed as:

$$p_{mi} = p_{fi} \dots\dots\dots 2-27$$

$$v_{mi} = -v_{fi} \dots\dots\dots 2-28$$

where $v_{mi} = \vec{v}_m \cdot \vec{n}$ and $v_{fi} = \vec{v}_f \cdot \vec{n}$, p_{mi} and p_{fi} are matrix and fracture pressures at the interface and \vec{v}_m and \vec{v}_f are velocities (Rasmussen et al., 1987; Beer and Watson, 1992).

Medium to long fractures

Boundary conditions along the medium and long fracture boundaries in this study are defined as:

$$p_{fi} = p_{av} \dots\dots\dots 2-29$$

$$v_{mi}^+ - v_{mi}^- = Q_i \dots\dots\dots 2-30$$

where $v_{mi}^+ = \bar{v}_m^+ \cdot \bar{n}$, $v_{mi}^- = \bar{v}_m^- \cdot \bar{n}$ are the normal velocity per unit area of fracture, p_{av} is the pressure in the fracture's central line and calculated by averaging the pressure values for the nodes located on the opposite sides of fracture boundaries at each boundary element to find a value for the centre line of fracture at that element. p_{fi} represents the pressure along the fracture nodes, \bar{v}_{mi}^+ and \bar{v}_{mi}^- are velocities on the opposite nodes on the fracture faces and Q_i is depended on the source strength of the fracture and represents the flow interaction between the matrix m and fracture i . Matrix pressure on the common matrix-fracture interface and on the exterior boundaries of the area around the fracture is unknown and can be calculated by applying the periodic boundary condition during the solution process.

Boundaries of grid block

Periodic boundary conditions are considered for nodes along the block boundaries, which require treating all fracture edges as being inside the grid block (Lough, 1998). This type of boundary condition was discussed in section 1.2.4 in chapter 1. Assuming that Γ_1 and Γ_3 are two opposite faces of the grid-block in the x_1 direction and Γ_2 and Γ_4 are two opposite faces of the grid-block in the x_2 direction as shown in **Error! Reference source not found.** Pressure at an arbitrary point $x = (x_1, x_2)$ in the grid-block can be expressed as (Durlflosky, 1991):

$$p(x) = p_0 + J(x - x_0) \dots\dots\dots 2-31$$

where x_o is the centre of the region under consideration, p_o is the pressure at x_o and $J = (j_1, j_2)$ is the local pressure gradient.

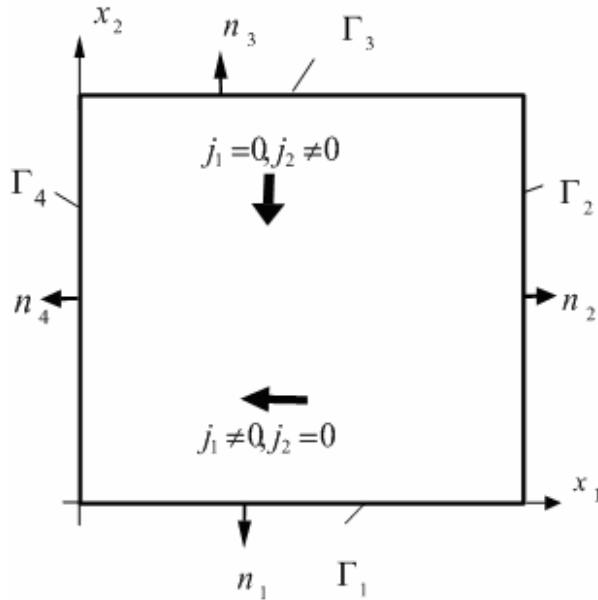


Figure 2-8: Periodic boundary condition over the grid-block.

Periodic boundary conditions over the unit cell are written as (Durlafsky, 1991):

$$p(x_1, x_2 = 0) = p(x_1, x_2 = 1) - j_2 \quad \text{On } \Gamma_1 \text{ and } \Gamma_3, \dots \dots \dots 2-32$$

$$v(x_1, x_2 = 0) \vec{n}_1 = -v(x_1, x_2 = 1) \vec{n}_2 \quad \text{On } \Gamma_1 \text{ and } \Gamma_3, \dots \dots \dots 2-33$$

$$p(x_1 = 0, x_2) = p(x_1 = 1, x_2) - j_1 \quad \text{On } \Gamma_2 \text{ and } \Gamma_4 \text{ and} \dots \dots \dots 2-34$$

$$v(x_1 = 0, x_2) \vec{n}_2 = -v(x_1 = 1, x_2) \vec{n}_4 \quad \text{On } \Gamma_2 \text{ and } \Gamma_4 \dots \dots \dots 2-35.$$

A constant pressure difference in the x_1 direction and a zero pressure difference in the x_2 direction ($j_1 \neq 0$ and $j_2 = 0$) are applied to calculate the first two terms of the permeability tensor k_{xx} and k_{yx} .

Having solved Laplace's equation under the above boundary conditions, the average velocity through the unit block is determined as follows:

$$\langle v_1 \rangle = - \int_{\partial\Gamma_3} v \cdot n_3 dx_2 \dots\dots\dots 2-36$$

$$\langle v_2 \rangle = - \int_{\partial\Gamma_1} v \cdot n_1 dx_1 \dots\dots\dots 2-37.$$

Assuming $j_1 \neq 0$ and $j_2 = 0$, the two components (k_{xx} and k_{yx}) of permeability tensor can be easily determined from the following equations:

$$\langle v_1 \rangle = -(k_{xx} j_1 + k_{xy} j_2) \dots\dots\dots 2-38$$

$$\langle v_2 \rangle = -(k_{yx} j_1 + k_{yy} j_2) \dots\dots\dots 2-39.$$

The remaining two components (k_{xy} and k_{yy}) of permeability tensor can be calculated in the same way by varying the direction of pressure gradient to $j_1 = 0$ and $j_2 \neq 0$.

2.5 Solution of the integral equation

The numerical methods used for solution of integral equations are usually based on an approximate method of solution. The type of method used may have an effect on the accuracy and the length time required for solution. Unfortunately, it is difficult to compare different methods as there are varieties of techniques for solving integral equations with

unrelated approximating techniques. The majority of these methods try to replace the integrals by a quadrature formula or by a weighted residual function such as the Galerkin method. In what follows, a quadrature based formula is used to develop a particular boundary element method.

2.5.1 Discretisation using the boundary element method

BEM is a relatively new numerical method developed in the shadow of the FEM and FDM. Recently, BEM has been a comparative interest for solving engineering problems with small number of books available on subject such as Chen and Zhou (1992). The BEM utilises information only at the boundary of the region because the solution of the problem is a combination of the exact solutions inside the region. BEM works extremely well for problems with a high ratio of volume to surface area but not very well for those with a low ratio. The opposite is the case for FEM. BEM treats the problems as a boundary value problem, solves the integrals at the boundary (or surface in three- dimensional analysis) and reduces meshing complexities significantly (Beer and Watson, 1992).

A constant or linear BEM is preferable to the FEM and FDM in the simulation of naturally fractured reservoirs as it is discussed in chapter 4. In fact, in BEM only the boundary requires sub-division, while in the FEM or FDM the whole domain of the partial differential equations are required to be discretised. The advantages associated with the boundary element method arise from the reduction of dimension by one which is important in cases of large three-dimensional systems. BEM also has the advantage that complex geometry can be considered in a shorter time by calculating the integrals at the boundaries only instead of solving them in the whole domain.

Similar to FEM, BEM can solve the integral equations by a quadrature formula or by a weighted residual method such as the well-known Galerkin method. The potential shortcoming of BEM is that it requires the fundamental solution of the governing partial differential equation to be known. Although BEM has some problems in modelling of non-homogeneous media, the application of this method in the solution of boundary integral equations in many engineering problems is appreciated (Brebbia, 1978; Huyakorn and

Pinder, 1983). It is also widely employed in the calculation of effective permeability in fractured porous media with constant matrix permeability (Lough et al., 1998; Lee et al., 2001 and Nakashima et al., 2000).

In the implementation of BEM, the whole domain A is divided into NC triangular elements, A_1, \dots, A_{NC} with centres of x_1, \dots, x_{NC} . The boundary S is discretised into N boundary elements as S_1, S_2, \dots, S_N over which displacements are chosen to be piecewise interpolated between the nodal points. Figure 2-9 shows a number of regions which are considered in this method. In this figure, short fractures and matrix porous media are defined as region 1, whereas medium and long fractures marked as region 2. The portion of matrix which is located around the medium and long fractures is marked as 3. Interconnected fractures are not included in this figure, but shown in figure 2-11.

Short fractures and matrix porous media

For modelling of short fractures only the boundaries of fractures and grid block are discretised using the constant type of BEM. In this case, the values of p and v are assumed to be constant and equal to the value at the mid point of the element. Equation 2-22 for a given ‘i’ can be written in discretised form as:

$$c^i(\mathbf{x}) p(\mathbf{x}) + \sum_{j=1}^{NS} \int_{S_j} F(x, \mathbf{x}) p(x) ds(x) = \sum_{j=1}^{NS} \int_{S_j} G(x, \mathbf{x}) v(x) ds(x), \dots \dots \dots 2-40$$

term $\int_{S_j} F(x, \mathbf{x}) ds(x)$ relate the ‘i’ node with the element ‘j’ over which the integral is carried out.

Medium to long fractures and interconnected fractures

In the case of medium, long and interconnected fractures, the Poisson’s equation is used for fracture and their surrounded matrix. For this purpose, all medium to long fractures are evaluated and are grouped into their corresponding blocks. Long fractures crossing a

Terms $\int_{S_j} F(x, \bar{x}_i) ds(x)$ and $\int_{S_j} G(x, \bar{x}_i) ds(x)$ relate node 'i' with the element 'j' over which the integral is carried out. Let us call these integrals \hat{A}_{ij} and \hat{B}_{ij} respectively. The second term on the right hand side is the contribution of fluid flow from the matrix to fracture and is termed as b_i . Assuming $A_{ij} = \hat{A}_{ij} + \frac{1}{2}I$, where I is the identity matrix, equation 2-42 can be written as:

$$[A]p = [B]v + b \dots\dots\dots 2-43$$

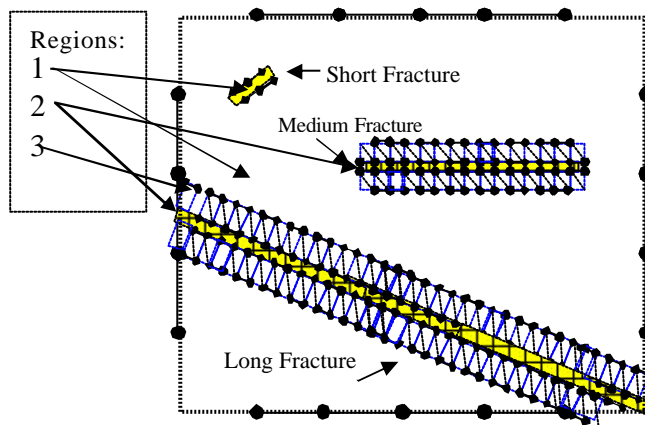


Figure 2-9: Boundary nodes on fractures and block and interior discretisation in two dimensions.

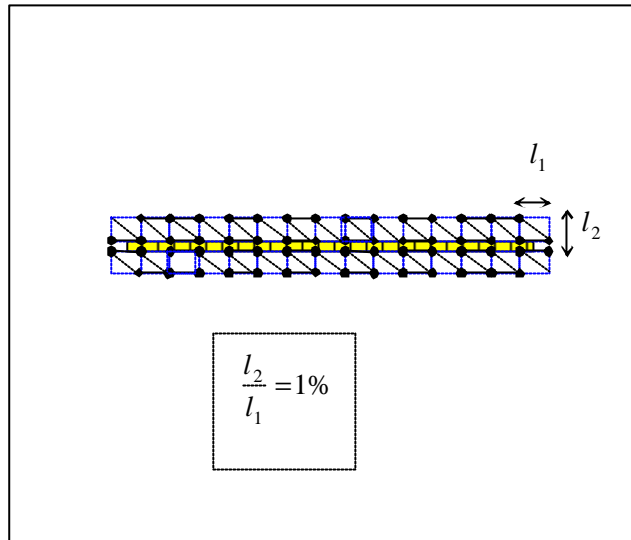


Figure 2-10: Defining the Poisson's region around the medium and long fractures. l_1 and l_2 are the boundary elements along the length and edge of fracture.

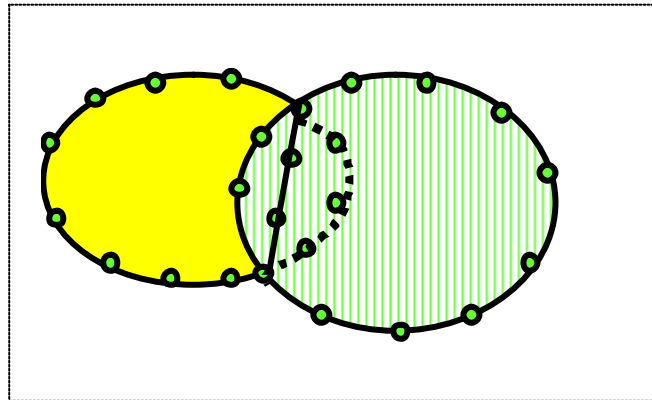


Figure 2-11: Intersected line between interconnected fractures with circular shapes

2.5.2 Boundary element solution of the system of equations

In this part the solution method for discretised boundary integral equations are briefly presented. Applying periodic boundary conditions in conjunction with boundary conditions along the fracture boundaries enables us to solve the system of linear equations in equation (2-43).

Equation 2-43 can be summarised as follows,

$$[A][X] = [B] \dots\dots\dots 2-44$$

where:

- A = coefficient matrix
- X = nodal displacement vector (unknown functions of p and v)
- B = load vector (boundary conditions and injection, production well information)

[A] is a dense, non-symmetric and a large matrix (commonly in thousands) and can be solved by the use of FORTRAN or LAPAC libraries. The size of stiffness matrix in this study can be calculated directly by use of the number of fractures inside the grid block. An example of the matrix vector system resulting from the collocation of equations in each block can be determined by considering a block containing single fracture with 400 elements along the grid block, 20 elements along the fracture boundaries and 20 elements along the Poisson's region (see figure 2-12). Size of the stiffness matrix for this example is equal to 960×960 as shown in figure 2-13.

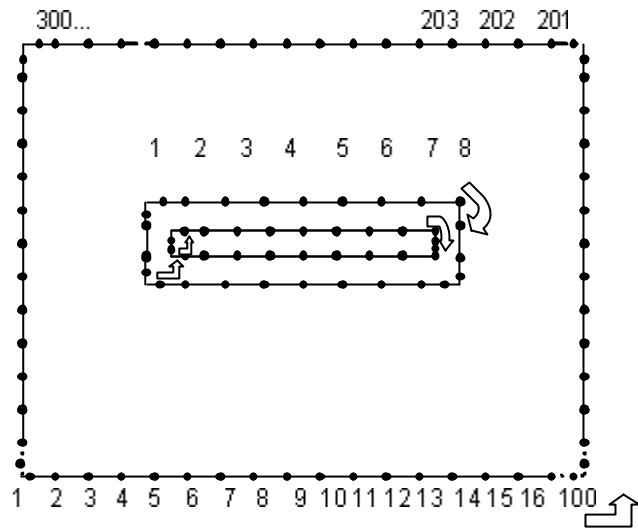


Figure 2-12: A block containing a single fracture to show the elements of stiffness matrix.

In equation 2-44, unknowns ($[X]$) are pressure and normal velocity at the grid-block boundaries, pressure and velocity at the fracture faces and edges, the portion of matrix around the fracture and fluid flow rate in fractures as well as at the lines of intersection between the interconnected fractures. The source term at the fracture boundaries and flow rate inside the fracture are calculated once the pressure and velocities at fracture and block boundaries are known. Calculations of velocity at the intersection line for intersected fractures and average pressure inside the fracture involves an iterative method as discussed earlier. Matrix and fractures are coupled with M node on the block, the N node on the region around the fractures and the N node along the fracture boundaries. This leaves us with $2M+4N$ unknowns and $M+2N$ equations.

The boundary conditions for fractures as specified in the mathematical formulation section gives us $2N$ equations. The periodic boundary condition gives us the remaining M equations when a constant pressure gradient between the opposite nodes on the grid-block boundaries is considered. In figure 2-13, A represents the fundamental solution and B represents the derivatives of A and C represents the boundary conditions at each collocation point.

The main advantage of this approach is that by modelling the short and medium to long fractures separately, it saves computation time and reduces the numerical error during the solution process. The source code to implement the above problem is written in the FORTRAN 90 and the flowcharts for calculation of effective permeability from short and medium to long fractures are shown in figure 2-14. It is shown that the input data first are examined in the geometric terms to be converted into 2D and also divided into short and medium to long fractures in each grid block. In each block, short fractures are formulated using the Laplace's equation using the periodic boundary conditions. The resulted local permeability from the short fractures is then used as matrix permeability for medium and long fractures which are treated inside the matrix porous media as source/ sink.

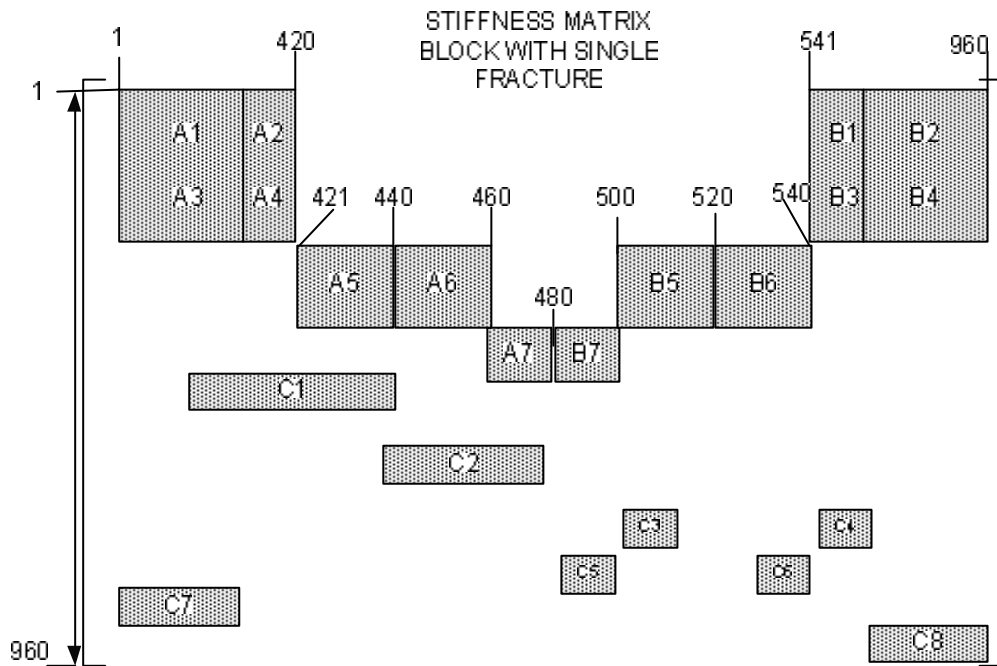


Figure 2-13: Stiffness matrix for block in figure 2-12 containing single fracture, F is the fundamental solution and G is its derivative B and C represent the boundary conditions around fracture, surrounding part and along the block boundaries.

Calculation of the components of effective permeability tensor in x and y directions, requires solving the above problems twice: the first two components are calculated by applying a unit pressure difference between the two opposite sides of the grid block in x -direction and zero pressure difference between the other two opposite sides of the grid block in y -direction. In the same way, the other two components of the tensor are calculated by applying a unit pressure difference to the two opposite sides of the grid block in y -direction and zero pressure difference in x -direction. This process is directly related to the application of periodic boundary condition which was explained previously in section 2.4.1 in this chapter.

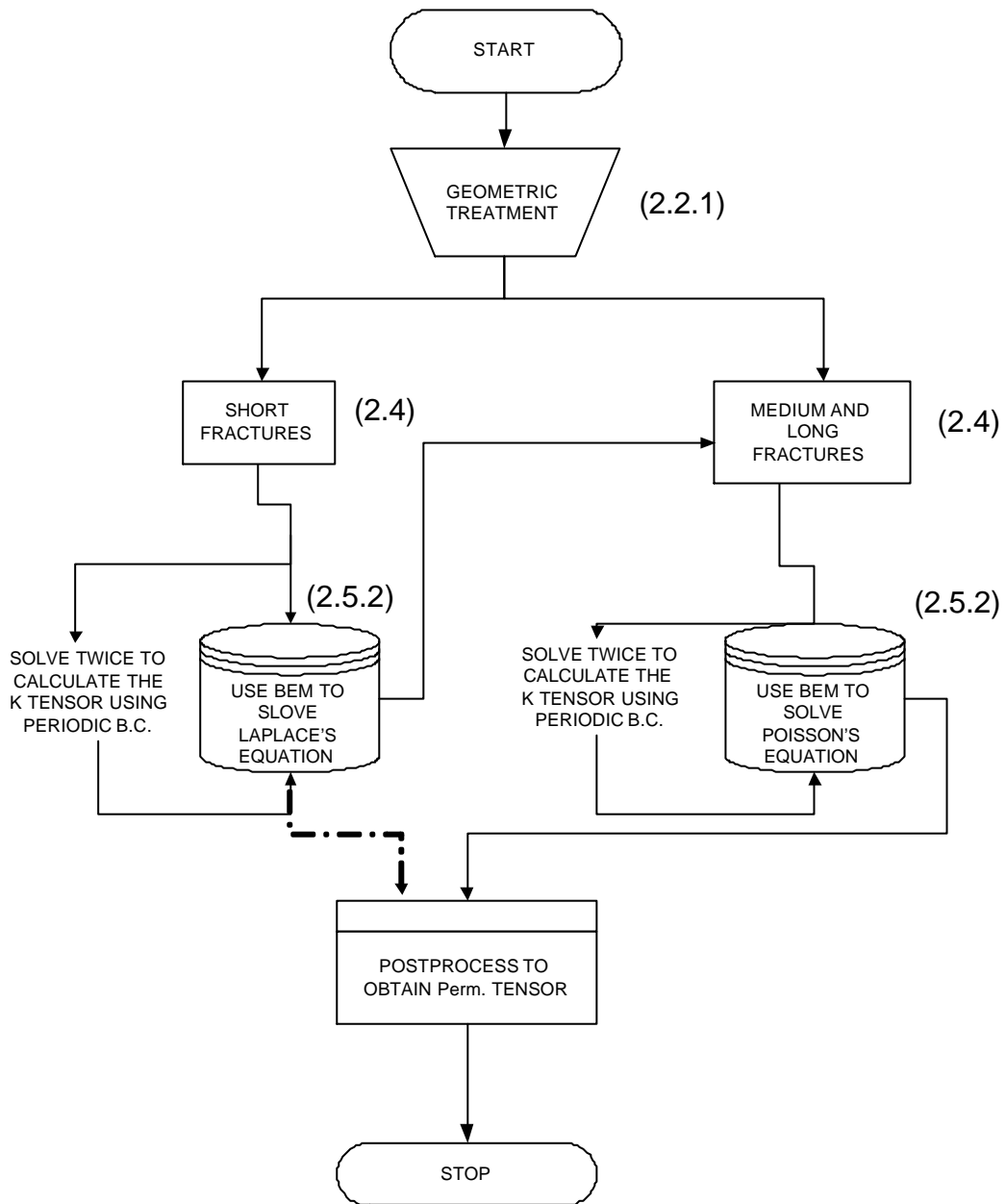


Figure 2-14: Flow chart for calculation of the effective permeability of naturally fractured reservoirs with multiple blocks and multiple fractures. Each part of the figure is connected to its related section in the text by addressing the related section number.

2.6 Comparative analysis between analytical and numerical results

The purpose of this section is to compare the results from the effective permeability algorithm with the results from an analytical formula which is believed to be a useful tool for measuring the consistency of the variation in the effective permeability (Lough et al., 1998). This will provide us with useful comparative results and to show us that the method is able to provide accurate results. This method has been used by (Lough et al., 1998) to validate the results of their effective permeability calculation model.

To proceed with this method we know that effective grid block permeability is depended on the fracture orientation so that it takes the form

$$K(\mathbf{q}) = \begin{pmatrix} K_{xx}(\mathbf{q}) & K_{xy}(\mathbf{q}) \\ K_{yx}(\mathbf{q}) & K_{yy}(\mathbf{q}) \end{pmatrix} \dots\dots\dots 2-45$$

Moreover, if when $\mathbf{q} = 0$ the effective permeability of the block is

$$K(0) = \begin{pmatrix} K_1 & 0 \\ 0 & K_2 \end{pmatrix} \dots\dots\dots 2-46$$

then it follows that the components given in equation 2-45 can be written as

$$K_{xx}(\mathbf{q}) = K_1 \cos^2 \mathbf{q} + K_2 \sin^2 \mathbf{q}$$

$$K_{yy}(\mathbf{q}) = K_1 \sin^2 \mathbf{q} + K_2 \cos^2 \mathbf{q} \dots\dots\dots 2-47$$

$$K_{xy}(\mathbf{q}) = K_{yx}(\mathbf{q}) = (K_1 - K_2) \sin \mathbf{q} \cos \mathbf{q}$$

Therefore, analytical results for fracture with varying orientations (rotation angle) can be calculated by the following equation:

$$K = \begin{bmatrix} k_{xx} \cos^2 \mathbf{q} + k_{yy} \sin^2 \mathbf{q} & (k_{xx} - k_{yy}) \sin \mathbf{q} \cos \mathbf{q} \\ (k_{xx} - k_{yy}) \sin \mathbf{q} \cos \mathbf{q} & k_{yy} \sin^2 \mathbf{q} + k_{xx} \cos^2 \mathbf{q} \end{bmatrix} \dots\dots\dots 2-48$$

where \mathbf{q} is the rotation angle and k_{xx} and k_{yy} are x and y components of the effective permeability tensor for a horizontal fracture, respectively (Lough et al., 1998).

To compare the results of this study with the results from the above analytical equation, calculations were carried out at several rotation angles or orientations for a single fracture with the length of 0.6 units and aperture of 1.0×10^{-4} units, inside a block with unit matrix permeability and length, (see **figure 2-15**). Each edge of the fracture is discretised into 7 nodes and 100 elements are considered along the block boundaries.

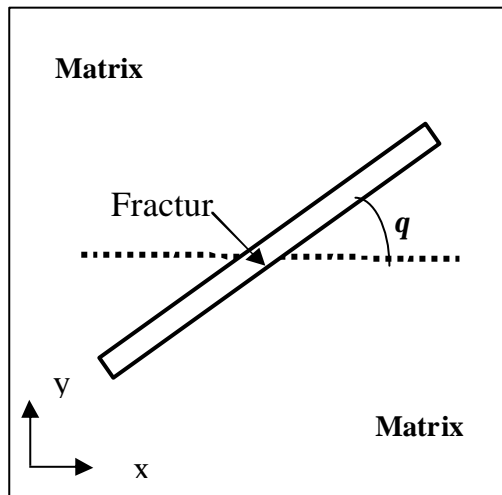


Figure 2-15: Validation of the method against the analytical solution by rotating a single fracture inside the matrix block

The diagonal and off-diagonal components of effective permeability tensor are compared with those calculated by analytical solution method for different angle \mathbf{q} between 0-90

degrees and the results are presented in figure 2-16 and figure 2-17 . It is shown in these figures that the results computed by using both methods are virtually indistinguishable and that they are within acceptable accuracy. The numerical results are consistent with those of analytical calculation as described by equation 2-41.

In Table 2-1 and Table 2-2 the calculated values of the diagonal and off-diagonal elements of the permeability tensor as a function of increase in the rotation angle for both the permeability algorithm and the analytical solution are presented. The results show a very good correlation between two methods and indicate that both methods are producing similar results.

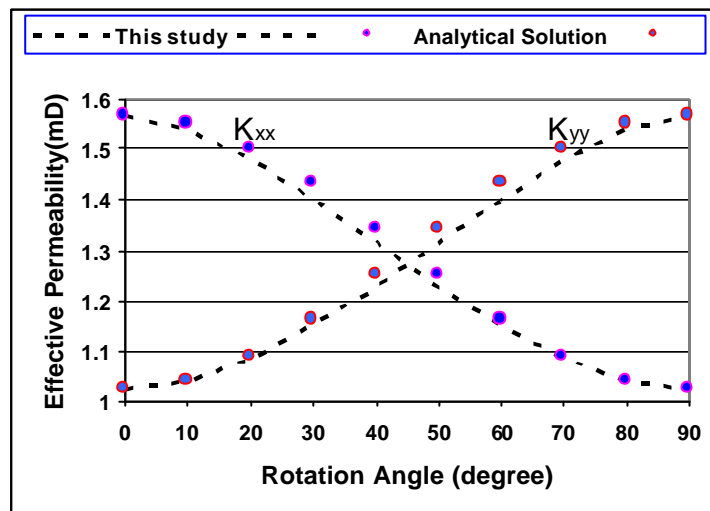


Figure 2-16: Comparison of analytically and numerically calculated diagonal elements of the permeability tensor for single fracture rotating in a block.

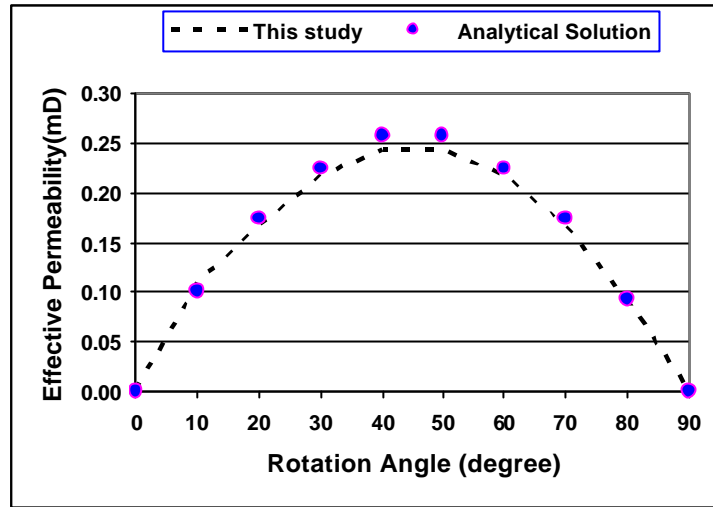


Figure 2-17: Comparison of analytically and numerically calculated off-diagonal elements of the permeability tensor for single fracture rotating in a block.

Rotation Angle q	Results calculated by Permeability Model		
	K_{xx}	$K_{xy} = K_{yx}$	K_{yy}
0	1.566	0.000	1.023
10	1.540	0.109	1.039
20	1.478	0.166	1.083
30	1.398	0.217	1.148
40	1.312	0.243	1.226
50	1.226	0.243	1.312
60	1.148	0.217	1.398
70	1.083	0.165	1.478
80	1.039	0.091	1.540
90	1.023	0.000	1.566

Table 2-1: Results of the numerically calculated diagonal and off-diagonal elements of the permeability tensor using this study.

Rotation Angle q	Resultscalculated by Analytical Solution		
	K_{xx}	$K_{xy} = K_{yx}$	K_{yy}
0	1.566	0.000	1.023
10	1.550	0.100	1.039
20	1.502	0.175	1.087
30	1.430	0.225	1.159
40	1.342	0.257	1.247
50	1.247	0.257	1.342
60	1.159	0.225	1.430
70	1.087	0.175	1.502
80	1.039	0.093	1.550
90	1.023	0.000	1.566

Table 2-2: Results of the analytically calculated diagonal and off-diagonal elements of the permeability tensor using

2.7 Closure

In this chapter, the algorithm to calculate effective permeability tensor in NFRs has been discussed. The fractured grid block has been replaced with a homogeneous block having a full tensor effective permeability, in which the fracture properties remain the same throughout the grid block. The effective permeability calculation is based on the treatment of fractures as sink/source plans in the matrix and the resulting equations are solved using the boundary element method. Short fractures are assumed to act as large pores belong to local permeability and medium to long fractures are treated as sink/source in their surrounding matrix porous media.

Fluid flow in matrix porous media was found very important in NFRs and it could not be ignored in simulation of fluid flow in these reservoirs. Most previous works did not consider the effect of matrix permeability and the effect of disconnected fractures.

Fluid flow in matrix, fracture, matrix-fracture interface and intersected fractures are considered. The boundary element method and periodic boundary conditions are then used to calculate effective permeability tensor in each grid block. The boundary element method simplifies discretisation process and the periodic boundary conditions have the advantage that provides symmetric and positive definite tensors (results always have a physical meaning).

Results of this study are validated against analytical solution and the difference between the two was found negligible. The application of effective permeability tensors in simulation of fluid flow in NFRs is presented in chapters 3 and sensitivity analysis are presented in chapter 4.

CHAPTER 3

SIMULATION OF FLUID FLOW IN NFR USING CONTROL VOLUME MIXED FINITE ELEMENT METHOD

CHAPTER 3

SIMULATION OF FLUID FLOW IN NFR USING CONTROL VOLUME MIXED FINITE ELEMENT METHOD

3.1 Overview

In previous chapter a method to calculate the effective permeability tensor in NFR was presented. The objective of this chapter is to employ the effective permeability tensors in the simulation of fluid flow and prediction of production from NFR using a flux-continuous control volume mixed finite element method. The control volume is employed to discretise the reservoir into grids assuming each grid block as a control volume. The mixed finite element method is employed to calculate fluid pressure and velocities in the reservoir, directly by providing a system of first order equations of Darcy's law and conservation of mass' law. Firstly, a rather general description is provided in which the present study is compared with similar studies, followed by a discussion of the problems associated with the applications of this current approach. Next, the mathematical formulation and the discretisation technique is presented. Finally, the results of this study are compared against data available in the literature.

3.2 Theory of simulation of fluid flow in NFRs

In the simulation of fluid flow in porous media, velocity or flux is usually of primary interest. In chapter 1, the previous methods of simulation of fluid flow in NFR were classified including a single continuum method, a double porosity/permeability method and a discrete fracture method or a control volume mixed method. It was concluded that the control volume mixed finite element (CVMFE) method is one of the most appreciated methods in the simulation of NFRs. It was first introduced by Russell (1995) and then improved by Cai et al. (1997) to include the irregular grid blocks. The CVMFE method accounts for accurate calculation of velocity in the block and between the neighbouring blocks by providing flux-continuous formulation of velocity. It also accounts for heterogeneity of the fractured reservoir using the effective permeability tensor.

In fractured reservoirs, often sharp changes in lithology can cause sudden changes in fluid properties (Sutopo et al., 2001). These changes cause the pressure to change rapidly and thus may lead to errors in the calculation of velocities using the conventional techniques where the diffusivity equation has been applied to the simulation of fluid flow in NFR. Moreover, conventional techniques require the solution of second order system of equations to calculate the pressure and then differentiate the pressure to calculate velocity. However, in CVMFE method velocity and pressure are directly calculated by solving a system of first order equations containing conservation of mass and Darcy's equation. It also overcomes the problems inherent in previous works regarding matrix and fracture characteristics, using effective permeability tensor for each block. CVMFE method has been used by a number of investigators in the simulation of fluid flow in NFRs (Sutopo et al., 2001; Cia et al., 1997 and Chou and Kwak, 2000).

In this chapter, CVMFE method is used to simulate fluid flow and to predict pressure and velocity distribution profiles. This follows the same basics as Cia et al.(1997) but incorporates full tensor effective permeability in the simulation of fluid flow in naturally fractured reservoirs. A computer program is written in FORTRAN to calculate the velocity

at the edges and pressure at the centre of each grid block taking into account the properties of individual fractures by using the effective permeability tensor.

3.3 Governing equations

Fluid flow in naturally fractured reservoirs is formulated using a system of first order equations for incompressible, single-phase flow. The algorithm is derived for regular grids and can be applied to the reservoirs with irregular grids (see Cia et al., 1997). Darcy's law for single-phase flow, neglecting the gravitational effect, is written as:

$$v = -\frac{K}{m} \frac{\partial P}{\partial x} \dots\dots\dots 3-1$$

and conservation of mass for an incompressible fluid can be described as follows:

$$\nabla \cdot v = q \dots\dots\dots 3-2$$

where, v (cm/sec) is the velocity, $\frac{\partial P}{\partial x}$ (atm/cm) denotes the pressure gradient field, K (Darcy), m (cp), q (cm^3 / sec) are permeability, fluid viscosity and flow rate, respectively. Single phase flow with unit density is assumed in this formulation. To derive the related integral equations using the finite element method, equation 3-1 is written as $mK^{-1}v + \nabla P = 0$, which generalises the usual harmonic averaging of K in a simple way as described by Cai et al. (1997).

Combining the Darcy's law and the conservation of mass results in the following system of first order equations in reservoir or domain Ω (Sutopo et al., 2001):

$$\begin{cases} mK^{-1}v + \nabla P = 0 \\ \nabla \cdot v = q \end{cases} \dots\dots\dots 3-3.$$

The Mixed Finite Element (MFE) method is used to define a solution to this problem, providing a direct solution of the first order equations 3-3 for v and P . In the above equations, K is the full tensor effective permeability, defined as:

$$K = \begin{bmatrix} K_{xx} & K_{xy} \\ K_{yx} & K_{yy} \end{bmatrix} \dots\dots\dots 3-4$$

where K_{xx} and K_{yy} are diagonal terms and K_{xy} and K_{yx} are off-diagonal terms of the permeability tensor K . In general, it is necessary for effective permeability tensor to be symmetric ($K_{xy} = K_{yx}$) and positive definite ($K_{xx}K_{yy} > K_{xy}^2, K_{xx} > 0, K_{yy} > 0$), in order to have a physical meaning (Durlafsky, 1991).

To derive the integral equation, it is necessary to define a weak form (defining a weak formulation is essential in the finite element methods) of the system of equations defined in equation 3-3. This study uses the format which is used by Wilson (2001) in deriving the appropriate weak form. In general, it is required to prove the existence and uniqueness of the weak form, or mixed variational form. It is also necessary to define appropriate function spaces which are conveniently used in finite element methods. The mathematical formulation for deriving the weak form is presented in detail by Wilson (2001).

To derive the integral equation, let's multiply the first term of equation 3-3 by a vector test function w and integrate over Ω giving

$$\int_{\Omega} \mathbf{n}K^{-1}v \cdot w d\Omega + \int_{\Omega} \nabla p \cdot w d\Omega = 0 \dots\dots\dots 3-5.$$

Integration by parts and applying the Neumann boundary condition for above equation yields (Sutopo et al., 2001):

$$\int_{\Omega} \mathbf{n}K^{-1}v \cdot w d\Omega - \int_{\Omega} \nabla p \cdot w d\Omega = - \langle w \cdot \mathbf{n}, q \rangle \partial\Omega \dots\dots\dots 3-6.$$

Next, multiplying the second term in equation 3-3 by a scalar test function z and integrating over Ω gives (Sutopo et al., 2001),

$$\int_{\Omega} \nabla \cdot v z dx = \int_{\Omega} q z dx \dots\dots\dots 3-7$$

where the function z and the components of w are chosen such that the divergence $\nabla \cdot w$ is square-integrable and $w \cdot n = 0$ at the boundary $\partial\Omega$. The above differential equations are still considered to be continuous, with P and v satisfying the same conditions as z and w respectively.

3.3.1 Boundary conditions

The Neumann boundary condition is then applied to the external boundaries of the reservoir. This type of boundary condition specifies a value for velocity on the boundaries. For example, the value of the velocity at the boundary may change if reservoir has an active aquifer, see figure 3-1.

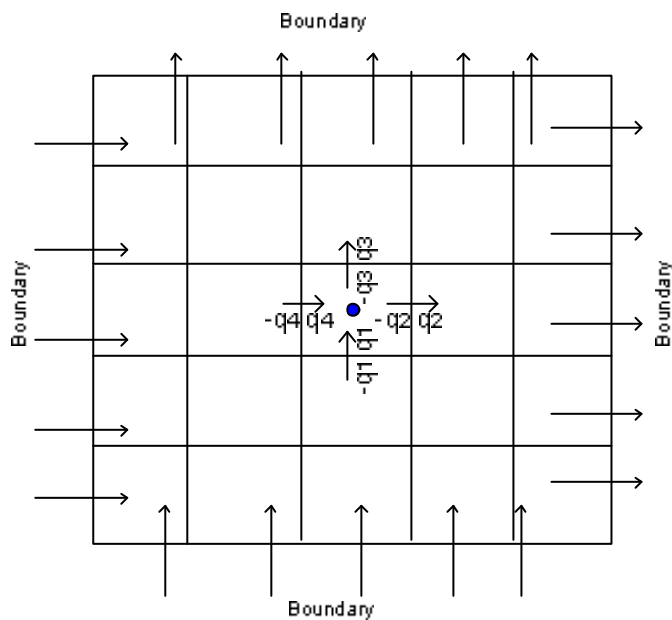


Figure 3-1: Describes Neumann type of boundary condition at the external boundaries of the reservoir

The flux-continuous boundary condition is used at the interfaces between grid blocks. This means that velocity vectors at the edges of each block are equal to the velocity vectors of their neighbouring blocks with the reverse sign (see figure 3-1).

3.4 Discretisation using the Control Volume

Block-centred control volume method is currently recognised by many researchers as an effective tool in discretisation of the integrals of equations (3-6) and (3-7) (Cai et al., 1997; Forsyth, 1989; Heinemann et al., 1989 and Rozon, 1989). Control volume discretisation helps to avoid the complexities that appear if one employs the standard mixed finite element method. The purpose of using the control volume in this formulation is to find a good combination of the finite volume method and the cell placements of flow variables. The main assumption for this method is that the pressure unknowns are assigned to the centres and the normal components of the velocity or fluxes are averaged and assigned to the edges of the grid blocks. Control volumes and nodal points of the pressure and velocity are shown in figure 3-2 and figure 3-3.

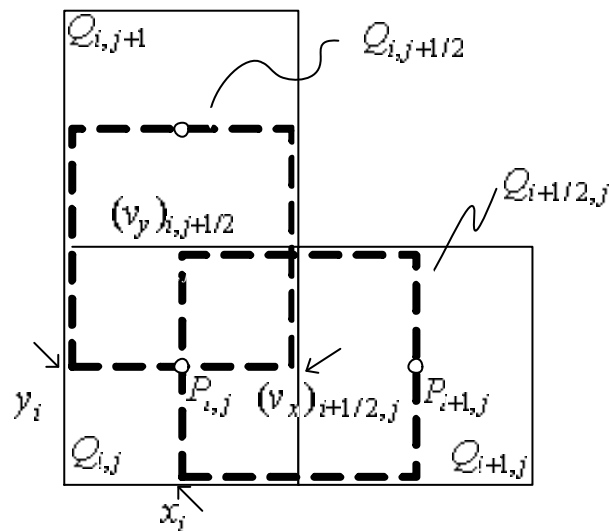


Figure 3-2: Control volume and unknowns for rectangular grid.

In figure 3-2, $Q_h = \{Q_{i,j}\}$ is a partition of the reservoir into a union rectangular grid block $Q_{i,j}$ with centre $c_{i,j}$ having the pressure $P_{i,j}$ at the centre of block (i, j). The subindices $\{i+1, j\}$, $\{i-1, j\}$, $\{i, j+1\}$ and $\{i, j-1\}$ are assigned to the eastern, western, northern and southern adjacent rectangles, respectively, if they exist. $Q_{i,j}$ is defined as:

$$Q_{i,j} = [x_{i-1/2}, x_{i+1/2}] \times [y_{i-1/2}, y_{i+1/2}]. \dots\dots\dots 3-8.$$

In figure 3-2, $c_{i+1/2,j} = (x_{i+1/2}, y_j)$ and $c_{i-1/2,j} = (x_{i-1/2}, y_j)$ are two midpoints of $Q_{i,j}$ in its vertical edges and $c_{i,j+1/2} = (x_i, y_{j+1/2})$ are the midpoints of $Q_{i,j}$ in its horizontal edges. Unknowns of the approximate velocity v are assigned to the edges of the block and the unknowns of the approximate pressure p to the centres of the partition $\{Q_{i,j}\}$ of the same block.

In the next step, a dual grid is introduced, which is obtained by shifting the original grid along x and y axes, to provide a finite volume around each unknown. Let $c_{i,j} = (x_i, y_j)$ and $c_{i+1/2,j} = (x_{i+1/2}, y_j)$ etc., define

$$Q_{i+1/2,j} = (x_i, x_{i+1}) \times (y_{i-1/2}, y_{i+1/2}) \dots\dots\dots 3-9$$

$$Q_{i,j+1/2} = (x_{i-1/2}, x_{i+1/2}) \times (y_j, y_{j+1}) \dots\dots\dots 3-10.$$

It is important to define control volumes over p_{ij} , $(v_x)_{i+1/2,j}$ and $(v_y)_{i,j+1/2}$, which are defined as $Q_{i,j}$, $Q_{i+1/2,j}$, $Q_{i,j+1/2}$, respectively. In order to have a physical description, one can consider $Q_{i+1/2,j}$ as a tank with pressures $p_{i,j}$ and $p_{i+1,j}$ at the two ends as shown in figure 3-2. Similarly, for $Q_{i,j+1/2}$, $p_{i,j}$ and $p_{i,j+1}$ are defined towards its two ends. As illustrated in figure 3-2, unknowns are denoted by $(v_x)_{i+1/2,j}$ on the vertical edge centred at $(x_{i+1/2}, y_j)$ and $(v_y)_{i,j+1/2}$ on a horizontal edge centred at $(x_i, y_{j+1/2})$. Throughout this chapter, $P_{i,j}$ is denoted as the nodal value of p at centre $C_{i,j}$. Since the approximate

pressure is assigned at the centre of control volume $Q_{i,j}$, it is usual to assume that it is piecewise constant with respect to the original control volume $\{Q_{i,j}\}$ on the whole reservoir domain (Chou and Kwak, 2000).

To perform the integration over the equation 3-3 using the control volume discretisation, let v_x and v_y denote the component of velocity such that $(v_x, v_y)^t = v$, then the equation 3-3 can be rewritten in the form of a first-order system (Sutopo et al., 2001):

$$\left[\begin{array}{l} (IDetK)^{-1}(K_{yy}v_x - K_{yx}v_y) + \frac{\partial p}{\partial x} = 0 \\ (IDetK)^{-1}(-K_{xy}v_x + K_{xx}v_y) + \frac{\partial p}{\partial y} = 0 \\ \frac{\partial v_x}{\partial y} + \frac{\partial v_y}{\partial x} = q_t \end{array} \right] \dots\dots\dots 3-11$$

with boundary conditions,

$$v_x(l) = g(l), \dots l \in \partial\Omega_{east} \cup \partial\Omega_{west}$$

$$v_y(l) = g(l), \dots l \in \partial\Omega_{south} \cup \partial\Omega_{north}$$

where Ω represents the reservoir under consideration and Ω_{south} , Ω_{north} , Ω_{east} and Ω_{west} represent its external boundaries. The first two terms of equation 3-6 are integrated over the control volume $Q_{i+1/2,j}$ and $Q_{i,j+1/2}$, respectively as (Sutopo et al., 2001):

$$\int_{x_i}^{x_{i+1}} \int_{y_{i-1/2}}^{y_{i+1/2}} \frac{1}{IDetK} (K_{yy}v_x - K_{yx}v_y) dx dy + \int_{x_i}^{x_{i+1}} \int_{y_{i-1/2}}^{y_{i+1/2}} \frac{\partial p}{\partial x} dx dy = 0 \dots\dots\dots 3-12$$

$$\int_{y_i}^{y_{i+1}} \int_{x_{i-1/2}}^{x_{i+1/2}} \frac{1}{IDetK} (-K_{xy}v_x + K_{xx}v_y) dx dy + \int_{y_i}^{y_{i+1}} \int_{x_{i-1/2}}^{x_{i+1/2}} \frac{\partial p}{\partial y} dx dy = 0 \dots\dots\dots 3-13.$$

Using the shape functions for p , v_x and v_y as described above, one can rewrite the integrals in equations 3-7 and 3-13 in terms of the unknowns: $P_{i,j}$, $P_{i+1,j}$, $P_{i,j+1}$, $(v_x)_{i-1/2,j}$, $(v_x)_{i+1/2,j}$, $(v_x)_{i+3/2,j}$, $(v_y)_{i,j-1/2}$, $(v_y)_{i,j+1/2}$, $(v_y)_{i,j+3/2}$, see figure 3-3.

Finally the discrete Darcy equations in x-direction for $Q_{i+1/2,j}$ becomes ,

$$\begin{aligned} & \frac{h^2 K_{yy;i,j}}{8(I(S) \det[K])_{i,j}} v_{x;i-1/2,j} + \frac{3h^2 K_{yy;i,j}}{8(I(S) \det[K])_{i,j}} v_{x;i+1/2,j} + \\ & \frac{3h^2 K_{yy;i+1,j}}{8(I(S) \det[K])_{i,j}} v_{x;i+1/2,j} + \frac{h^2 K_{yy;i+1,j}}{8(I(S) \det[K])_{i+1,j}} v_{x;i+3/2,j} + \dots \dots \dots 3-14. \\ & \frac{h^2 K_{xy;i,j}}{4(I(S) \det[K])_{i,j}} (v_{y;i,j-1/2} + v_{y;i,j+1/2}) + \frac{h^2 K_{xy;i,j}}{4(I(S) \det[K])_{i+1,j}} \\ & (v_{y;i+1/2,j-1/2} + v_{y;i+1/2,j+1/2}) + h(P_{i+1,j} - P_{i,j}) = 0 \end{aligned}$$

Similarly in y-direction for $Q_{i+1/2,j}$ becomes,

$$\begin{aligned} & \frac{h^2 K_{xx;i,j}}{8(I(S) \det[K])_{i,j}} v_{y;i,j-1/2} + \frac{3h^2 K_{xx;i,j}}{8(I(S) \det[K])_{i,j}} v_{y;i,j+1/2} + \\ & \frac{3h^2 K_{xx;i,j+1}}{8(I(S) \det[K])_{i,j}} v_{y;i,j+1/2} + \frac{h^2 K_{xx;i,j+1}}{8(I(S) \det[K])_{i,j+1}} v_{y;i,j+3/2} + \dots \dots \dots 3-15 \\ & \frac{h^2 K_{yx;i,j}}{4(I(S) \det[K])_{i,j}} (v_{x;i-1/2,j} + v_{x;i+1/2,j}) + \frac{h^2 K_{yx;i,j}}{4(I(S) \det[K])_{i,j+1}} \\ & (v_{y;i-1/2,j+1/2} + v_{y;i+1/2,j+1/2}) + h(P_{i,j+1} - P_{i,j}) = 0 \end{aligned}$$

where p is constant and v_x varies linearly with x but remains constant in the y direction (Sutopo et al., 2001). Similarly, v_y is constant in the y direction and varies linearly with x , h denotes the size of the grid block edges in both the vertical and horizontal directions and

changes to h_1 and h_2 , respectively, if the grid block is not square. I is the mobility ratio in the case of multiple phases and simplifies to viscosity in single phase flow.

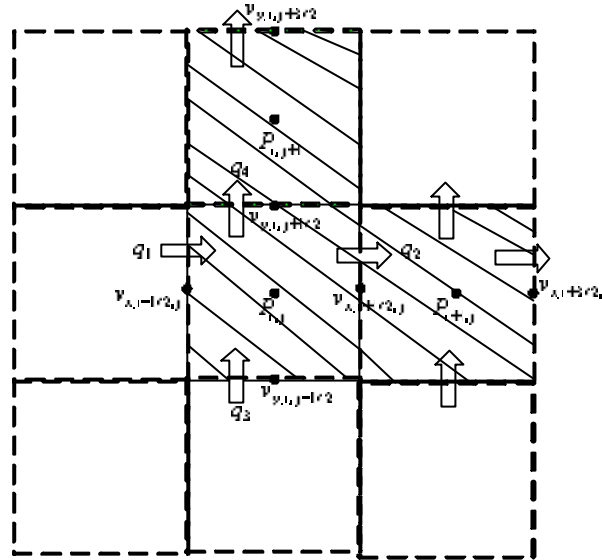


Figure 3-3: The Fluxes, pressure and velocities of block (i,j) in CVMFE method.

In case of a rectangular grid block (figure 3-3), equation 3-14 can be written in the x direction in the following form (Sutopo et al., 2001):

$$\begin{aligned} & \frac{h^2}{8} (K_{yy} (IDet[k]^{-1})) \{v_{x,i-1/2,j} + 3v_{x,i+1/2,j} + v_{x,i+3/2,j}\} \\ & + \frac{h^2}{4} (K_{yx} (IDet[k]^{-1})) \{v_{y,i,j-1/2} + v_{y,i,j+1/2} + v_{y,i+1,j-1/2} + v_{y,i+1,j+1/2}\} \dots\dots\dots 3-16. \\ & + h(P_{i+1,j} - P_{i,j}) = 0 \end{aligned}$$

Jones (1995) presented a similar equation in the following form:

$$\begin{aligned} & \frac{h^2}{8} (K_{yy} (Det[k]^{-1})) \{v_{x,i-1,j} + 6v_{x,i,j} + v_{x,i+1,j}\} \\ & - \frac{h^2}{4} (K_{yx} (Det[k]^{-1})) \{v_{y,i-1,j+1} + v_{y,i-1,j} + v_{y,i,j+1} + v_{y,i,j}\} \dots\dots\dots 3-17. \\ & + h(P_{i,j} - P_{i-1,j}) = 0 \end{aligned}$$

Next, equation 3-7 is integrated over the control volume $Q_{i,j}$ which is in fact a matter of applying the divergence theorem. From the definition of v_x and v_y , we have (Sutopo et al., 2001):

$$\int_{Q_{i,j}} \nabla \cdot v dx dy = \int_{Q_{i,j}} \left(\frac{\partial v_x}{\partial x} + \frac{\partial v_y}{\partial y} \right) dx dy = \int_{Q_{i,j}} q_i dx dy \dots\dots\dots 3-18.$$

Due to the assumption that v_x and v_y are constants at the edges of the block, applying the Gauss divergence theorem to the left hand side of equation 3-18 enables it be converted into a surface integrals as (Sutopo et al., 2001):

$$\begin{aligned} \int_{Q_{i,j}} \nabla \cdot v dx dy &= \int_{\partial Q_{i,j}} v \mathbf{h} ds = \int_{\partial Q_{i,j}^e} v_x(x_{i+1/2}, y) dy - \\ &\int_{\partial Q_{i,j}^w} v_x(x_{i-1/2}, y) dy + \int_{\partial Q_{i,j}^n} v_y(x, y_{i+1/2}) dx - \dots\dots\dots 3-19 \\ &\int_{\partial Q_{i,j}^s} v_y(x, y_{i-1/2}) dx \end{aligned}$$

where e, w, n and s denote the east, west, north and south edges of control volume Q , respectively. As v_x and v_y are constant at the edges of the control volume, the mass conservation equation can be expressed in terms of $(v_x)_{i-1/2,j}$, $(v_x)_{i+1/2,j}$, $(v_y)_{i,j+1/2}$ and $(v_y)_{i,j-1/2}$ as:

$$h(v_{xi+1/2,j} - v_{xi-1/2,j} + v_{xi,j+1/2} - v_{xi,j-1/2}) = -|Q|q_{ti,j} \dots\dots\dots 3-20$$

where $q_{ti,j}$ on the right hand side of equation 3-20 denotes the values of q at the node $c(i,j)$ and c is the centre of the block with position (i, j) . The CVMFE method produces discrete version of Darcy's law, which relates the pressure drop between cells to a linear combination of velocities for each volume in the x and y directions. Equations 3-16, 3-17

and 3-20 provide a system of linear equations which can be solved to calculate the pressure at block centres and the flux across the edges.

The resulting system of equations is written in the following form:

$$\begin{bmatrix} M_{xx} & M_{xy} & N_x \\ M_{yx} & M_{yy} & N_y \\ N_x^T & N_y^T & 0 \end{bmatrix} \begin{bmatrix} V_x \\ V_y \\ P \end{bmatrix} = \begin{bmatrix} 0 \\ 0 \\ -|Q|q_t \end{bmatrix} \dots\dots\dots 3-21.$$

In problems with a diagonal permeability tensor, the off-diagonal elements of the effective permeability tensor tend to be zero and the above system of equations can be simplified by assuming a symmetric system of linear equations with zero elements for M_{xy} and M_{yx} as:

$$\begin{bmatrix} M_{xx} & 0 & N_x \\ 0 & M_{yy} & N_y \\ N_x^T & N_y^T & 0 \end{bmatrix} \begin{bmatrix} V_x \\ V_y \\ P \end{bmatrix} = \begin{bmatrix} 0 \\ 0 \\ -|Q|q_t \end{bmatrix} \dots\dots\dots 3-22.$$

In equations 3-21 and 3-22 M_{xx} and M_{yy} are tridiagonal matrixes, defined as:

$$M_{xx} = \begin{bmatrix} T_x a_{1,1} + T_x a_{2,1} & T_x b_{2,1} & & & \\ T_x b_{2,1} & T_x a_{1,1} + T_x a_{2,1} & T_x c_{3,1} & & \\ & T_x c_{3,1} & T_x a_{2,1} + T_x a_{3,1} & - & \\ & & - & - & \\ & & & - & - \end{bmatrix} \dots\dots\dots 3-23$$

$$M_{yy} = \begin{bmatrix} T_y a_{1,1} + T_y a_{1,2} & \cdot & \cdot & T_y a_{1,2} \\ \cdot & T_y a_{2,1} + T_y a_{2,2} & \cdot & \cdot & T_y a_{2,2} \\ \cdot & & & & \\ T_y a_{1,2} & & T_y a_{3,1} + T_y a_{3,2} & & \\ & & & - & \\ & T_y a_{2,2} & & & - \end{bmatrix} \dots\dots\dots 3-24$$

where $Ta_x, Tb_x, Tc_x, Ta_x, Tb_x$ and Tc_x are transmissibility functions and expressed in the following form as (Sutopo et al., 2001):

$$T_x a = \frac{h^2 K_{yy;i,j}}{8(I(S) \det[K])_{i,j}} \dots\dots\dots 3-25$$

$$T_x b = \frac{3h^2 K_{yy;j,j}}{8(I(S) \det[K])_{i,j}} \dots\dots\dots 3-26$$

$$T_x c = \frac{h^2 K_{yy;i,j}}{4(I(S) \det[K])_{i,j}} \dots\dots\dots 3-27$$

$$T_y a = \frac{h^2 K_{xx;i,j}}{8(I(S) \det[K])_{i,j}} \dots\dots\dots 3-28$$

$$T_y b = \frac{3h^2 K_{xx;i,j}}{8(I(S) \det[K])_{i,j}} \dots\dots\dots 3-29$$

$$T_y c = \frac{h^2 K_{xx;i,j}}{4(I(S) \det[K])_{i,j}} \dots\dots\dots 3-30.$$

Matrices N_x and N_y contain 1 and -1 elements. M_{xy} and M_{yx} have four non-zero terms corresponding to pressures of the two adjacent blocks as stated in equations 3-14 and 3-15.

3.5 Solution to the system of linear equations

Equation 3-21 for full effective permeability tensor or equation 3-22 for diagonal effective permeability tensor can be solved easily by making use of standard methods. Equations 3-21 or 3-22 are similar to the method presented in chapter 2 and can be summarised as follows:

$$[A][X]=[B] \dots\dots\dots 3-31$$

where:

- [A] = coefficient matrix
- [X] = nodal displacement vector (unknown functions of p and v)
- [B] = load vector (boundary conditions and injection, production well information)

Equation 3-31 can be solved by commercial libraries such as the FORTRAN library. The size of stiffness matrix in the method can be directly calculated given the number of blocks in the reservoir. In equation 3-31 the coefficient matrix [A] contains the transmissibility values for blocks in x and y directions. The unknown vector [X] contains the velocity values at the edges of the grid blocks in x and y directions and pressure unknowns at the centre of the blocks. Applying the boundary conditions around the reservoir boundaries can result in equations equal to the number of unknowns. Source code to implement the above problem is written in FORTRAN. The flowchart of the method is presented in figure 3-4 which shows a schematic diagram for calculation of fluid flow in naturally fractured reservoirs using the CVMFE approach.

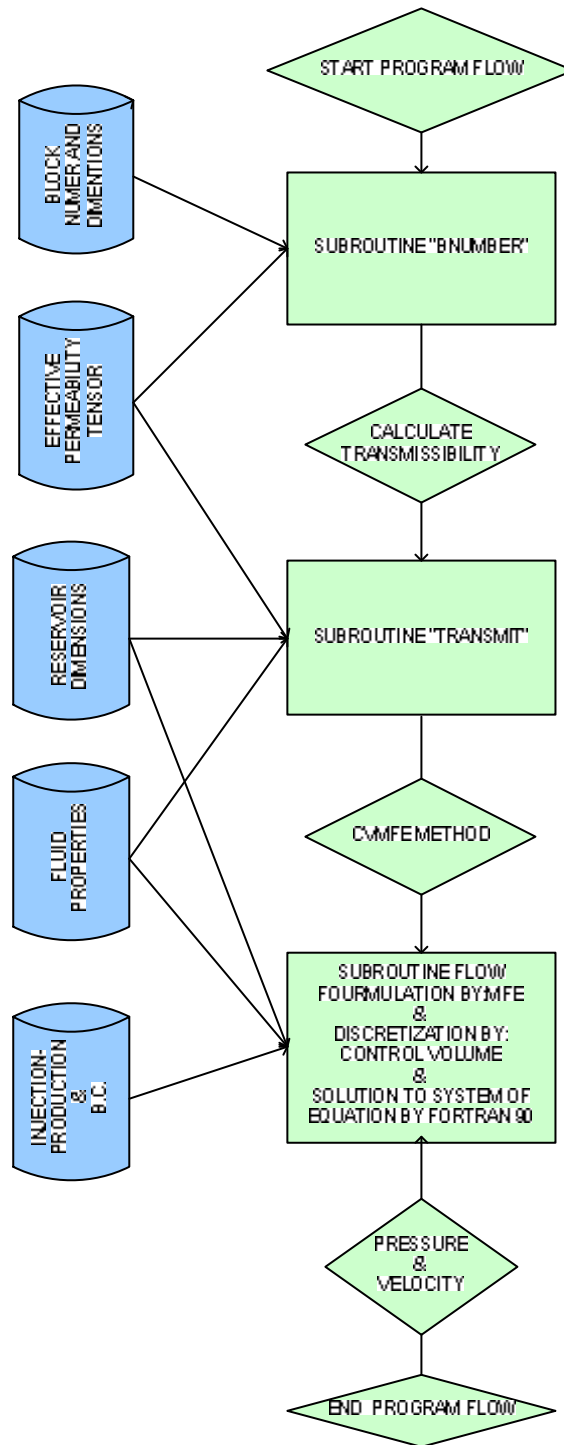


Figure 3-4: Flow chart of production simulation from naturally fractured reservoirs using code written in the FORTRAN using the CVMFE method described in this chapter.

3.6 Comparative analysis

In this section, two examples are presented to verify the production algorithm against data received from Sutopo et al., (2001) and the results from IMEX.

In the first example, a homogeneous region containing 16 square blocks with unit length and diagonal effective permeability equal to one in each grid block is considered. The fluid flow is considered single phase with unit viscosity. Two wells, one injector and one producer, with unit flux are located in grid blocks (1, 1) and (4, 4), respectively. Pressure in block (1, 1) is set to one and pressure and velocity vectors in other grid blocks are then calculated. Unknowns are shown in figure 3-5 which are the value of velocity vectors at the edges of grid block and pressure at the centre of each block.

The results of production estimation model for pressure and velocity distribution maps in this example are shown in figure 3-6 and figure 3-7. Figure 3-6 shows that in the homogeneous region pressure is distributed based on the distance from the injector and producer. It can be seen that the maximum pressure difference (0.2 Pa) is related to the contour map which is located in the centre and then decreases towards the injector or producer. From figure 3-7, it can be seen that there is a uniform velocity distribution in the region between the injector and producer. In this example, velocity vectors in y-direction are equal to the results in x-direction for each block and the average velocity in each grid block is the resulted vector between the velocities in x- and y-directions. The results of this study and the results received from Sutopo et al. (2001) are presented in table 3-1 and table 3-2. The comparative results between the results from both studies for pressure and the average velocity of each grid block are presented in figure 3-8. From the figure, it can be seen that the results from both studies match and the difference between the two is negligible. The similarity between the models is due to the fact that both models are following the same methodology in applying the CVMFEM (the mathematical formulation was introduced by Russell (1995) and Cai et al. (1997) as discussed in section 3.2). This study employs CVMFEM in simulation of fluid flow in NFRs with multiple length

fractures using the block effective permeability tensor. The study also applies the CVMFEM for the optimization of drilling program and well locations in NFRs.

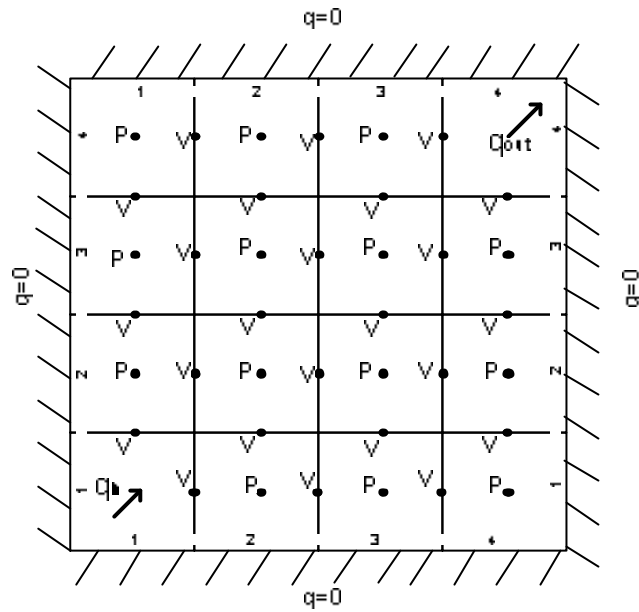


Figure 3-5: Schematic diagram of the example which shows boundary conditions and unknowns as well as the position of injector (q_{in}) and producer (q_{out}).

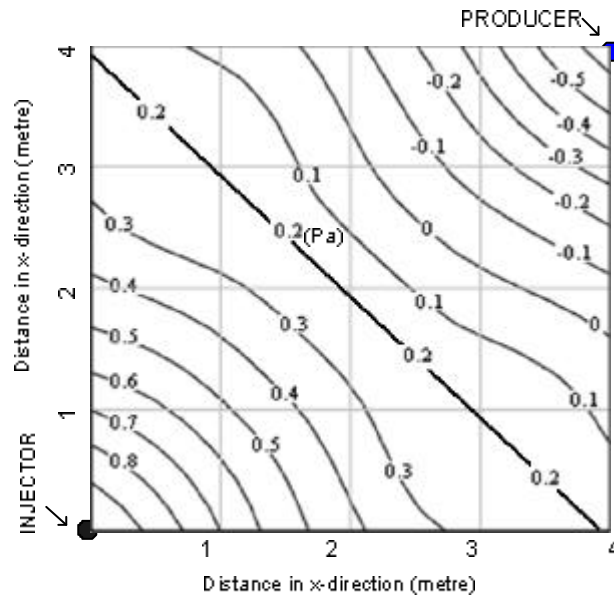


Figure 3-6: Pressure profile for homogeneous system.

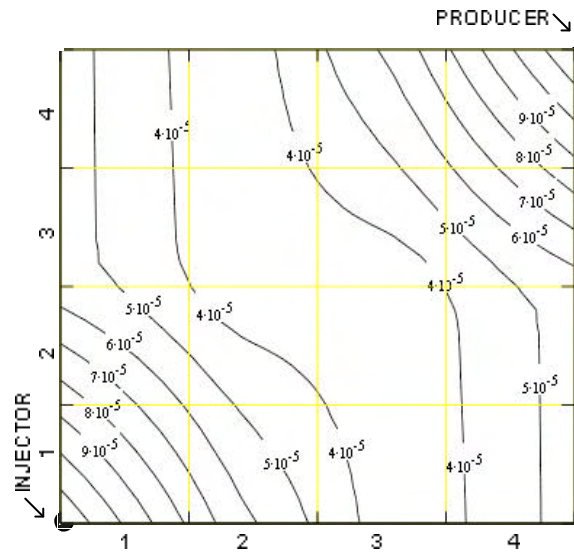


Figure 3-7: Velocity profile for a homogeneous system in (m/sec)

Block No.	Results calculated by this study		
	Pressure	Vx	Vy
(1,1)	1.0000	0.5000	0.5000
(1,2)	0.5909	0.2720	0.2720
(1,3)	0.3079	0.1326	0.1326
(1,4)	0.1746	0.0000	0.0000
(2,1)	0.5909	0.2279	0.2279
(2,2)	0.3915	0.2279	0.2279
(2,3)	0.1746	0.1397	0.1397
(2,4)	0.4136	0.0000	0.0000
(3,1)	0.3079	0.1397	0.1397
(3,2)	0.1746	0.2279	0.2279
(3,3)	-0.4228	0.2279	0.2279
(3,3)	-0.2418	0.0000	0.0000
(4,1)	0.1746	0.1323	0.1323
(4,2)	0.4136	0.2720	0.2720
(4,3)	-0.2417	0.5000	0.5000
(4,4)	-0.6507	0.0000	0.0000

Table 3-1: Results of the pressure and velocity in X- and Y-directions from this study.

Block No.	Results calculated by Sutopo et al. (2001)		
	Pressure	Vx	Vy
(1,1)	1.0000	0.5000	0.5000
(1,2)	0.5909	0.2720	0.2719
(1,3)	0.3078	0.1327	0.1326
(1,4)	0.1746	0.0000	0.0000
(2,1)	0.5909	0.2279	0.2278
(2,2)	0.3915	0.2279	0.2279
(2,3)	0.1746	0.1397	0.1397
(2,4)	0.4136	0.0000	0.0000
(3,1)	0.3079	0.1396	0.1397
(3,2)	0.1746	0.2279	0.2279
(3,3)	-0.4227	0.2279	0.2278
(3,3)	-0.2418	0.0000	0.0000
(4,1)	0.1745	0.1323	0.1324
(4,2)	0.4136	0.2720	0.2720
(4,3)	-0.2417	0.5000	0.5000
(4,4)	-0.6508	0.0000	0.0000

Table 3-2: Results of the pressure and velocity in X- and Y-directions from Sutopo et al. (2001).

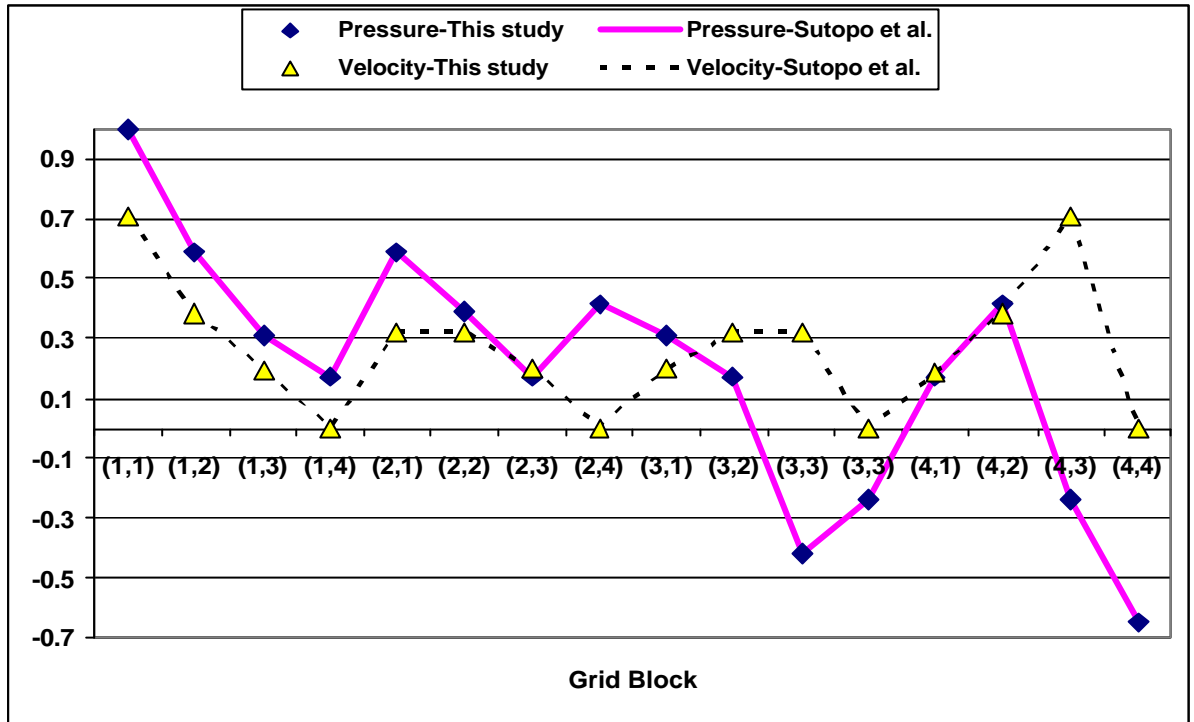


Figure 3-8: Comparison of the results of this study and the results calculated by Sutopo et al. (2001) for pressure and average velocity of the Grid blocks.

In the second example, a homogeneous region with dimension of 500 m × 500 m containing 121 blocks and diagonal effective permeability equal to 50 mD in each grid block is considered. Three wells, one injector in block (6, 6) with injection rate of 100,000 bbl/day and two producers in blocks (1, 1) and (11, 11) with producing rate of 50,000 bbl/day of single phase flow with viscosity of 0.35 cp are considered. Below is list of parameters used in this example:

Wellbore skin factor:	0
Well spacing:	352 m between injector and producer assuming one injector and two producers
Reservoir boundary conditions:	No flow (Neumann boundary condition)
Grid system	Array of 11*11 grids

Some other parameters have been varied within the following range in this study:

Matrix permeability:	50 mD
Well production rate:	50,000 bbl/day
Fluid viscosity:	0.35 cp
Thickness:	1.00 ft

The results of this study were compared against the results calculated by IMEX considering the above geometry and reservoir properties. IMEX mainly does two and three-phase flow simulation and requires relative permeability as input data. However, when oil water contact is set very low, such that the grid block is fully in water zone, this could be considered as the case for single-phase flow. It is also important for the IMEX program to reach the steady state condition as the CVMFEM simulates fluid flow in steady state condition. This requires assigning enough time for the IMEX program (i.e. 350 days in the above example) before comparing the results with CVMFEM.

Comparative results between this study and the results of IMEX program for the above example are presented in figures 3-8 and 3-9. From the figures, it can be seen that the results of pressure difference from this study are very close to the results of IMEX program with an accuracy of 99% (8337.38 against 8325.48). The slight difference between the results are due to the fact that CVMFEM is a block centred method and does not account for wellbore radius, well index and also it requires entering relative permeability data. The other difference might be from the fact that CVMFEM is a steady state program whereas IMEX is a time dependent program as discussed above. However, the above example shows that the fluid flow simulation program in this thesis produces very similar results to IMEX and that provides good confidence in simulation of fluid flow in NFRs. The main advantage of CVMFEM to IMEX is that it can simulate NFRs considering the effect of individual fractures (using the block effective permeability tensor).

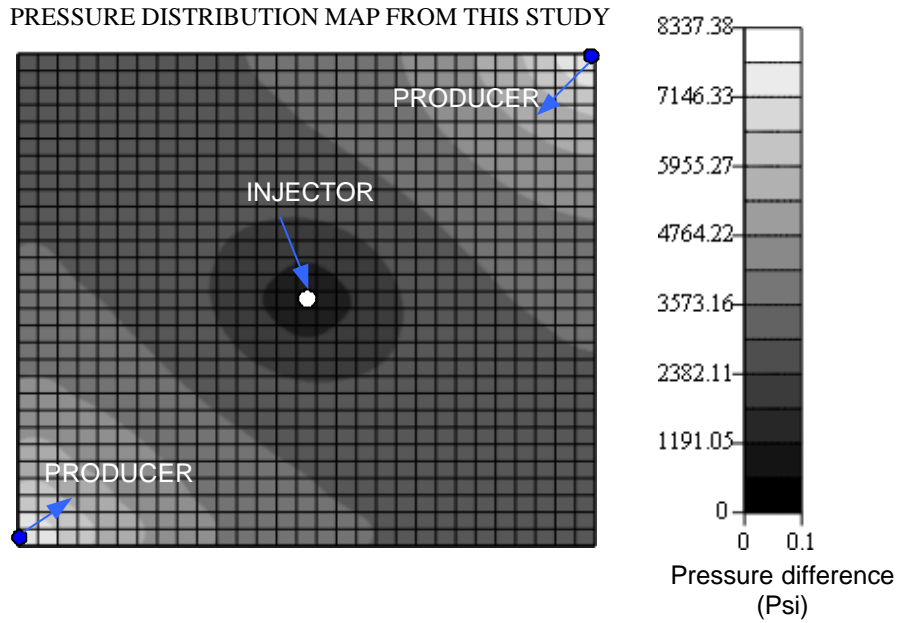


Figure 3-9: Pressure difference for a reservoir with unit thickness calculated in this study for injection rate of 100,000 bbl/day and block permeability of 50 mD.

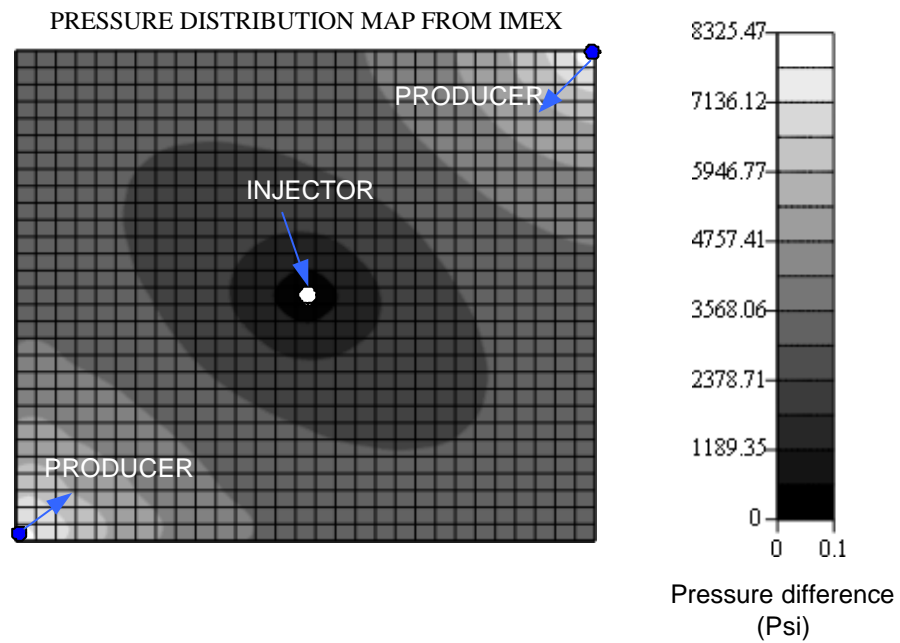


Figure 3-10: Pressure difference for a reservoir with unit thickness calculated by IMEX for injection rate of 100,000 bbl/day and block permeability of 50 mD.

3.7 Closure

In this chapter, the algorithm for simulation of fluid flow in NFRs by the use of the effective permeability tensor has been reviewed. The effective permeability simplifies the complexities caused by fractures and allows the detailed simulation of fluid flows in NFRs.

Fluid velocity in conventional simulators is calculated by indirect methods. Most simulators calculate the velocity by differentiation of the pressure in a system of second order equations. In contrast, a mixed finite element method calculates fluid velocities and pressure directly and simultaneously by use of a system of first order equations (Darcy's law and mass conservation's law). Unlike mixed finite difference method, the mixed finite element method is applicable to reservoirs with irregular geometry (with irregular grids). The control volume technique is a block-centred approach which calculates pressure in the centre of each grid block. It also accounts for the continuity of flux between the neighbouring blocks. Combination of control volume and mixed finite element methods discretises the fractured reservoir into a number of control volumes (blocks) and calculates the fluid pressure and velocity distributions throughout the reservoir.

The fluid pressure and velocity distributions obtained from this algorithm represent the effect of fracture systems on production from NFRs. They will be considered for further studies in hydraulic fracturing and targeting of the location of the proposed wells in the reservoir. Examples and sensitivity studies against the reservoir parameters as well as a case study are discussed in chapter 4.

CHAPTER 4

RESULTS AND CASE STUDY

CHAPTER 4

RESULTS AND CASE STUDY

4.1 Overview

In chapters 2 and 3, the algorithms to calculate the effective permeability and the production estimation models in NFR have been presented. This chapter is aimed to evaluate the algorithms and their applicability in simulation of NFRs with large number of fractures. First, the effective permeability calculation algorithm is evaluated through a number of examples and its sensitivity is discussed against changes in properties of rock, fluid and model parameters. Next, the performance of production model is evaluated through a number of examples and its sensitivity is tested against changes in reservoir and fluid properties. Finally, both algorithms are presented in a case study. The case study is aimed to show the applicability of the present models in the near real reservoirs with fracture network.

4.2 Evaluation of the permeability calculation algorithm

The effective permeability algorithm calculates local permeability for the effect of short fractures assuming that large pores belong to matrix. The calculated local permeability is then used by the program to calculate the full tensor effective permeability for medium size fractures which serve as source/sink in the matrix porous media. Long fractures are divided into a length equal to the blocks intersected by them and analysed in the same manner as medium size fractures.

In the examples presented throughout this chapter, it is assumed that short fractures have a length lower than 0.05 % of the grid block size and long fractures are those that have a length of higher than the grid block diagonal.

In the following, a number of examples are presented to show the performance of the effective permeability model in a region containing multi-scale fracture. A schematic of a region containing multi-scale fractures is presented in figure 4-1. Examples-1 to 3 present the calculation of the effective permeability of short, medium to long and interconnected fractures. Example-4 calculates the effective permeability tensor for whole region with multi scale length and different fracture systems.

4.2.1 Example-1: Short Fractures

A schematic of a region containing short fractures is presented in figure 4-2. The figure shows the discretisation using the boundary element method over the boundaries of the fractures and grid block. In this example, for calculation of local permeability from short fractures, numbers of boundary nodes at the boundaries of grid block and along the boundaries of fracture are set to 400 and 14, respectively.

Figure 4-3 shows a region measuring 60×60 feet and containing 316 short fractures with length of 0.5 (ft) for each fracture. The region is divided into 4×4 rectangular grids, matrix permeability is set at 0.1 (mD), fluid viscosity is set at 1 (cp) and fracture aperture is assumed to be equal to 0.001 (ft).

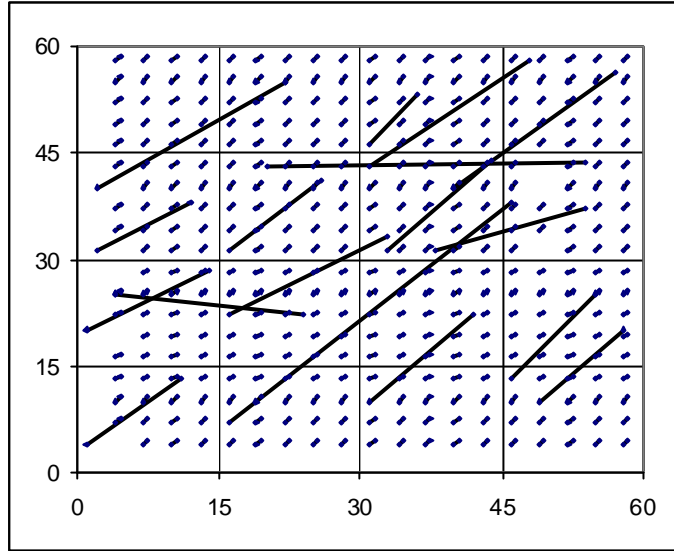


Figure 4-1: Region containing multiple fractures to calculate permeability and to investigate its sensitivity against different parameters.

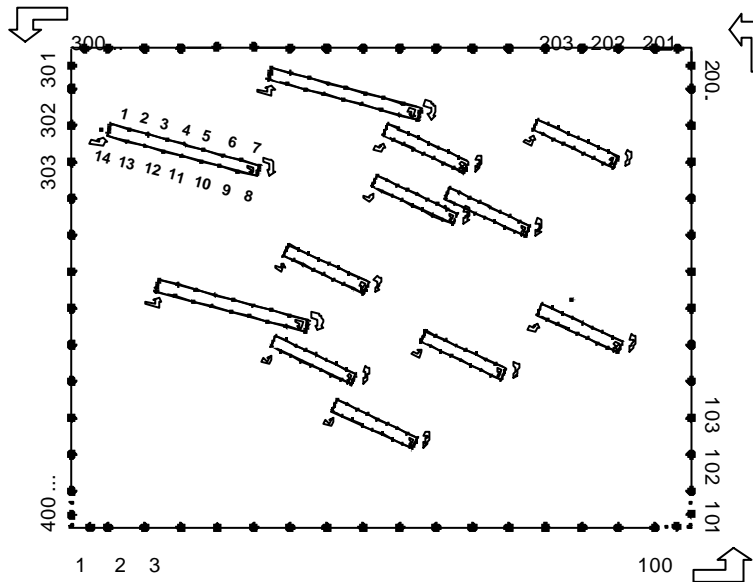


Figure 4-2: Schematic of a block containing short fractures presenting the number of boundary elements around the grid block and fractures.

First, interface boundary conditions are applied over the boundaries of short fractures assuming that they are large pores inside the matrix. Then, periodic boundary conditions are applied over the boundaries of grid block to calculate the permeability tensor for short fractures as: $\begin{bmatrix} K_{xx} & K_{xy} \\ K_{yx} & K_{yy} \end{bmatrix}$. Finally, diagonal elements of the tensor are averaged using the

equation: $K = \sqrt{\frac{1}{2}(K_{xx}^2 + K_{yy}^2)}$ to calculate the local permeability.

The results of local permeabilities are presented in table 4-1. From the table it can be seen that the effective permeabilities of block (2, 1) containing 20 fractures and block (2-2) with 25 fractures are 0.201 (mD) and 0.329 (mD), respectively. This means that the local permeability is highly influenced by the number of short fractures in the block. This effect can be seen by comparing the results of local permeability for other blocks in the region.

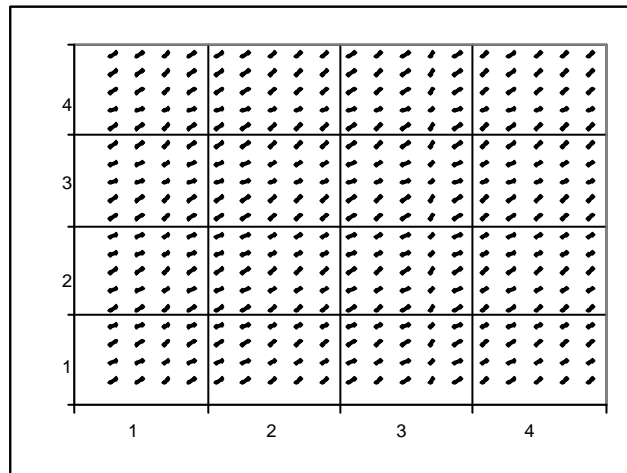


Figure 4-3: Short fractures in an array of 4×4 blocks in a region of $60(ft) \times 60(ft)$.

Block	(1-1)	(1-2)	(1-3)	(1-4)	(2-1)	(2-2)	(2-3)	(2-4)
Local effective permeability (mD)	0.150	0.237	0.237	0.237	0.201	0.329	0.329	0.329
Block	(3-1)	(3-2)	(3-3)	(3-4)	(4-1)	(4-2)	(4-3)	(4-4)
Local effective permeability (mD)	0.201	0.329	0.329	0.329	0.201	0.329	0.329	0.329

Table 4-1: Local permeability for shorts fractures shown in figure 4-3.

4.2.2 Example-2: Medium to long fractures

A schematic view of a region containing medium size fractures is presented in figure 4-4. The figure presents the boundary elements at the boundaries of grid block, fractures and the boundaries of Poisson's region. The latter is the part of matrix porous media around the fracture that is affected by fluid flow inside the fracture. In this example, region containing a number of medium size fractures has been considered and divided into array of 4×4 grids containing 16 fractures as shown in figure 4-5. Table 4-2 presents the coordinates of the fractures. Matrix permeability and fracture aperture are assumed to be constant and equal to 0.01 (mD) and 0.001 (ft), respectively. The boundary elements at boundary of the block, fracture and at the boundary of Poisson's region for medium size fractures are set at 400, 24 and 24, respectively.

In chapter 2, it was mentioned that the medium fractures act as sink/ source in the matrix. They were analysed by the use of Poisson's equation for the fractures and their surrounding matrix (Poisson's region). The effective permeability tensor in each grid block was calculated by applying the periodic boundary conditions and discretisation using the boundary element method. Based on this algorithm, the effective permeability tensors are calculated for this example and the results are presented in figure 4-6. The results are also shown in graphical form in figure 4-7 where tensors are replaced by ellipses. In each ellipse, the horizontal and vertical lines of the ellipse represent the x- and y-diagonal

elements. The direction of ellipse represents the off-diagonal terms of the effective permeability tensor. In fact, shape of the ellipse captures the directional variation of the horizontal and vertical permeability, in both magnitude and direction.

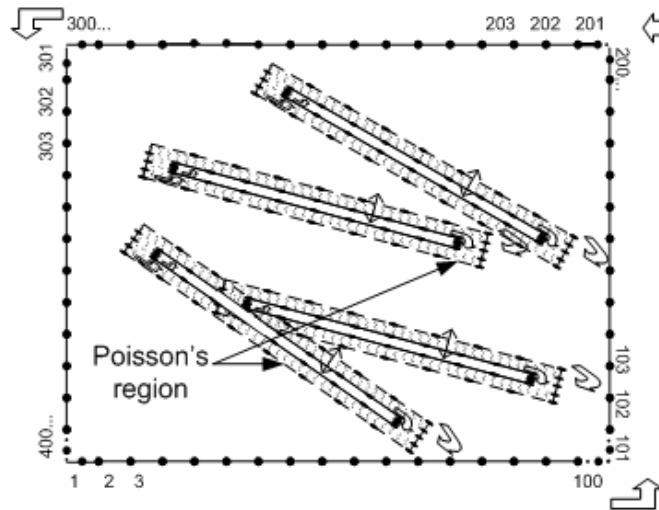


Figure 4-4: Schematic of the block containing medium size fractures to show the boundary elements around the grid block, fractures and Poisson's region.

Comparing the results in different blocks it is observed that as the number of fractures increases from one block to another block, the vertical and horizontal permeability of the grid block increases, which is to be expected. For example, the existence of fractures in block (1, 1) has resulted a horizontal permeability of 1.34 and vertical permeability of 1.27, compared to the block's initial permeability of 0.01 (mD). It is also shown that long fractures which are crossing a number of blocks, have significant effect on the effective permeability of blocks both in their value and their orientation, see blocks (2-1), (2-2), (3,2) and (3-3) for example.

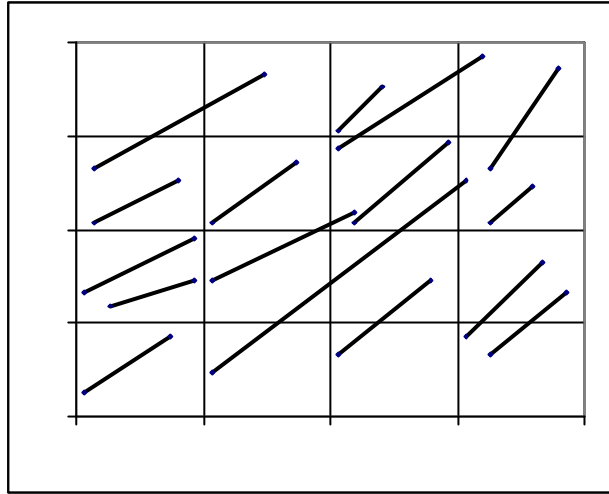


Figure 4-5: Arbitrary oriented fractures in an array of 4×4 blocks.

(x_1, y_1)	(x_2, y_2)	(x_1, y_1)	(x_2, y_2)
(1, 4)	(11,13)	(16,31)	(26,41)
(4, 18)	(14,22)	(31,10)	(42,22)
(1,20)	(14,28.5)	(31,46)	(36,53)
(2,31)	(12,38)	(31,43)	(48,58)
(2,40)	(22,55)	(33,31)	(44,44)
(16,7)	(46,38)	(49,40)	(57,56)
(16,22)	(33,33)	(49,31)	(54,37)
(46,13)	(55,25)	(49,10)	(58,20)

Table 4-2: Coordinates of the fractures (x (feet), y (feet)) related to figure 4-5.

4	$\begin{bmatrix} 1.12 & 0.09 \\ 0.09 & 1.07 \end{bmatrix}$	$\begin{bmatrix} 1.16 & 0.12 \\ 0.12 & 1.09 \end{bmatrix}$	$\begin{bmatrix} 1.99 & 0.49 \\ 0.49 & 1.49 \end{bmatrix}$	$\begin{bmatrix} 1.79 & 0.29 \\ 0.29 & 1.90 \end{bmatrix}$
3	$\begin{bmatrix} 1.49 & 0.19 \\ 0.19 & 2.34 \end{bmatrix}$	$\begin{bmatrix} 2.39 & 0.02 \\ 0.02 & 1.51 \end{bmatrix}$	$\begin{bmatrix} 2.89 & 0.21 \\ 0.21 & 3.60 \end{bmatrix}$	$\begin{bmatrix} 1.34 & 0.05 \\ 0.05 & 2.18 \end{bmatrix}$
2	$\begin{bmatrix} 1.99 & 0.34 \\ 0.34 & 1.6 \end{bmatrix}$	$\begin{bmatrix} 2.21 & 0.06 \\ 0.06 & 2.28 \end{bmatrix}$	$\begin{bmatrix} 1.74 & 0.09 \\ 0.09 & 2.68 \end{bmatrix}$	$\begin{bmatrix} 1.59 & 0.19 \\ 0.19 & 1.54 \end{bmatrix}$
1	$\begin{bmatrix} 1.34 & 0.31 \\ 0.31 & 1.27 \end{bmatrix}$	$\begin{bmatrix} 1.19 & 0.19 \\ 0.19 & 1.06 \end{bmatrix}$	$\begin{bmatrix} 1.06 & 0.07 \\ 0.07 & 1.07 \end{bmatrix}$	$\begin{bmatrix} 1.23 & 0.05 \\ 0.05 & 1.11 \end{bmatrix}$
	1	2	3	4

Figure 4-6: The results of the effective permeability tensors for fractures in figure 4-5.

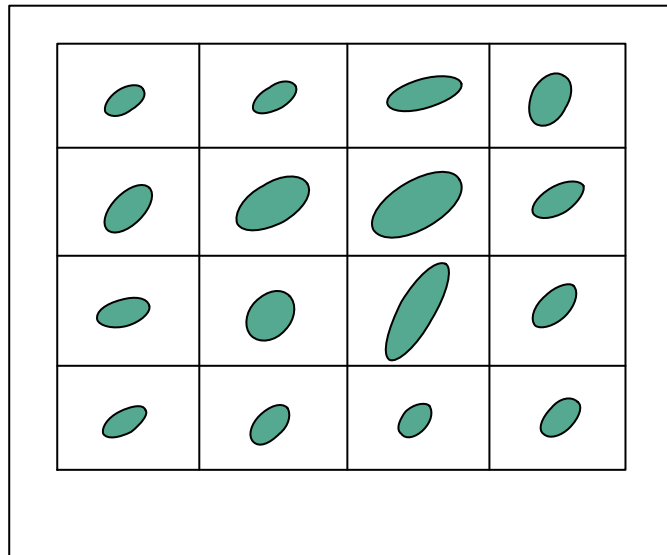


Figure 4-7: Elliptical form of the effective permeability tensors presented in figure 4-6.

4.2.3 Example-3: Interconnected fractures

Example-2 is modified with a number of interconnected fractures as shown in figure 4-8. Coordinates of fractures are presented in Table 4-3 with the matrix permeability and fracture aperture equal to 0.01 (mD) and 0.001 (ft), respectively. The calculated effective permeability tensors in each grid block are presented in figure 4-9 and figure 4-10 in tensor form and elliptical form. When the results in blocks with connected fractures are compared with the results in blocks without connected fractures it is observed that fracture connectivity has strong influence on block permeability. It is also seen that the number of connected fractures and their orientation have a strong effect on the effective permeability. This is obtained by comparing the results calculated in blocks (2-2), (2-3) and (3-3) in figure 4-10 with and without interconnected fractures.

Fracture connectivity has also effect on off-diagonal elements of the effective permeability tensor and defines the fluid path way in grid block, see off-diagonal elements of blocks (3, 2) and (3, 3) in figure 4-9. When the results of block (2, 1) for horizontal and vertical permeability (2.05 mD and 1.3 mD) are compared with that for block (2, 2) (2.53 mD and 2.81 mD), it can be seen that the fracture density also plays an important role in estimating the effective permeability of grid block.

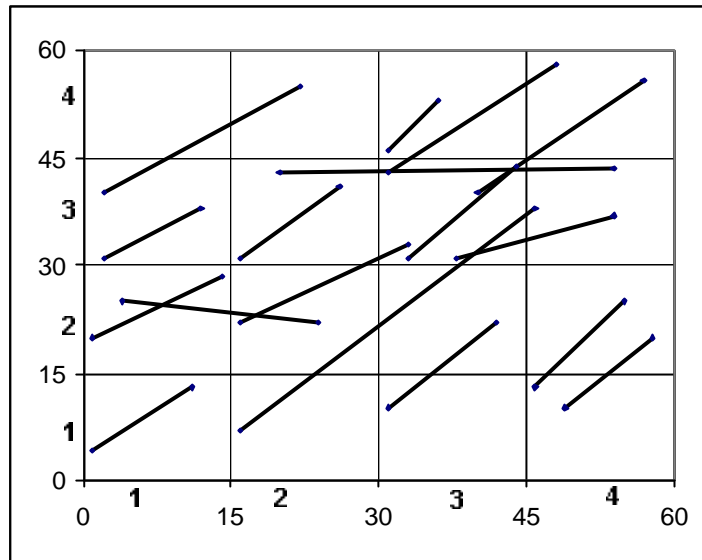


Figure 4-8: Arbitrary connected fractures in an array of 4×4 blocks

(x_1, y_1)	(x_2, y_2)	(x_1, y_1)	(x_2, y_2)
(1, 4)	(11,13)	(16,31)	(26,41)
(4, 25)	(24,22)	(20,43)	(54,43.5)
(1,20)	(14,28.5)	(31,10)	(42,22)
(2,31)	(12,38)	(31,46)	(36,53)
(2,40)	(22,55)	(31,43)	(48,58)
(16,7)	(46,38)	(33,31)	(44,44)
(16,22)	(33,33)	(40,40)	(57,56)
(46,13)	(55,25)	(38,31)	(54,37)

Table 4-3: Coordinates of the fractures (x (feet), y (feet)) related to figure 4-8.

4	$\begin{bmatrix} 1.12 & 0.09 \\ 0.09 & 1.07 \end{bmatrix}$	$\begin{bmatrix} 1.16 & 0.12 \\ 0.12 & 1.09 \end{bmatrix}$	$\begin{bmatrix} 1.99 & 0.49 \\ 0.49 & 1.49 \end{bmatrix}$	$\begin{bmatrix} 1.74 & 0.18 \\ 0.18 & 2.12 \end{bmatrix}$
3	$\begin{bmatrix} 1.49 & 0.19 \\ 0.19 & 2.34 \end{bmatrix}$	$\begin{bmatrix} 2.61 & 0.27 \\ 0.27 & 3.15 \end{bmatrix}$	$\begin{bmatrix} 4.48 & 0.47 \\ 0.47 & 5.14 \end{bmatrix}$	$\begin{bmatrix} 1.60 & 0.07 \\ 0.07 & 2.17 \end{bmatrix}$
2	$\begin{bmatrix} 2.05 & 0.34 \\ 0.34 & 1.3 \end{bmatrix}$	$\begin{bmatrix} 2.53 & 0.08 \\ 0.08 & 2.81 \end{bmatrix}$	$\begin{bmatrix} 1.74 & 0.09 \\ 0.09 & 2.68 \end{bmatrix}$	$\begin{bmatrix} 1.59 & 0.19 \\ 0.19 & 1.54 \end{bmatrix}$
1	$\begin{bmatrix} 1.34 & 0.31 \\ 0.31 & 1.27 \end{bmatrix}$	$\begin{bmatrix} 1.19 & 0.19 \\ 0.19 & 1.28 \end{bmatrix}$	$\begin{bmatrix} 1.06 & 0.07 \\ 0.07 & 1.07 \end{bmatrix}$	$\begin{bmatrix} 1.23 & 0.05 \\ 0.05 & 1.11 \end{bmatrix}$
	1	2	3	4

Figure 4-9: Calculated the effective permeability tensors for interconnected fractures related to the figure 4-8.

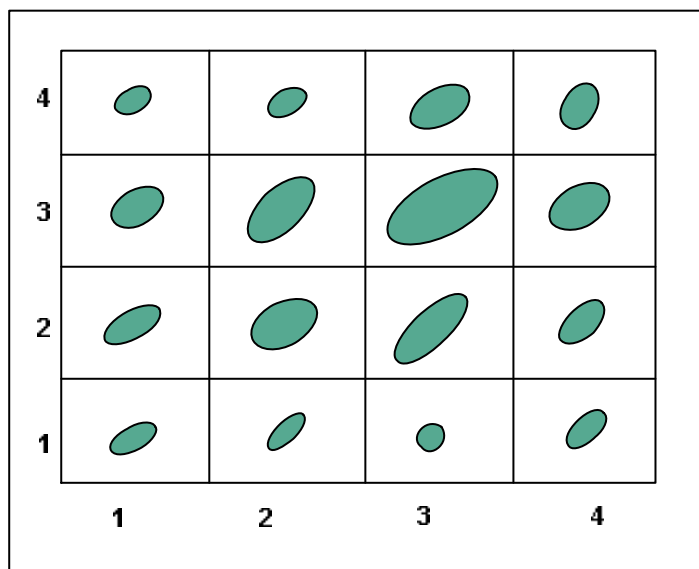


Figure 4-10: Results of the effective permeability tensors presented in figure 4-9.

4.2.4 Example-4: Multiple length fractures

In this example a fractured region is considered as combination of examples-1 to 3 containing all types of fractures, see figure 4-11. The region contains 320 fractures of different sizes and has similar properties for reservoir and model parameters with the previous examples. Calculation of the effective permeability involves the following steps: First, the local permeability is calculated for effect of short fractures as explained in example-1. Next, long fractures are divided into parts and treated in a same manner as medium size fractures. Finally, the model calculates the effective permeability tensor taking into account the effect of all types of fractures.

The results of effective permeabilities are presented in tensor form and elliptical from in figure 4-12 and figure 4-13, respectively. When the results of figure 4-12 are compared with the results for medium to long fractures in figure 4-9, it can be seen that the effective permeability in each block with presence of large number of short fractures is increased significantly. For instance, horizontal and vertical permeabilities of block (3,3) are 21.3 and 26.7 (mD) in figure 4-13 and 4.48 and 5.14 (mD) in figure 4-10, respectively. The results clearly show that the directional permeability which was originally contained in the fracture system is now contained in the effective permeability values.

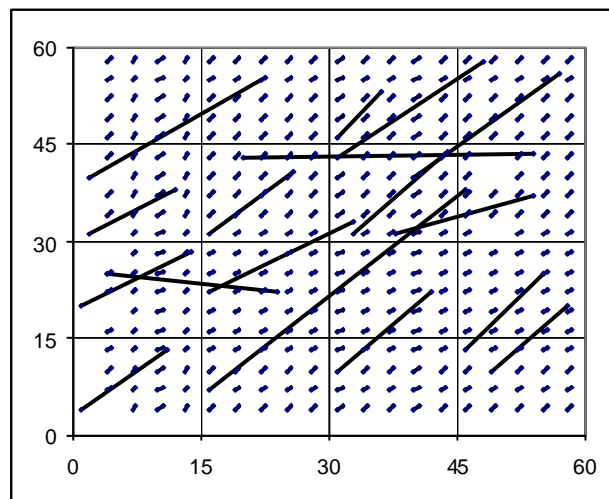


Figure 4-11: Multiple scale length fractures in calculation of effective permeability.

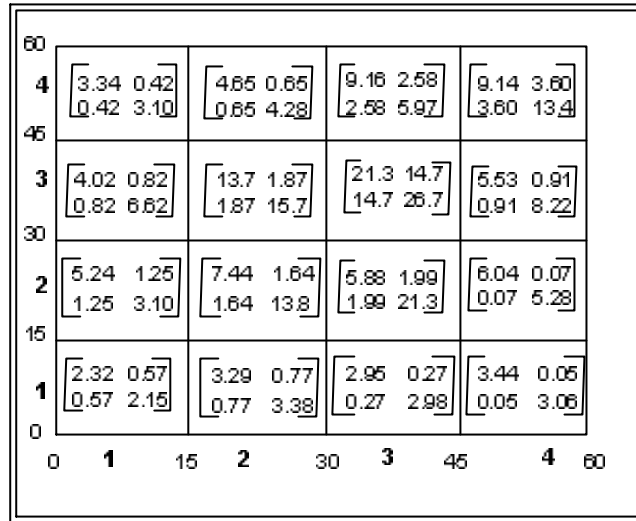


Figure 4-12: The calculated effective permeability tensors for fractures in figure 4-11.

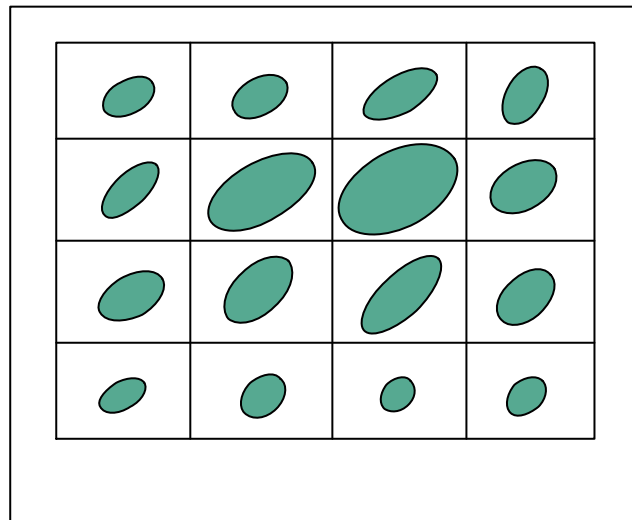


Figure 4-13: Elliptical presentation of the tensors in figure 4-12.

4.2.5 Sensitivity studies for the effective permeability algorithm

In this section, major properties of fractured porous media such as fracture aperture, matrix permeability, fracture orientation and density are investigated. This is followed by investigation of the effect of model parameters such as the number of elements at the boundaries of grid block, size of the Poisson's region and aspect ratio.

Effect of aperture

Based on the cubic law (equation 2-1), fracture aperture has a direct influence on fracture permeability. In this section, example-4 containing multiple-scale length fracture is used to investigate the effect of aperture. The effective permeability tensor is calculated when the matrix permeability is set at $K_m=0.1$ (mD) and fracture permeability is calculated at fracture aperture of: $H=0.001$, $H=0.002$, $H=0.005$, $H=0.01$ and $H=0.1$ (ft) in different cases. The calculated local permeabilities from short fractures are plotted in figure 4-14 against the block number. Local permeabilities are then used in the model to calculate the full tensor effective permeability in each grid block for medium and long fractures. To compare the results for different apertures, the diagonal terms of the effective permeability in x and y -directions, are presented in figure 4-15 and figure 4-16.

When compared, it can be seen that the changes in local permeabilities in all cases are consistent. This is true for results from short fractures and medium to long fractures presented in figure 4-14, figure 4-15 and figure 4-16. In each figure, the top curve is related to the highest aperture size of 0.1 (ft) and the bottom curve is related to the lowest aperture size of 0.001 (ft). When the results of local permeability for top curve are compared with those related to the bottom curve, it can be seen that by increasing the aperture from 0.001 (ft) to 0.1 (ft), the local permeability is slightly increased. It is also shown through the above figures that blocks 1, 5, 9 and 13 have the minimum permeability due to the paucity of fractures. Finally, it can be seen that the aperture (fracture permeability) has only slight effect on the total effective permeability of the block. This is because of the assumption that short fractures are considered as large pores in the matrix and do not act as sink/source inside the matrix.

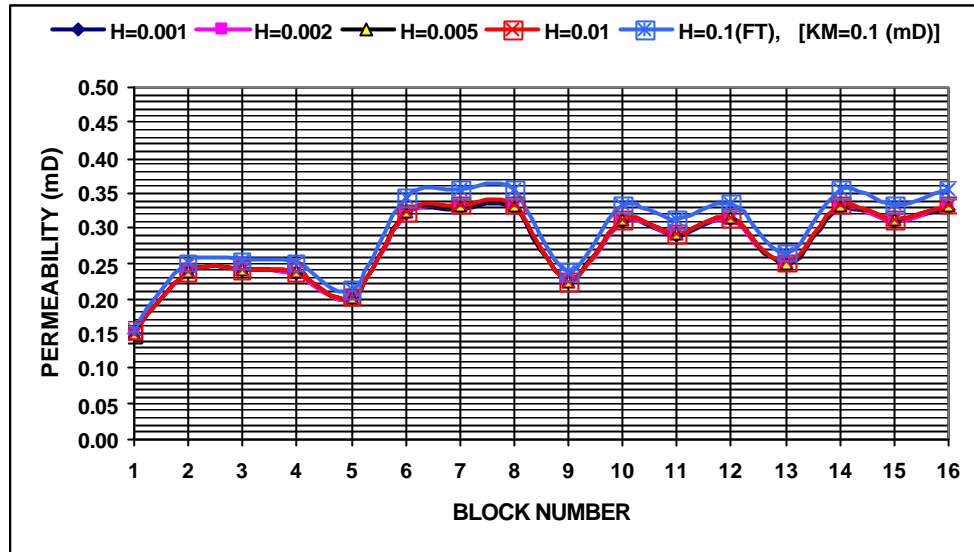


Figure 4-14: Sensitivity analysis for short fractures. Effect of aperture on local permeability assuming matrix permeability of $K_m=0.1$ (mD).

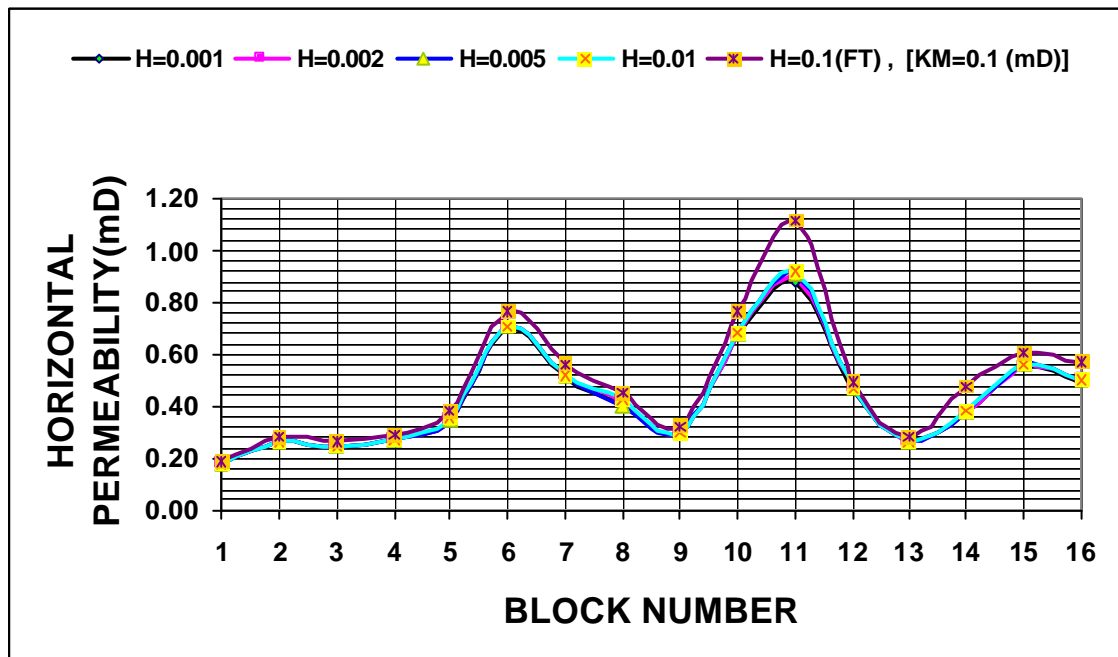


Figure 4-15: Normalised horizontal permeability values of the effective permeability tensor versus fracture aperture with matrix permeability of $K_m=0.1$ (mD).

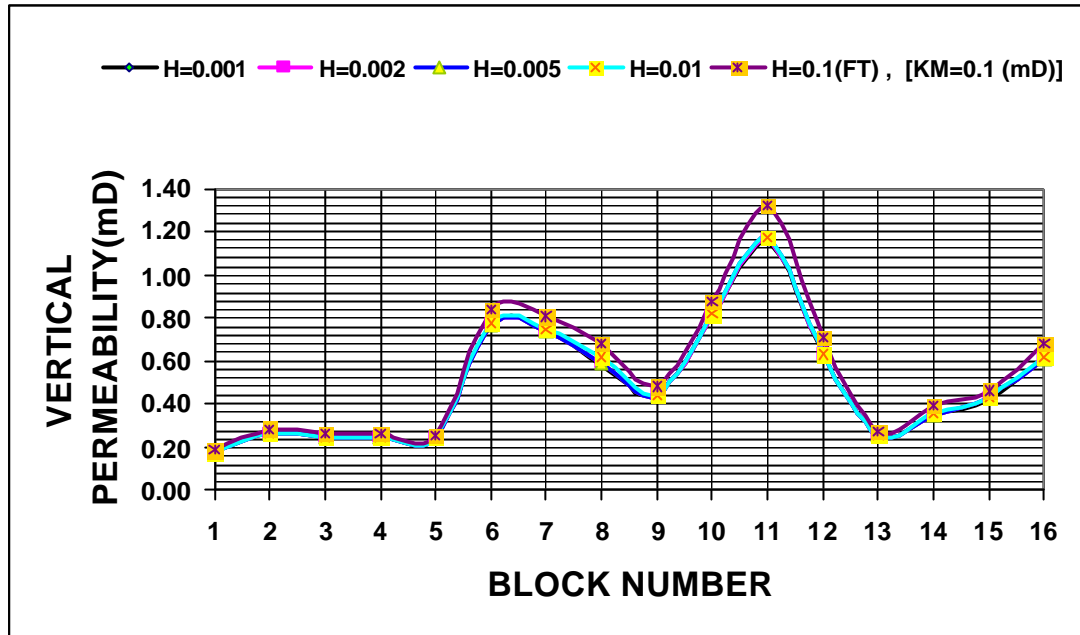


Figure 4-16: Normalized permeability in y-direction from the effective permeability tensor versus fracture aperture with matrix permeability $K_m=1$ (mD).

Effect of matrix permeability

As explained in example-4, matrix permeability is allowed to vary from $K_m=0.1$, $K_m=0.2$, $K_m=0.3$, $K_m=0.4$ and $K_m=0.5$ (mD) where the aperture is set at $H=0.001$ (ft). The calculated local matrix permeabilities from short fractures are presented in figure 4-17. Results of the block effective permeability tensors are also presented in figure 4-18 and figure 4-19 with their x - and y -components in each grid block.

When the results (figure 4-17, figure 4-18 and figure 4-19) for matrix permeability, are compared with the results (figure 4-14, figure 4-15 and figure 4-16) for different apertures, it can be seen that changes in matrix permeability has greater effect on effective permeability compared to fracture aperture. This is due to the fact that fluid flow in this study is mainly considered through the matrix porous media as discussed in chapter 2.

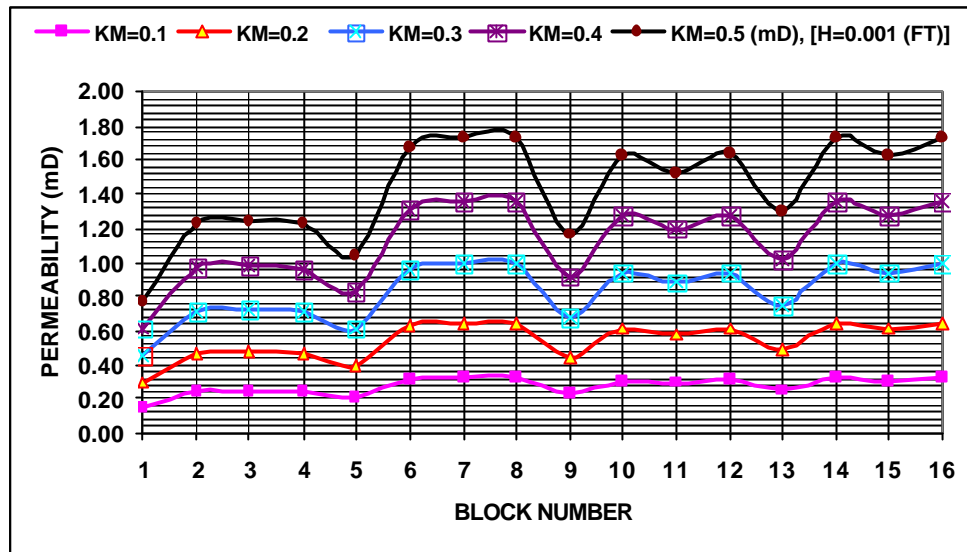


Figure 4-17: Sensitivity analysis for short fracture model. Effect of Matrix permeability on the block effective permeability with fracture aperture $H=0.001$ (ft).

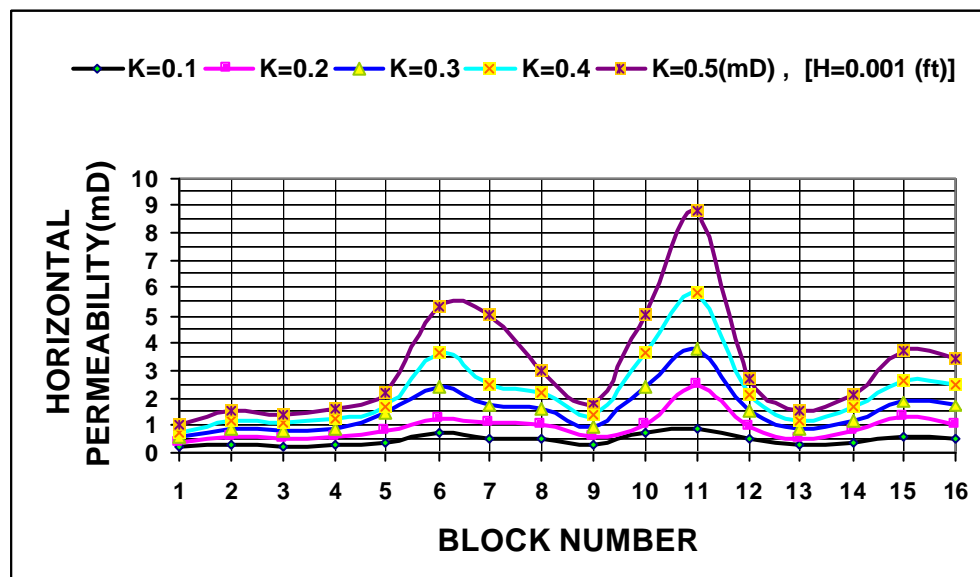


Figure 4-18: Normalized horizontal permeability values of the effective permeability tensor for different matrix permeability and constant fracture aperture $H=0.001$ (ft).

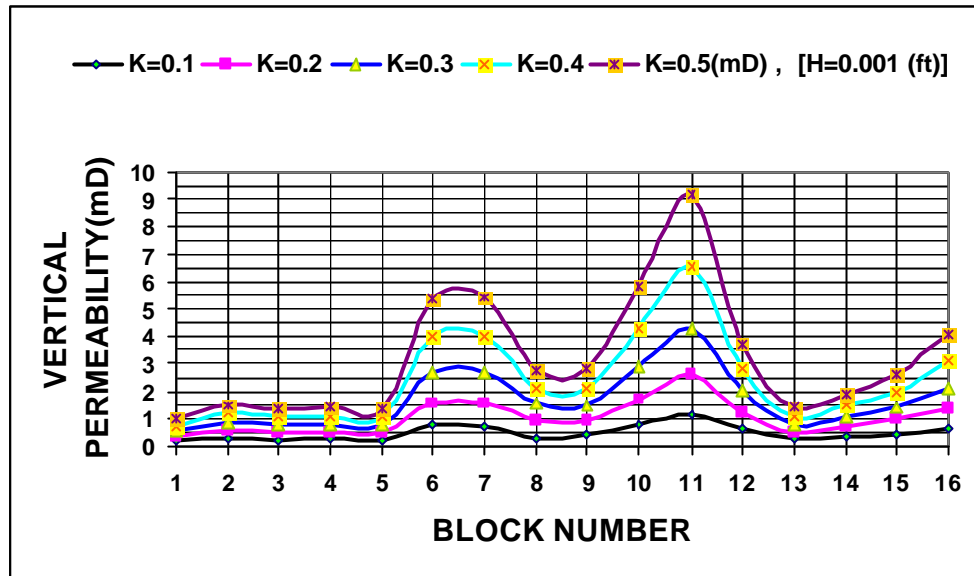


Figure 4-19: Normalized vertical permeability values of the effective permeability tensor for different matrix permeability and constant fracture aperture $H=0.001$ (ft).

Effect of Fracture density and orientation

In this section, the effect of fracture density and orientation on the block effective permeability tensor is investigated. For this purpose, a region containing 4 blocks with 13 arbitrary oriented fractures in an array of 2×2 with measuring $100(m) \times 100(m)$ is selected (see figure 4-20). Starting with an initial configuration of two fractures in a grid block, the fractures are rotated inside the block and successively added to show how the effective permeability tensor changes. Coordinates of fractures are presented in Table 4-4 and matrix permeability and fracture aperture are set at 1 (mD) and 0.001 (ft), respectively.

(x_1, y_1)	(x_2, y_2)	(x_1, y_1)	(x_2, y_2)
(10, 40)	(60,45)	(55,180)	(75,130)
(10, 30)	(60,35)	(110,140)	(160,145)
(185,30)	(165,80)	(110,130)	(160,135)
(155,80)	(175,30)	(185,110)	(165,180)
(10,140)	(60,145)	(155,190)	(175,110)
(10,130)	(60,135)	(110,120)	(160,125)
(85,130)	(65,180)		

Table 4-4: Coordinates of fractures in figure 4-20 to investigate the effect of fracture orientation and density.

The effective permeabilities for this array of grid blocks are depicted in figure 4-21 in tensor form and in figure 4-22 in elliptical form. In figure 4-22, the effective permeability for each block is represented by ellipses where the horizontal line of the ellipse represent the permeability in x-direction and the vertical line of ellipse represents the permeability in y-direction. These lines are shown by solid and dashed lines in horizontal and vertical directions, respectively. Permeability values ranges from 1.064 (mD) to 2.057 (mD) for this example. The off-diagonal elements are shown by direction of ellipses, which varies from -0.08 (mD) to 0.0181 (mD). When compared, it can be seen that as more fractures are added and the fracture density within the block is increased, the vertical permeability in block (1, 2) and horizontal permeability in block (2, 2) increases, as expected. When the results in blocks (1, 1) are compared with that of block (2, 1) in figure 4-22, it is clear that the model accounts for effect of fracture orientation in calculation of full tensor effective permeability. This is shown by increase in vertical permeability and decrease in horizontal permeability when blocks (1, 2) and (2, 2) are compared. The shape of ellipse in block (2, 2) shows the complexity of interaction even for just five fractures.

In summary, from the above examples, it can be concluded that the effective permeability algorithm is confidently sensitive to the reservoir properties and can handle the fractured reservoirs containing fractures of different sizes, density and aperture in a wide range of matrix permeability.

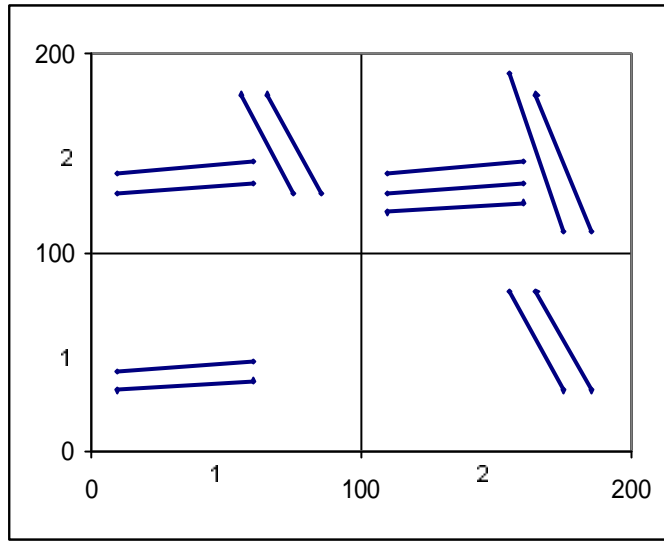


Figure 4-20: Arbitrary oriented fractures in a region containing 4 grid-blocks to show the effect of fracture density and orientation on the effective permeability tensor.

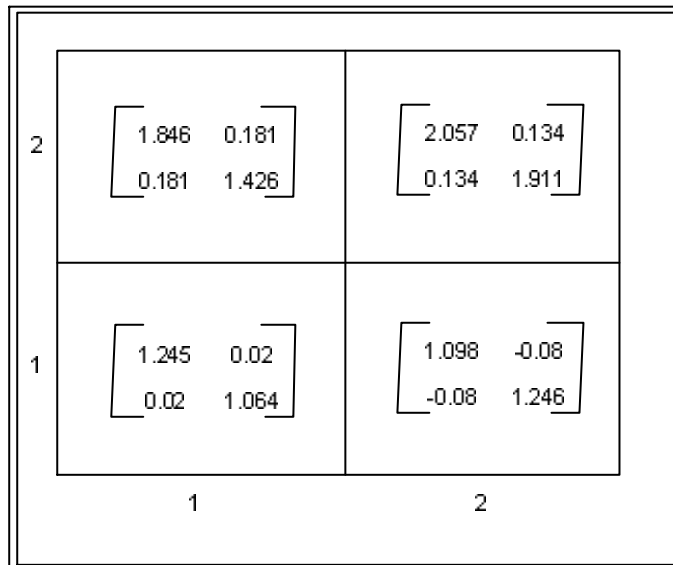


Figure 4-21: Effective permeability tensors calculated for fractures in figure 4-20 to show the effect of fracture density and orientation.

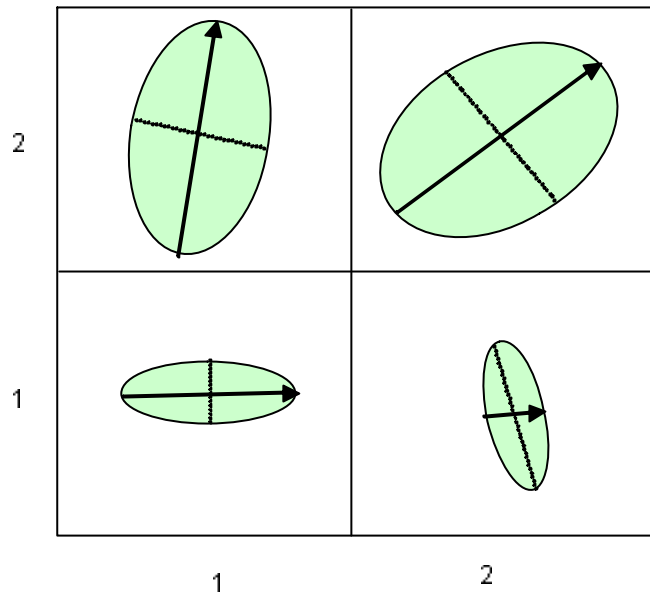


Figure 4-22: The elliptical presentation of the block effective permeability tensors related to figure 4-20 and figure 4-21.

Effect of the number of boundary elements

It was mentioned that the number of elements at the grid block boundary is set to 400 (100 elements per edge of the block), see figure 4-2. In this section, effect of changes of the boundary elements at the block boundaries is investigated through a square block containing a single fracture. The block has a length of 100 feet with matrix permeability equal to 1(mD) and the fracture has a length of 80(ft) and aperture of 0.01(ft) as depicted in figure 4-23. Effective permeability tensor was calculated for permeability of 1.525 (mD) in x-direction and 1.019(mD) in y-direction. Repeating the example with different number of elements (800, 1200, 1600 and 2000) at the grid block boundaries has resulted negligible changes in the effective permeability (less than one percentage). It should be also considered that the increase in number of elements results a higher computing time.

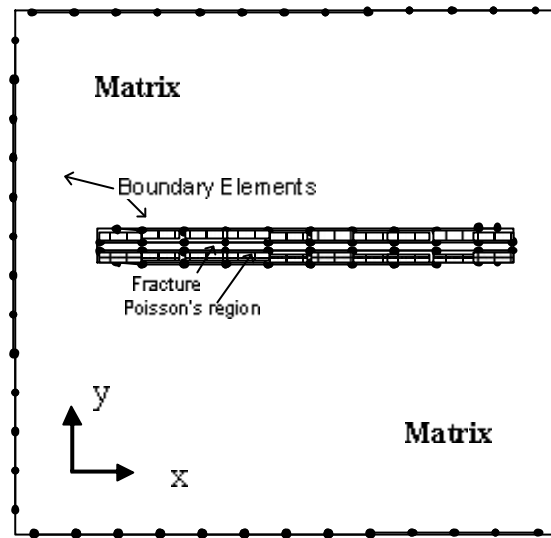


Figure 4-23: Square block with single fracture to investigate the sensitivity against the number of boundary elements along the boundaries of block, fracture and Poisson's region.

Effect of aspect ratio

Rasmussen et al. (1987) showed that aspect ratio, which is the ratio of distance between nodes at the boundary of fracture to the fracture's aperture, has a strong effect on the calculated effective permeability, see figure 4-24. They used linear types of boundary elements in discretisation part and showed that the error for aspect ratio of 10, 20 and 25 are 0.2%, 5.9% and 25.4%, respectively. They concluded that the aspect ratio should be less than 10 to have a reasonably accurate result. Given this, it is almost impossible to apply their method as it would require about 1000×1000 elements at each side of the surface of a fracture with 1(m) length and aperture of 10-100 μm in petroleum engineering problems.

In the present work, this issue is solved by the use of constant type of boundary elements at the boundaries of fractures and grid block. In fact, constant type of boundary elements requires normal vector at the midpoint of each element whereas the linear type elements

requires normal vectors at both ends of element. The later may create error at the corners where the direction of normal is not perpendicular to the element, see figure 4-25.

The previous example (figure 4-23) is considered and repeated with different aspect ratios to check the sensitivity of the program and the results are presented in figure 4-26. It can be seen that in all cases with different aspect ration, the program has produced very similar results with errors in order of less than 1 percent and the results from this model are insensitive to the aspect ratio. Additionally, based on the above discussion the new model can boast of increases in efficiency resulting from fewer elements and therefore fewer integral evaluations.

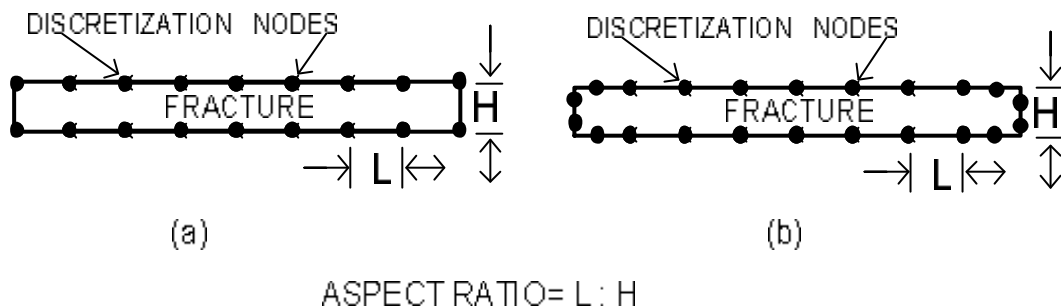


Figure 4-24: (a) Description of aspect ratio which is defined as the ratio of distance between nodes to the width of fracture without considering boundary elements along the fracture edges. (b) Discretisation method using constant elements in this thesis with a number of boundary elements at the edges of the fractures.

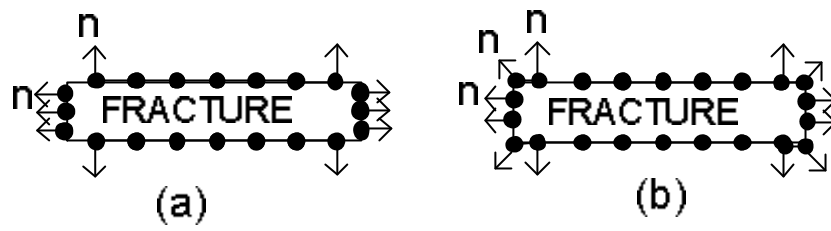


Figure 4-25: Normal to the boundary (a) constant type boundary elements (b) linear type boundary elements.

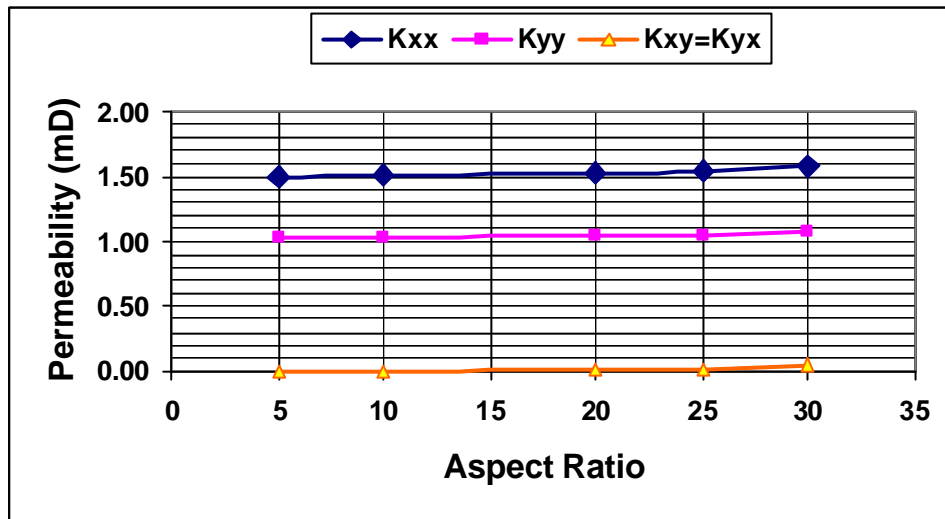


Figure 4-26 Effect of aspect ratio on diagonal and off-diagonal terms of the effective permeability tensor.

Effect of Poisson's region

The last parameter is Poisson's ratio which is the ratio of distances between the size of Poisson's region (H_1) to the distance between the nodes at the fracture boundary (L), as shown in figure 4-27.

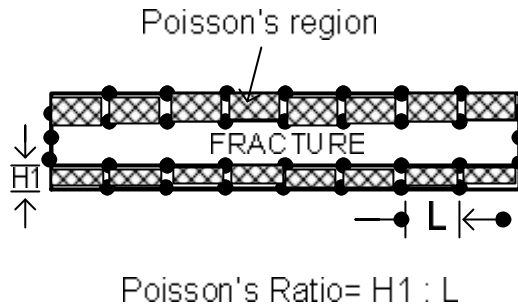


Figure 4-27: Definition of Poisson's ratio which is the proportion of distance between the nodes on Poisson's region from the corresponding nodes on the fracture boundary to the distance between nodes on the fracture boundary.

To test the sensitivity of the model against changes in Poisson's ratio, the example of figure 4-23 is repeated for Poisson's ratio of: 0.002 (1/500), 0.0025 (1/400), 0.0033 (1/300), 0.005 (1/200), 0.0067 (1/150) and 0.01 (1/100). The diagonal and off-diagonal elements of the effective permeability tensor for above cases are presented in figure 4-28. When compared, it can be seen that changes in Poisson's ratio do not cause significant differences in the results. Throughout the examples presented in this chapter, Poisson's ratio is set at 0.005 (1/200).

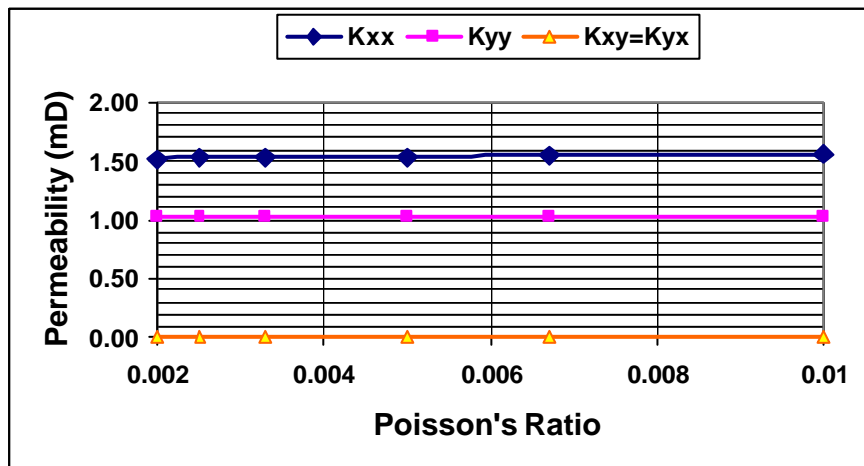


Figure 4-28: Effect of Poisson's ratio on diagonal and off-diagonal terms of effective permeability.

From the study of model parameters, it can be concluded that the model is insensitive to the changes in the number of boundary elements, aspect ratio, or size of the Poisson's region do not lead to a significant error in the calculated effective permeability tensors.

4.3 Evaluation of the production algorithm

In this section production method is used to simulate flow and pressure drop across the block through a number of examples. Effect of heterogeneity on fluid velocity and pressure is presented in example-1. This is followed by example-2, where the pressure and velocity in a fractured region with zero Neumann boundary conditions are investigated. Sensitivity of production estimation model was also studied by changing reservoir parameters and fluid properties.

Example-1: Region with no flow boundary

A region measuring $180(m) \times 225(m)$ and containing 180 blocks in an array of 12×15 is considered. Each block is assumed to have diagonal permeability tensor with elements of $K_{xx} = 50$ and $K_{yy} = 10$ in x and y directions, respectively (figure 4-29(a)). One injector and one producer are located at the centre of blocks (1, 1) and (12, 15) with flow rate set at 100 (bbl/day) and the fluid viscosity of 1 (cp). A schematic view of the model is presented in figure 4-29(b) which shows the zero Neumann boundary conditions at the reservoir boundaries.

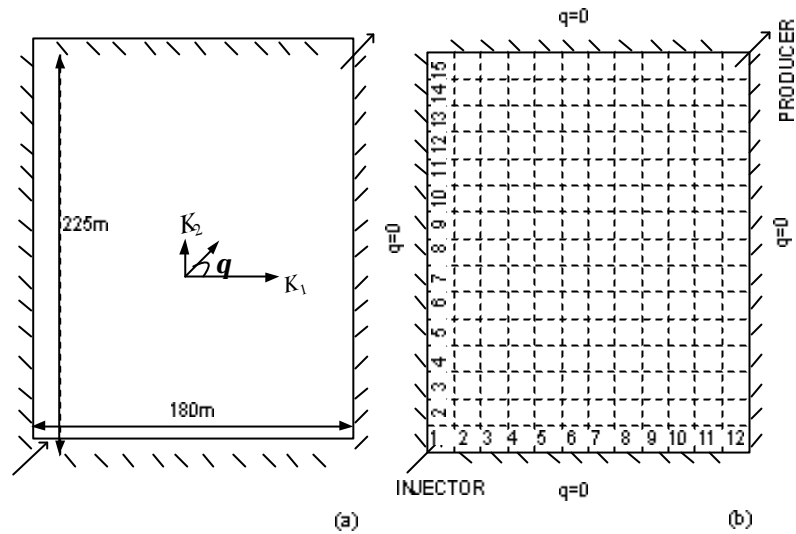


Figure 4-29: (a) Heterogeneous region in array of 12×15 blocks and Neumann boundary conditions. (b) no-flow Neumann boundary conditions.

The results of pressure distribution (psi) and the average velocity distribution (ft/s) are presented in figure 4-30 and figure 4-31. The average velocities are calculated from the velocity vectors in x and y directions in each grid block and presented in figure 4-31. When the results in figure 4-30 and figure 4-31 are compared, it can be seen that flow in the reservoir is generally dominated by permeability in x direction as expected. This effect is shown in figure 4-30 where the pressure lines are behaving as straight lines far from the injector and producer in horizontal direction. Such an effect can be seen in velocity distribution map in figure 4-31. The pressure difference between the injector and producer is equal to 404.5 (psi) in this example.

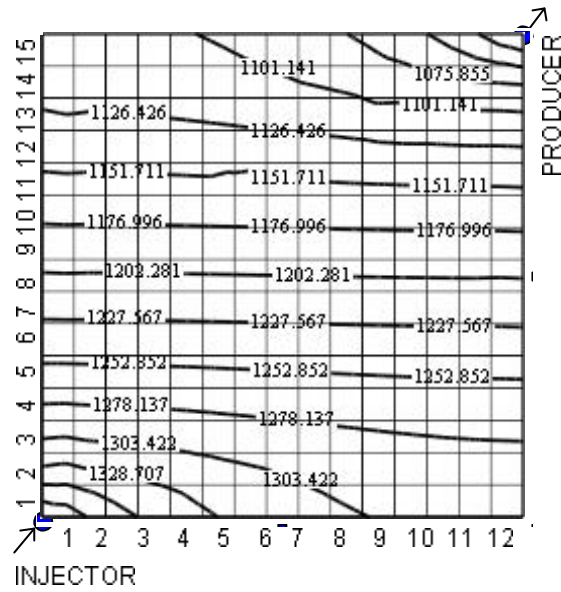


Figure 4-30: Pressure distribution in steady state conditions in homogeneous reservoir explained in example-1, (psi).

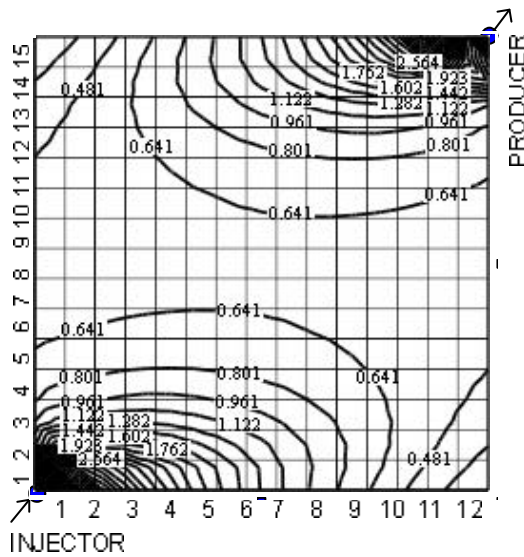


Figure 4-31: Velocity field distribution in steady state conditions in heterogeneous reservoir in example-1, (ft/sec).

Example-2: Fractured region with no-flow boundaries

In this example, the effect of heterogeneity caused by fractures on velocity distribution is investigated. A region measuring $144(m) \times 144(m)$ and containing a single fracture is divided into 144 blocks in an array of 12×12 . Matrix permeability is set at 1 (mD), fluid viscosity is assumed to be 1cp and fracture aperture is 0.01 (ft). The coordinates of start and end points of fracture are $(X_1=24, Y_1=24)$ and $(X_2=120, Y_2=120)$ meters as depicted in figure 4-32. One injector and one producer with the rate of 100(bbl/day) are located in blocks (1, 1) and (12, 12), respectively. The effective permeability tensors for blocks are first calculated using the effective permeability model and then used in the production model. Figure 4-32 shows the velocity distribution when the fracture is oriented at angle 45. It can be seen from the figure that the fracture controls the fluid flow in the region. Pressure difference between the injector and producer is calculated as 4790 (psi) by the model, see figure 4-33.

Effect of fracture orientation was also investigated by rotating the fracture at an angle of 135, 0 and 90 degrees inside the region. Results of the velocity and the pressure distribution maps are presented in figure 4-34 to figure 4-38. The results show that the model can account for the heterogeneity and that the flow in the reservoir is generally dominated by fracture as the main conduit in the reservoir. The figures show that the pressure difference between the injector and producer are equal to 5298(psi), 5257(psi) and 5258(psi) when the fracture has the angle of 135, 0 and 90 degrees, respectively (see, figure 4-35, figure 4-37 and figure 4-39). Comparing the result in figure 4-33 and figure 4-33 with the pressure difference 4790 (psi) and 5257 (psi), one can see the effect of fracture orientation on pressure distribution of the reservoir and that the production model is relatively sensitive to the fracture orientation.

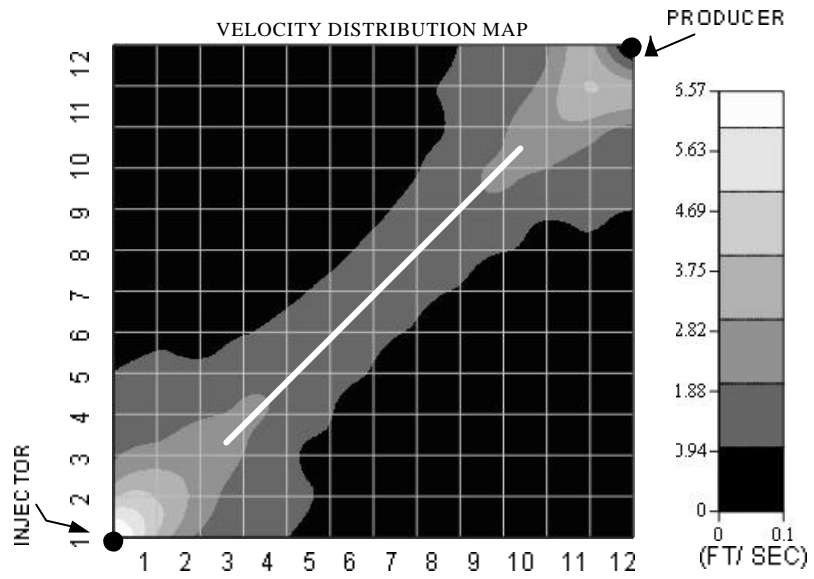


Figure 4-32: Velocity distribution in region with single fracture oriented at 45 degrees.

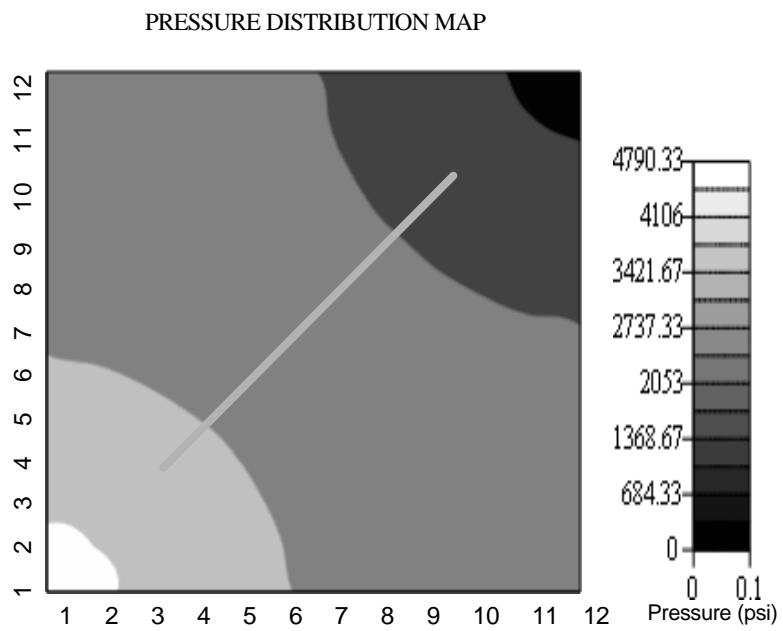


Figure 4-33: Pressure distribution in region with single fracture oriented at 45 degrees.

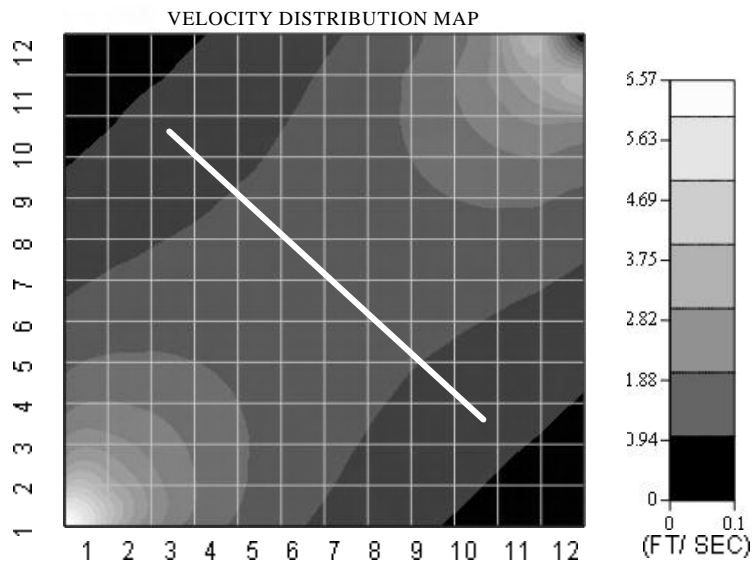


Figure 4-34: Velocity distribution in the region containing a single fracture with 135 degrees in.

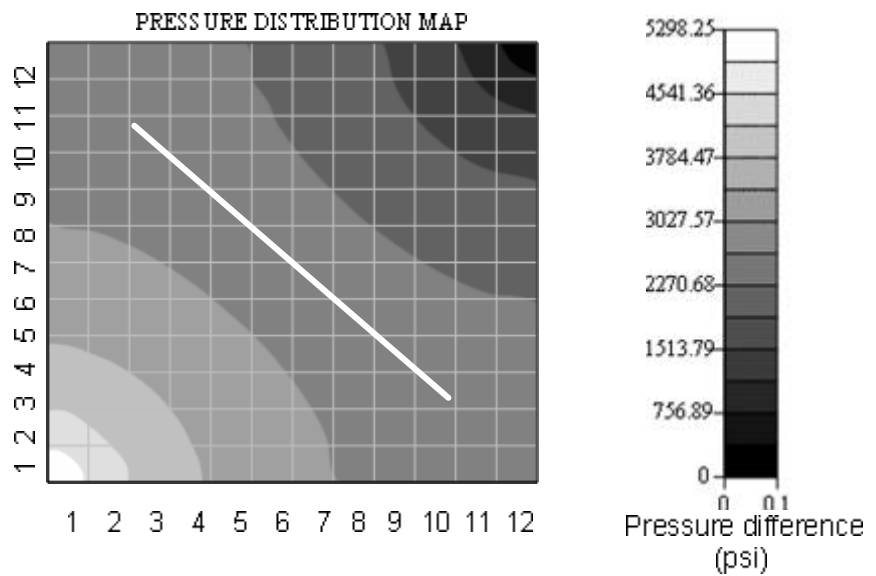


Figure 4-35: Pressure distribution in the region containing a single fracture with 135 degrees in.

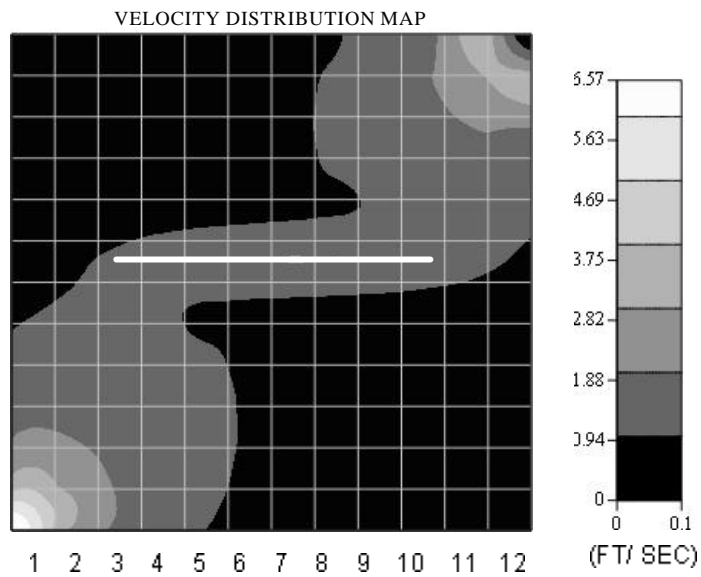


Figure 4-36: Velocity distribution in the region containing a horizontally distributed single fracture in.

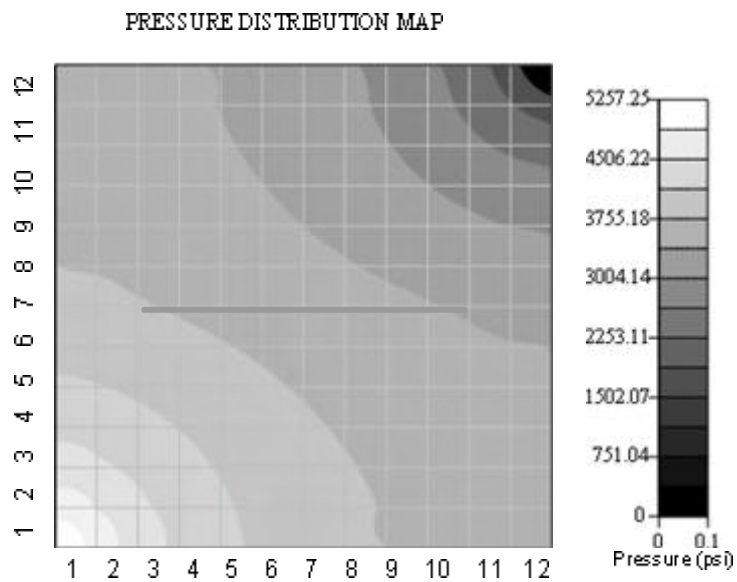


Figure 4-37: Pressure distribution in the region containing a horizontally distributed single fracture in.

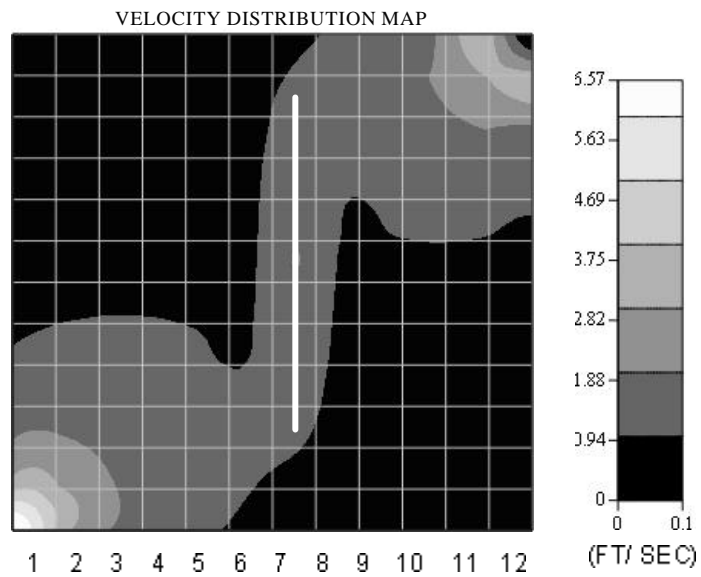


Figure 4-38: Velocity distribution in the region containing a single fracture oriented in y-direction.

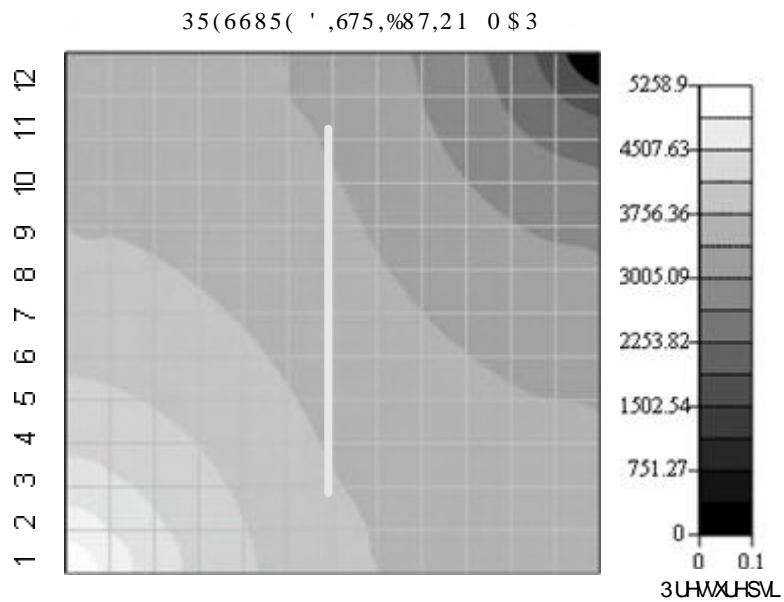


Figure 4-39: Pressure distribution in the region containing a single fracture oriented in y-direction.

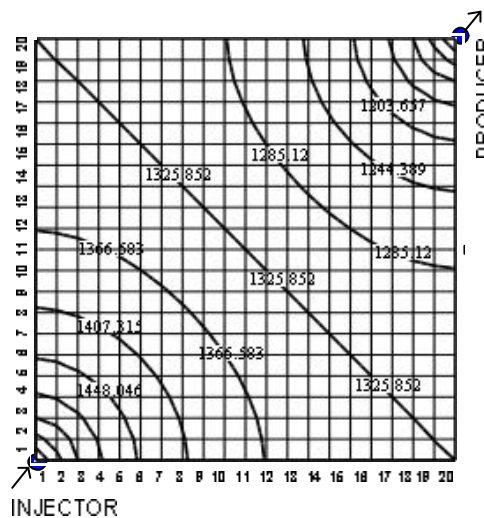
4.3.1 Sensitivity studies for production estimation algorithm

The production model is studied for its sensitivity against changes in fluid and reservoir parameters such as fluid viscosity, number and location of injection/ production wells and permeability of the reservoir.

Effect of fluid viscosity

The effect of viscosity is studied in a homogeneous region with Neumann boundary conditions and dimensions $240(m) \times 240(m)$ with 400 blocks in an array of 20×20 blocks. Region is assumed to have permeability of $K_{xx} = 10$ and $K_{yy} = 10$ in x and y -directions. Production model is applied to this example for fluid viscosity of 1(cp), 2(cp), 5(cp) and 10(cp). Results of pressure and velocity distribution are presented for viscosity values of 1(cp) and 10(cp) in

figure 4-40 to figure 4-42. The results of pressure difference for different fluid viscosities are presented in figure 4-43. When compared, it can be seen that there is a linear relation between changes in fluid viscosity and pressure difference in the reservoir, see figure 4-43. For instance, the figure shows that the pressure difference between the injector and producer has increased from 800 to 6500 psi when fluid viscosity changed from 1 to 10 cp.



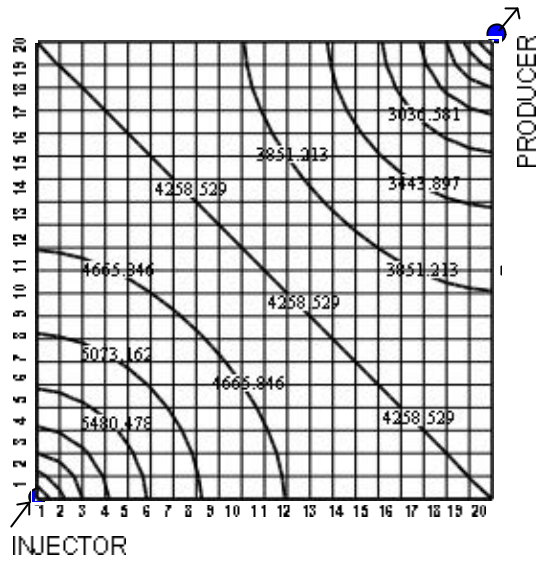


Figure 4-41: Pressure distribution for homogeneous reservoir with viscosity of 10(cp).

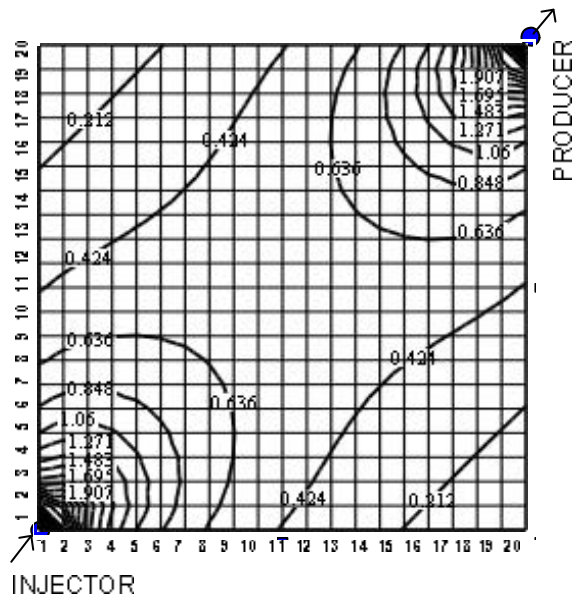


Figure 4-42: Velocity distribution for homogeneous reservoir in steady state condition

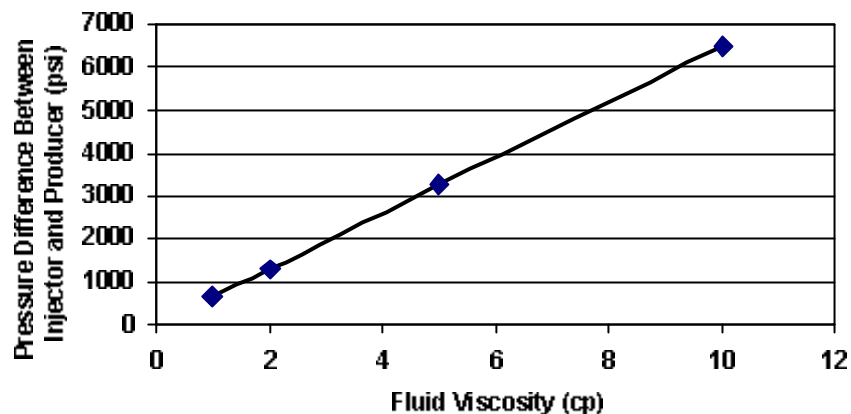


Figure 4-43: Sensitivity study for effect of fluid viscosity on pressure difference between the injector and producer.

Effect of number and location of injectors and producers

In this section two examples are provided to show how the model can be used to optimize the well locations and production from NFRs. For this purpose, a region is considered in an array of 30×30 blocks and dimension of $500\text{m} \times 500\text{m}$ with the formation thickness of 1m. Matrix permeability and fluid viscosity are assumed 50 mD and 1 cp, respectively.

In the first example, 1 producer with production rate of 100,000 bbl/day is located in the centre of the region (block (6,6)) and four injectors each with injection rates of 25,000 bbl/day are located in the corners with the well spacing of 352 m between the injectors and producer. The results of pressure distribution and velocity distribution are presented in figure 4-44. It can be seen that the pressure difference between the injectors and producer is 4288.6 psi per unit of reservoir thickness.

In the second example, the above region is revised such that the locations of injectors have been moved to grids (1, 3), (1, 14), (1, 16) and (1, 27). The producer is located in the centre of region similar to the above example. The results of pressure distribution are presented in figure 4-45. From the figure, it can be seen that pressure difference between the injectors and producer is 7108 psi per unit of reservoir thickness. When the results of this example are compared to the previous example with the same number of wells but different well locations (and pressure difference of 4288 psi.ft), it can be seen that well

location has a great effect on pressure loss and fluid flow in the reservoir. Comparing the results in figure 444 with the results presented in figure 4-45, it can be seen that the production from the reservoir can be optimize if a proper well location is considered.

From the numerical example and the sensitivity studies, it can be seen that the CVMFE method is an efficient method for simulation of production in a NFR and can handle a wide range of heterogeneity, different fluid properties and any number of injectors and producers in the simulation of NFRs.

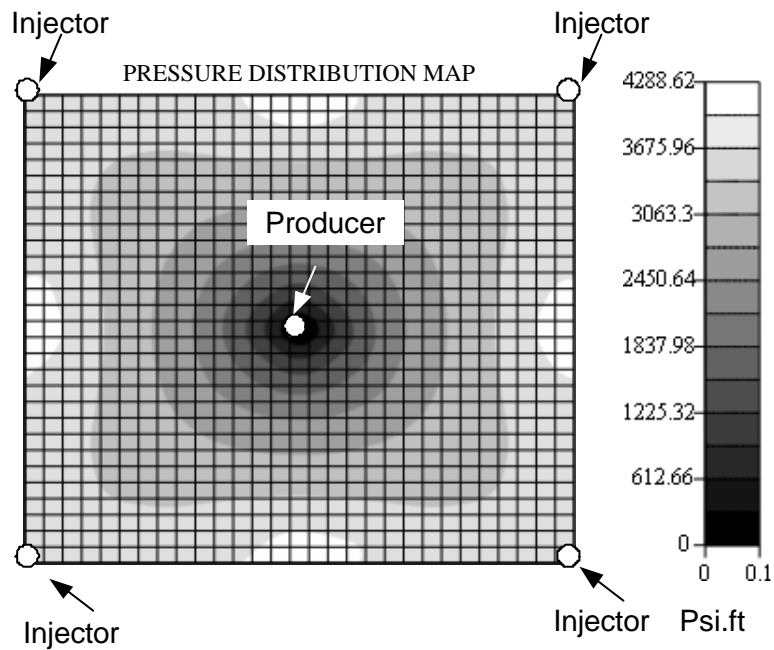


Figure 4-44: Pressure distribution in the homogeneous region with one producer located in the centre and four injectors located in the corners.

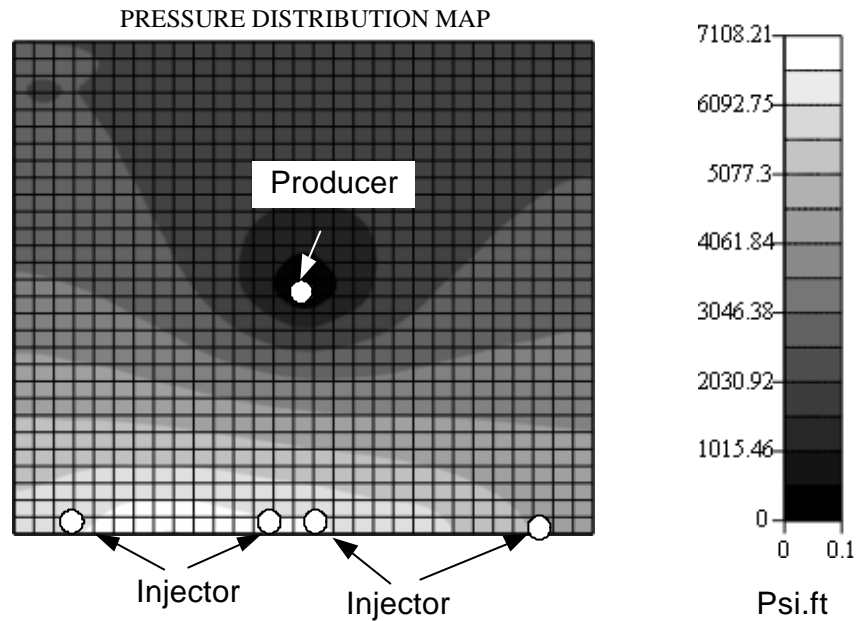


Figure 4-45: Pressure distribution in the homogeneous region with one producer in the centre and four injectors located in grids (1, 3), (1, 14), (1, 16) and (1, 27).

4.4 Case studies

In this section, two case studies have been simulated using the effective permeability and production algorithms to evaluate their performance in production optimization and fluid flow simulation in NFRs with high fracture density.

In the first case study, a geothermal reservoir located in South Australia has been selected to optimize the injection/ production rates and location of injectors and producers in the reservoir. In this project, two producers and one injector with 352 m well spacing have been proposed and the flow rates and wells locations were investigated in this study. The reservoir has the dimension of around 9000 m×9000m with the formation thickness around 500m.

A 2D cross section has been selected at depth of 2800 m the fractures are characterized for their geometry and directions using the work of Tran (2004). In calculation of effective permeability, the whole reservoir is discretised into 900 rectangular blocks in array of 30*30 in x and y directions with block size of 442 m. Fractures of different sizes are

considered and the effective permeability tensors are calculated assuming the matrix permeability equal to 200 (mD). The results of the effective permeability calculation are presented elliptical format in 2D for each grid block as shown in Figure 4-46. From the figure, it can be seen that the results of effective permeability differentiate the reservoir into a number of regions given the option to drill one of the areas with low, medium or high fracture density.

To investigate the effect of location on productivity, three different locations have been selected to run the production as shown in Figure 4-46. The production program has been run for those regions and the pressure difference between the injector and producers are calculated for an injection rate of 300 lit/sec and production rate of 150 lit/sec from each producer. The well trajectories for this case study are shown in Figure 4-48. The results of pressure distribution and velocity distributions for the area with high fracture density, low and without fractures are presented in Figure 4-48, Figure 4-49 and Figure 4-50. It can be seen that there is a considerable change in pressure difference (5955, 7166 and 8933 (psi.ft)) between injector and producers for cases with high, low and no fracture densities (the pressure difference is calculated per feet of the reservoir thickness). A sensitivity study has been carried out for this case study to calculate the pressure difference with the injection/ production rates for each of the above cases. Results of the simulation for matrix permeability equal to 200 mD are summarized in Table 4-5. Comparison of the results in this table for different injection rates and fracture density shows that fracture density is one of the key parameters in the simulation of fluid flow in the reservoir. It is shown that the directional permeability which was originally contained in the fracture system is now contained in the results of effective permeability model (Figure 4-46) and production simulation model (Table 4-5) for the homogenized grid block.

From the above case studies, it can be seen that the program can be used in production optimization and optimizing the well location, injection/production rates to achieve the maximum production with less pressure loss between the wells.

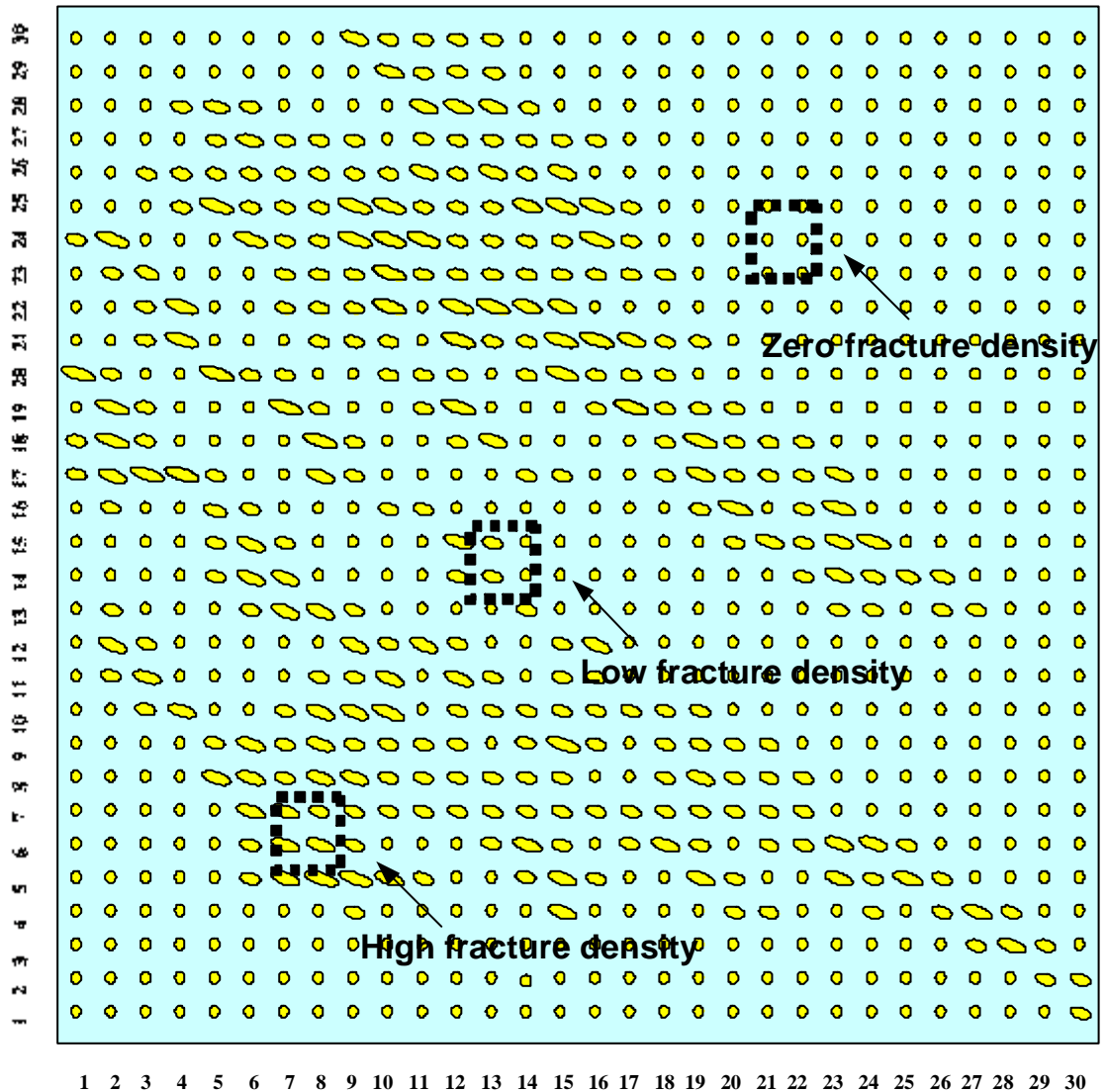


Figure 4-46: Elliptical presentation of the effective permeability tensors calculated for the first case study. Each ellipse shows the permeability values in x- and y-directions and the orientation of fractures in each grid-block.

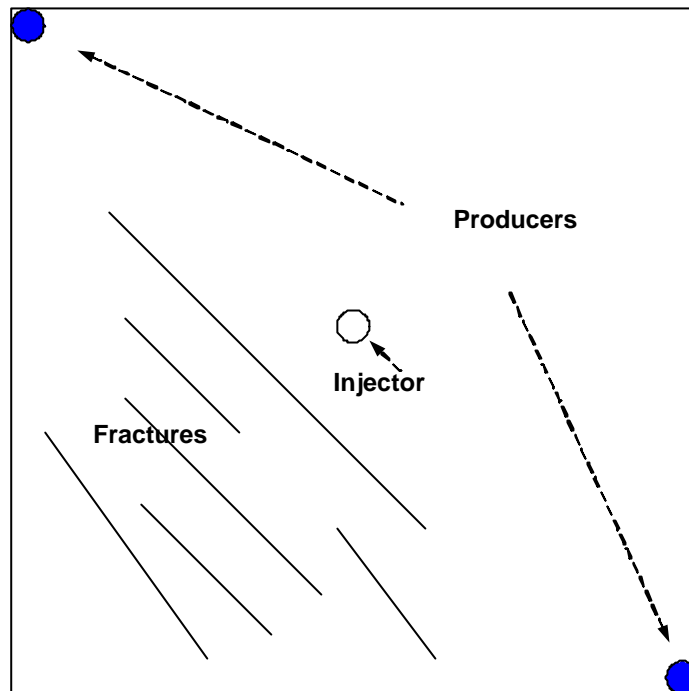


Figure 4-47: Well trajectories in case study 1.

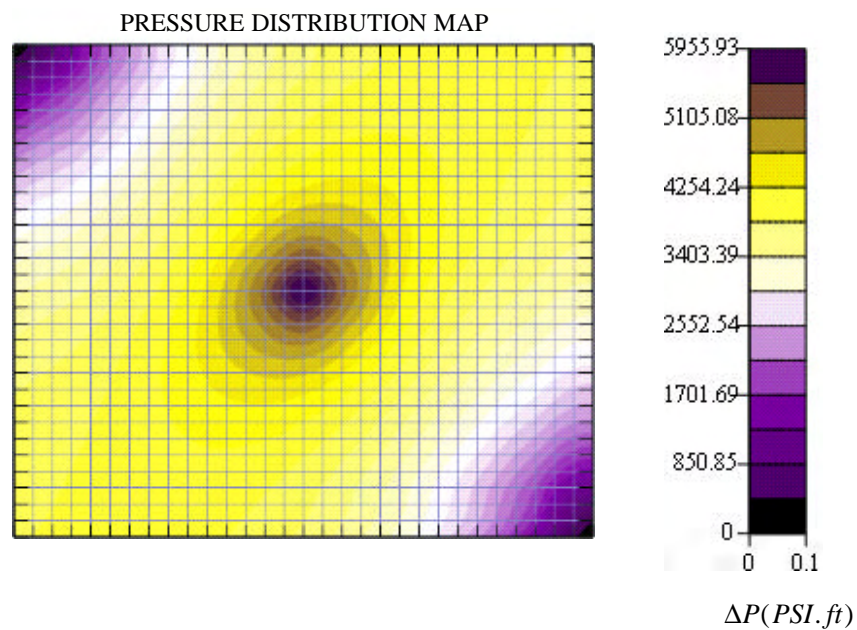


Figure 4-48: Pressure distribution for the high fracture density in case study 1.

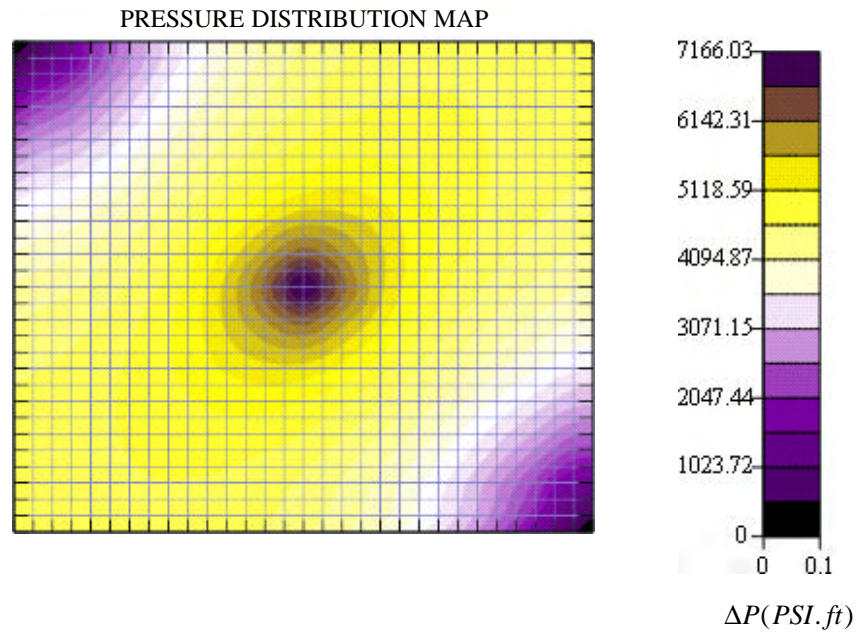


Figure 4-49: Pressure distribution for the low fracture density in case study 1.

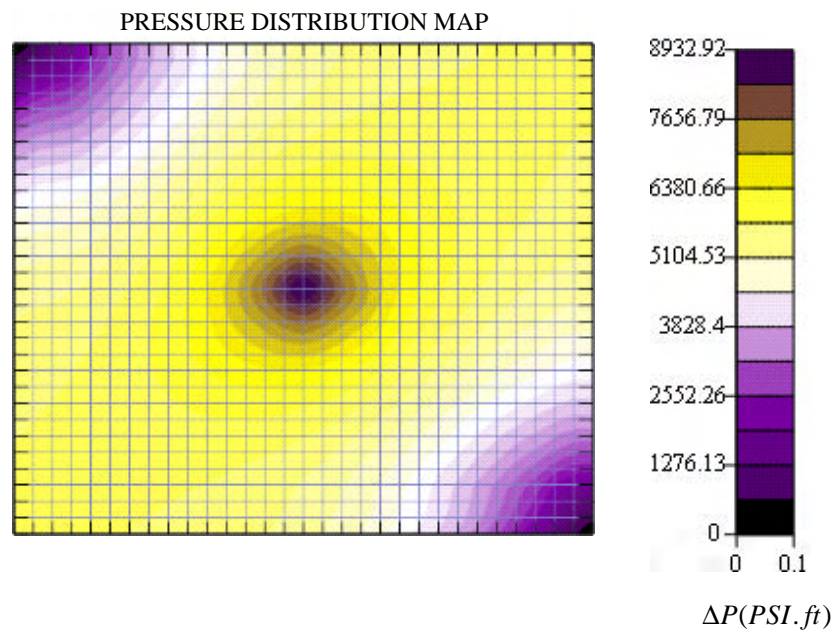


Figure 4-50: Pressure distribution for the region without fracture in case study 1.

Table 4-5: Results of the simulation for matrix permeability equal to 200 mD with different injection rate and fracture density.

Injection Rate (lit/s)	Fracture Density	Pressure difference (Psi.ft)
400	Without fracture	11900
400	Low	9554
400	High	7941
300	Without fracture	8933
300	Low	7166
300	High	5955
200	Without fracture	5956
200	Low	4777
200	High	3970
150	Without fracture	4666
150	Low	3583
150	High	2978
100	Without fracture	2978
100	Low	2389
100	High	1985

In the second case study, the effective permeability and production simulation algorithms are applied in a near real naturally fractured reservoir. In this case, the fault map of Otsego County and surrounding areas (New York, USA) is examined (figure 4-51) [<http://www.nywaterfind.com>]. The fault map has been recently characterised for properties of individual fractures by Tran (2004).

4.4.1 Otsego fault map

Otsego region has dimension of 100km (east west) by 70km (north south). This fault system covers parts of four counties of Otsego, Chenango, Delaware and Schoharie in New York, USA. A part of this fractured reservoir was characterized by Tran (2004). In this case study, fluid viscosity, matrix permeability and fracture aperture were set at 1(cp), 0.5(mD) and 0.01(ft), respectively. Otsego contains fractures of different sizes, orientations and is a good example to use to understand the performance of NFRs.

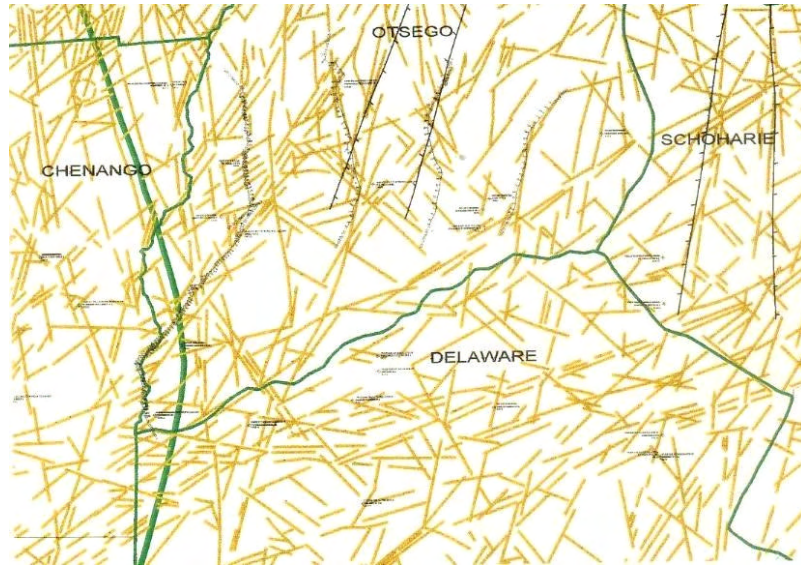


Figure 4-51: Fault map of Otsego County and the surrounding areas (New York, USA)[<http://www.nywaterfind.com/fractureotsego.JPG>]



Figure 4-52: Fault map of Otsego County and the surrounding areas (New York, USA)

In this case study, a block of Otsego is examined measuring $830(m) \times 830(m)$ with 442 fractures with high fracture density and a large number of interconnected fractures. The purpose is, thus, to simulate single phase incompressible fluid flow in a naturally fractured

reservoir with large number of fractures of different scales. Fracture lines are portrayed by x-y coordinates of their start and end points by section B1 in Appendix-B with a high density of fracture in each grid block. For the purpose of this study, the region is divided into an array of 12×12 blocks.

Similar to the previous examples, the local permeability values from short fractures are calculated using the effective permeability algorithm. The calculated local permeabilities are then used to calculate the effective permeability tensor for medium to long fractures in each grid block. The results of effective permeability tensors are presented by section B2 in Appendix-B. The results are also shown by ellipses in figure 4-54. From the results, it can be seen that long fractures have considerable influence on block's effective permeability. It is also shown that fracture density has a great influence on permeability tensor: high effective permeability corresponds to high fracture density, see blocks (2, 3) to (2, 5) for instance. Finally ellipses show that the fracture orientation relatively matches to the off-diagonal term of permeability tensor in the grid blocks.

In a second step, the pressure distribution and fluid velocity distribution maps are calculated using the production model for Otsego fault map. For this purpose, one injector and one producer with injection rate of 50 (bbl/day) are located in the lower left hand side and the upper right hand side of the region in blocks (1, 1) and (12, 12), respectively. The results of the average velocity and pressure distribution are presented in figure 4-55 and figure 4-56. The coordinates of centre, pressure and average velocity in each grid block are presented by section B3 in Appendix-B. From the results in figure 4-55, it can be seen that the velocity distribution is influenced by fracture distribution especially by long fractures in the region. Comparing the results in blocks with long fractures with other blocks, it can be seen that long fractures have strong effect on effective permeability and dominate the fluid flow in the reservoir, see blocks (3, 2) to (6,2) for example.

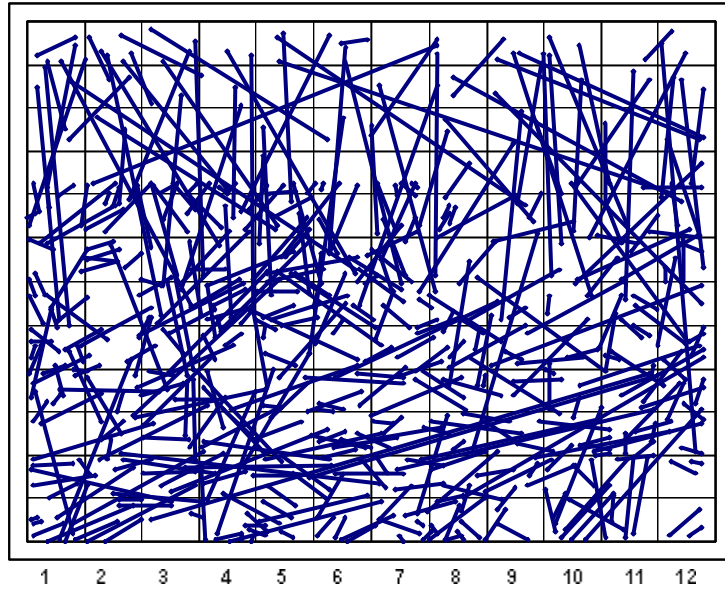


Figure 4-53: Arbitrary oriented fractures in a naturally fractured region containing different types of fractures in 144 grid-blocks (case study).

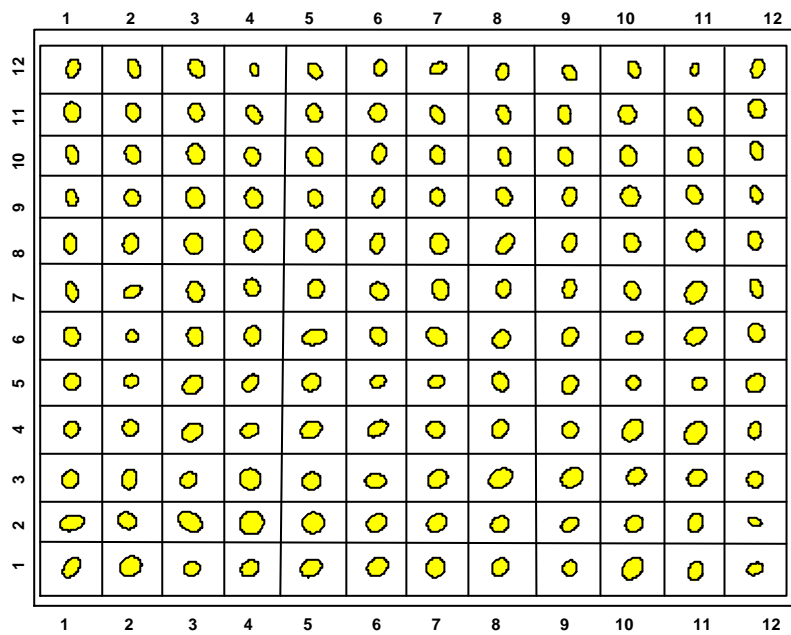


Figure 4-54: Elliptical presentation of the effective permeability tensors calculated for the case study 2. Each ellipse shows the permeability values in x- and y-directions and the orientation of fractures in each grid-block.

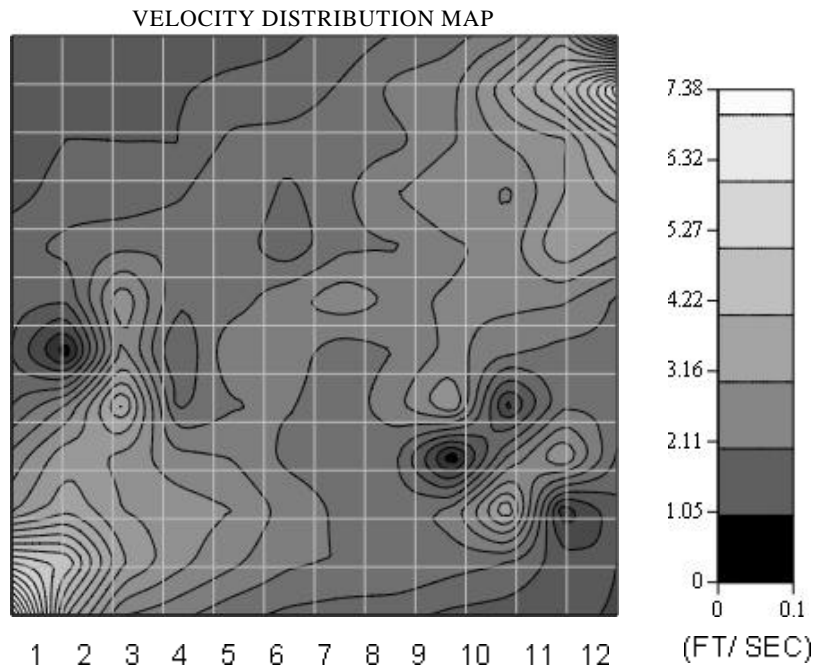


Figure 4-55: Velocity distribution in the region (related to the case study).

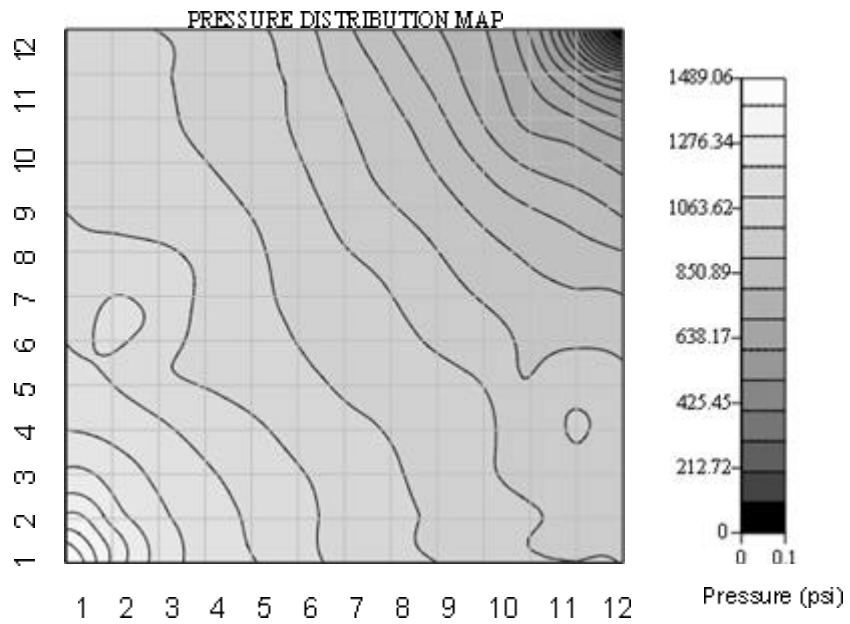


Figure 4-56 Pressure distribution in the region (related to the case study).

4.4.2 Discussion

In this chapter, a number of examples for the effective permeability calculation and production simulation algorithms have been presented. In the first part, examples-1 to 4 showed how the effective permeability is calculated for a block containing short, medium, long and interconnected fractures. The sensitivity study showed that the algorithm is positively sensitive against matrix permeability, fracture density and aperture. It was also shown that the algorithm does not create errors by changing the number of boundary elements, aspect ratio and the size of Poisson's ratio in the program.

In the second part, production simulation algorithm was successfully evaluated in the same way by presenting a number of examples and through the sensitivity studies. It was shown that fractures dominate the fluid flow in the reservoir and can have a strong effect of pressure distribution inside the reservoir.

Finally, a case study was presented from Otsego fault map containing large numbers of short, medium, long and interconnected fractures to evaluate the applicability of the effective permeability calculation and production simulation algorithms in NFRs with high fracture density. Similar to the examples presented in the previous sections, in this case the effective permeability tensors, fluid velocity and pressure distribution maps were calculated using both algorithms. From the results both algorithms have generated satisfactory results and simulations have been relatively fast as the fractures are replaced by the effective permeability tensor in the fluid flow calculation.

CHAPTER 5

CONCLUSIONS AND SCOPE OF FURTHER WORK

CHAPTER 5

CONCLUSIONS AND SCOPE OF FUTURE WORK

5.1 Conclusions and perspectives

Based on the results of this study, the following conclusions can be drawn:

1. Effective permeability tensor is a unique tool in simulation of fluid flow in naturally fractured reservoirs. It accounts for the effect of reservoir heterogeneity by using the characteristics of individual fractures.
2. The calculated effective permeabilities in this study and the sensitivity analyses, clearly show the effect of directional permeability which was originally contained in the fracture system.
3. The study proved that the periodic boundary condition and the boundary element method are the most effective tools in the calculation of the effective permeability tensor in NFRs. The principal strength of the boundary element method is its ability to simplify discretisation process and periodic boundary condition provides symmetric and positive definite tensors which always have physical meaning.
4. The results of this study show that fluid flow in matrix porous media is important and the simulation is based on the treatment of fractures as planner sources in the matrix.
5. The sensitivity analysis showed that the facture density has a greater effect on the block effective permeability than the fracture connectivity due to the strong coupling between matrix and fractures at the matrix/ fracture interface.
6. This study has improved the calculation of the block effective permeability tensor by applying the Poisson equation in the region around the medium and long fractures. The results of sensitivity analysis presented in section 4.2.5 in chapter 4, show that the model is insensitive to changes in aspect ration and Poisson's ratio.

7. Simulation of fluid flow in NFRs by use of the effective permeability tensor offers great flexibility in solving flow equations in NFR in large scale and high fracture density without dealing with complexities caused by fractures.
8. Control volume mixed finite element method is an efficient method in simulation of fluid flow in NFR and simplifies the calculation of fluid flow by using the block effective permeability tensor and calculates pressure and velocity simultaneously in a system of linear equation.
9. The fluid pressure and velocity distributions obtained from this study represent the effect of fracture systems on production from NFRs. They will be considered for further studies in hydraulic fracturing and production optimization of the wells in NFRs.
10. The results from the production simulation model also provide a basis to decide about the appropriate wellbore trajectory, location and orientation of injectors and producers in the reservoir to achieve the maximum production and the minimum draw down in the reservoir.

5.2 Recommendation for further studies

The following areas are recommended for further studies:

1. Further efforts are possible by three-dimensional calculation of the effective permeability tensor. This improvement allows consideration of actual three dimensional properties of fractures and provides more accurate results.
2. It is also possible to incorporate an up-scaling module to up-scale the fine scale the effective permeability tensor to coarse scale. This is important in NFR with very high density of fractures which requires the calculation of the effective permeability in fine scale grids. The results of the effective permeability tensors need to be up-scaled for the simulation purpose.

3. Further improvements in the production model are required for calculating pressure and velocity in any point inside the reservoir as a function of time, which is essential in the simulation of fluid flow as well as stimulation of hydraulic fracturing in NFRs.
4. The model can also be improved to simulate multi-phase fluid flow in NFRs by incorporating the methods which provide relative permeability, capillary pressures and account for the fluid compressibility.

BIBLIOGRAPHY

- Aavatsmark, I., Barkrve, T., Boe, Ø. and Mannseth, T. (1998a) Discretisation on unstructured grids for inhomogeneous, anisotropic media. Part I: Derivation of the methods. *SIAM J. SCI. Comput.*, 19(5).
- Aavatsmark, I., Barkrve, T., Boe, Ø. and Mannseth, T. (1998b) Discretisation on unstructured grids for inhomogeneous, anisotropic media. Part II: Discussion and numerical results. *SIAM J. SCI. Comput.*, 19(5).
- Aguilera, R. (2003) Geologic and Engineering Aspects of Naturally Fractured Reservoirs, Canadian Society of Exploration Geophysicists Recorder (February), pp. 44-49.
- Akif Atalay, M., Dilara Aydin, E. and Murat, A (2004) Multi-region heat conduction problems by boundary element method. *International Journal of Heat and Mass Transfer*, 47(6-7): 1549-1553.
- Anderson, J. and Dverstorp, B. (1987) Conditional simulations of fluid flow in three-dimensional networks of discrete fractures. *Water Resources Research*, 23: 1876-86.
- Anderson, J. and Thunvik, R. (1986) Predicting mass transport in discrete fracture networks with the aid of geometrical field data. *Water Resources Research*, 22(13): 1942-1950.
- Arbogast, T., Dawson, C.N., Keenan, P.T., Wheeler, M.F. and Yotov, I. (1998) Enhanced cell-centred finite differences for elliptic equations on general geometry. *SIAM J. Sci. Comput.*, 19(2): 404-425.
- Arbogast, T., Keenan, P.T., Wheeler, M.F. and Yotov, I. (1995) Logically rectangular mixed methods for Darcy flow on general geometry, paper SPE29099. Society of Petroleum Engineers Symposium on Reservoir Simulation, San Antonio, Feb.12-15.
- Arbogast, T., Wheeler, M.F. and Yotov, I. (1997) Mixed finite elements for elliptic problems with tensor coefficients as cell-centred finite differences. *SIAM J. Numer. Anal.*, 34(2): pp. 828-852.
- Barenblatt, G.I., Zheltov, Y.P. and Kochina, I.N. (1960) Basic concepts in the theory of seepage of homogeneous fluids in fissurized rocks. *Prikladnaya Matematika i Mekhanika*, 24, No. 5, pp. 852-864 (in Russian); *Journal of Applied Mathematics*

- and Mechanics (PMM), 24(5): 1286-1303 (English Translation).
- Bear, J. (1972) Dynamic of Fluids in Porous Media, American Elsevier, New York.
- Beer, G. and Watson, J.O. (1992) Introduction to Finite and Boundary Element Methods for Engineers. John Wiley & Sons, Chichester, 509 pp.
- Begg, S.H. and P.R., K. (1985) Modelling the Effects of Shales on Reservoir Performance: Calculation of Effective Vertical Permeability, SPE13529, Society of Petroleum Engineers.
- Berkowitz, B. and Balberg, I. (1993) Percolation theory and its application to groundwater hydrology. Water Resources Research, 29(4): 775-794.
- Brebbia, C.A. (1978) The Boundary Element Method for Engineers. (Pentech, London, 1978). Brown, E.T. (1981) Rock characterization testing and monitoring, p. 211. Pergamon Press.
- Brown, S.R. and Scholz, C.H. (1986) Closure of rock joints. Journal of geophysical research, 91: 4939-4948.
- Caces, M.C., Ledoux, E., Marsily, G. and Tillie, B. (1990) Modelling fracture flow with a stochastic discrete fracture network: calibration and validation. 1: The flow model. Water Resources Research, 26: 497-489.
- Cai, Z., Jones, J.E., McComick, S.F. and F., R.T. (1997) Control-volume mixed finite element methods. Computational Geoscience, 1: 289-315.
- Cai, Z., Mandel, J. and McCormick, S.F. (1991) The finite volume element method for diffusion equations on general triangulations. SIAM J.Numer.Anal., 28: pp.392 – 402.
- Chavent, G. and Jaffre, J. (1986) Mathematical Models and Finite Elements for Reservoir Simulation, North Holland and New York.
- Chen, G. and Zhou, J. (1992) Boundary Element Methods. Academic Press, San Diego.
- Chen, M., Bai, M. and Roegiers, J.C. (1999) Permeability tensor of anisotropic fracture networks. Journal of Mathematical Geology, 31(4): 355-373.
- Chernyshev, S.N. and Dearman, W.R. (1991) Rock Fractures, Butterworth- Heinemann, 272 pp.

- Chilingarian, G.V., Mazzullo, S.J. and Rieke, H.H. (1992) Carbonate reservoir Characterization: A Geologic-Engineering Analysis. Part I, Elsevier Publ. Co., Amsterdam, Developments in Petroleum Science 30.
- Chilingarian, G.V., Mazzullo, S.J. and Rieke, H.H. (1996) Carbonate reservoir Characterization: A Geologic-Engineering Analysis. Part II, Elsevier Publ. Co., Amsterdam, Developments in Petroleum Science 44.
- Chou, S.H. and Kwak, D.Y. (2000) Mixed co-volume methods on rectangular grids for elliptic problems. *SIAM J. Numer. Anal.*, 37(3): 758--771 (electronic).
- Dagan, G. (1979) Models of groundwater flow in statistically homogeneous porous formations. *Water Resources Research*, 15(1): 47-63.
- Dagan, G. (1989). *Flow and transport in porous formations*, Springer-Verlag, New York.
- Dagan, G. (1993) High- order correction of the effective permeability of heterogeneous isotropic formations of log- normal conductivity distribution. *Transport in Porous Media*, 12: 279-290.
- Desbarats, A.J. (1987) Numerical estimation of the effective permeability in sand- shale formations. *Water Resources Research*, 23(2): 273.
- Durlofsky, L.J. (1991) Numerical calculation of equivalent grid block permeability tensor for heterogeneous porous media. *Water Resources Research*, 27(5): 699-708.
- Durlofsky, L.J. (1993) A triangle based mixed finite element-finite volume technique for modelling two phase flow through porous media. *J. Comput. Phys.*, 105: 252.
- Durlofsky, L.J. (1994) Accuracy of mixed and control volume finite element approximations to Darcy velocity and related quantities. *J. Comput. Phys.*, 30(4): 965.
- Durlofsky, L.J., Enquist, B. and Osher, S. (1992) Triangle based adaptive stencils for the solution of hyperbolic conservation laws. *J. Comput. Phys.*, 98: pp.64 –73.
- Durlofsky, L.J., Jones, R.C. and Milliken, W.J. (1997) A nonuniform coarsening approach for the scale-up of displacement processes in heterogeneous porous media. *Advances in Water Resources*, 20(5-6): 335-347.
- Dverstorp, B. and Anderson, J. (1989) Application of the discrete fracture network concept

- with field data: possibilities of model calibration and validation. *Water Resources Research*, 25(3): 540-50.
- Edwards, M.G. (1998) Cross flow tensors and finite volume approximation with by deferred correction. *Computer methods in applied mechanics and engineering*, 151: 143- 161.
- Edwards, M.G. and Rogers, C.F. (1994) A flux continuous finite difference scheme for the full tensor pressure equation. In: *ECMOR IV (Editor)*, 4th European Conference on the Mathematics of Oil Recovery, Roros, Norway.
- Edwards, M.G. and Rogers, C.F. (1998) Finite volume discretisation with imposed flux continuity for the general tensor pressure equation (1998). *Computational Geosciences*, 2: 259.
- Faybishenko, B., Witherspoon, P.A. and Benson, S.M. (2000) *Dynamics of fluids in fractured rock*, American geophysical union, Washington DC.
- Feistauer, M., Felcman, J. and M., L.a.a. (1995) Combined finite element-finite volume solution of compressible flow. *J. Comput. Appl. Math.*, 63: pp.179 –199.
- Firoozabadi, A. and Ishimoto, K. (1994) Theory of re-infiltration in fractured porous media: Part I One dimensional model. *Advanced technology series*, 2(2): 35-44.
- Forsyth, P.A. (1989) A control volume finite element method for local mesh refinement, *Proceedings of the 10th Society of Petroleum Engineering Symposium on Reservoir Simulation* , Dallas, pp. 85–96.
- Galli, A. and al., e. (1996). Quick upscaling of flow and transport related parameters, Technical report LHM/96/RD/11 (Geoscience 2, Reservoir Eng. Project, Topic 4) Commission of the European Communities.
- Gaul, H.L. (2004) *Boundary Element Methods*. <http://www.bem.uni-stuttgart.de/home.htm>, Institute A of Mechanics, University of Stuttgart, Stuttgart.
- Gelhar, L.W. (1993) *Stochastic subsurface hydrology*. Prentice- Hall, Engelwood Cliffs, New Jersey.
- Gentier, S. and Ries, J. (1990) Quantitative description and modelling of joint morphology, *Proceeding of the International Symposium on Rock Joints*. W. Barton and E. Stephansson, eds. Rrterdam: A. A. Balkema, Loen, Norway, pp. 375-382 in *Rock Joints*.

- Gilman, J.R. and Kazemi, H. (1983) Improvements in simulation of naturally fractured reservoirs. *Society of Petroleum Engineers*, 23: 695-707.
- Gupta, A., Penuela, G. and Avila, R. (2001) An Integrated approach to the determination of permeability tensor for naturally fractured reservoirs. *Canadian Petroleum Technology*, 40(12): 43-48.
- Guyon, E., Hulin, J.P. and Lenormand, R. (1984) Application de la percolation a la physique des milieux poreux. *Annales des Mines*, 5(6): 17-40.
- Harstad, H., Teufel, W.T. and Lorenz, J.C. (1995) Characterization and simulation of naturally fractured tight gas sandstone reservoirs, SPE30573, Society of Petroleum Engineers Annual Technical Conference & Exhibition held in Dallas, USA, 22-25 October, 1995.
- Heinemann, Z.E., Brand, C., Munka, M. and Chen, Y.M. (1989) Modelling reservoir geometry with irregular grids, *Proceedings of the 10th Society of Petroleum Engineers Symposium on Reservoir Simulation*, Dallas, pp. 37–54.
- Hossain, M.M. (2000) Reservoir simulation by hydraulic fracturing: Complexities and remedies with reference to initiation and propagation of induced and natural fractures, The school of Petroleum Engineering, The University of New South Wales, Sydney, Australia.
- Huang, C. and Evans, D.D. (1985). A three-dimensional computer model to simulate fluid flow and contaminant transport through a rock fracture system, NUREG/CR-4042, US Nuclear Regulatory Commission.
- Hughes, R.G. and Blunt, M.J. (2000) Network modelling of multiphase flow in fractures. *Advances in Water Resources*, 24: 409-421.
- Iwai, K. (1976) Fundamental studies of fluid flow through a single fracture. PhD dissertation, University of California, Berkeley.
- Jensen, C.L., Lee, S.H., Milliken, W.J., Kamath, J., Narr, W. and Wu, H. (1998) Field simulation of naturally fractured reservoirs using effective permeabilities derived from realistic fracture characterisation, SPE58999, Society of Petroleum Engineering Annual Technical Conference and Exhibition held in New Orleans, Louisiana, 27-30 Sep.1998.
- Jones, J.E. (1995) A mixed finite volume element method for accurate computation of fluid

velocities in porous media, Denver.

- Karimi-Fard, M. and Firoozabadi, A. (2001) Numerical simulation of water injection in 2D fractured media using discrete-fracture model, Society of Petroleum Engineering Annual Technical Conference and Exhibition, New Orleans, Louisiana.
- Kasab, J.J., Karur, S.R. and Ramachandran, P.A. (1995) Quasilinear boundary element method for nonlinear Poisson type problems. *Engineering Analysis with Boundary Elements*, 15: 277-282.
- Kazemi, H. (1969) Pressure transient analysis of naturally fractured reservoirs with uniform fracture distribution. *Society of Petroleum Engineers Journal*: 451-462.
- Kazemi, H. and Gilman, J.R. (1989). Multiphase flow in fractured petroleum reservoirs, Proceedings, Advanced workshop on heat and mass transport in fractures rocks, Laboratorio Nacional de Engenharia Civil (LNEC), Lisbon, Portugal.
- Kazemi, H. and Gilman, J.R. (1993) Multiphase flow in fractured petroleum reservoirs, in flow and contaminant transport in fractured rock. Academic Press, J. Bear, Tsang, C.F. and Marsily, G., San Diego, Calif.
- Kazemi, H., Merrill, L.S., Porterfield, K.L. and Zeman, P.R. (1976) Numerical simulation of water-oil flow in naturally fractured reservoirs. *Journal of Society of Petroleum Engineering*, p. 317.
- Kazemi, H., Seth, M.S. and Thomas, G.W. (1969) The interpretation of interference tests in naturally fractured reservoirs with uniform fracture distribution. *Society of Petroleum Engineers Journal*: 463-472.
- Khalili-Naghadeh, N. (1991) Numerical modelling of flow through fractured media, PhD dissertation, University of New South Wales, Sydney, Australia.
- king, P.R. (1989) The use of renormalization for calculating effective permeability. *Transport in Porous Media*, 4: 37-58.
- Kitanidis, P.K. (1995) Groundwater flow in heterogeneous formations, In Second George Kovac's Colloquium. UNESCO, Paris.
- Koebbe, J. (1993) A computationally efficient modification of mixed finite element methods for flow problems with full transmissivity tensors. *Numer. Methods Partial Differential Equations*, 9: pp. 339-355.
- Krasilova, N.S. (1979) Analysis of rock fracturing in small-scale engineering- geological

- surveys, *Engineering geology*, 4: 38-46.
- Kunkel, J.R., Way, S.C. and Mckee, C.R. (1988) Comparative evaluation of selected continuum and discrete- fracture models. Us Nuclear Regulatory Commission, USA.
- Kwak, D.Y. and Kim, K.Y. (2000) Mixed co-volume methods for quasi-linear second-order elliptic problems, *SIAM J. Numer. Anal.*, 38(4): pp. 1057-1072.
- Kwon, T. H. (2001) Boundary Element Method., online lecture notes for boundary integral equation formulation for Poisson equation.
- Lee, C.H. and Farmer, I. (1993) *Fluid Flow in Discontinuous Rocks*. Chapman & Hall, London, 169 pp.
- Lee, C.H., Jensen, C.L. and Lough, M.F. (1999) An efficient finite difference model for flow in a reservoir with multiple length-scale fractures, SPE 56752, SPE Annual Technical Conference and Exhibition, Houston, U.S.A.
- Lee, S.H., Durlofsky, L.J., Lough, M.F. and Chen, W.H. (1997) Finite difference simulation of geologically complex reservoirs with tensor permeabilities, *SPE Reservoir Evaluation and Engineering*: 567-574.
- Lee, S.H., Durlofsky, L.J., Lough, M.F. and Chen, W.H. (1998) Finite difference simulation of geologically complex reservoir with tensor permeabilities, *SPE RE&E*: 567.
- Lee, S.H., Jensen, C.L. and Lough, M.F. (2001) Hierarchical modelling of flow in naturally fractured reservoirs with multiple length scales. *Water Resources Research*, 37(3): 443-455.
- Lee, S.H., Jensen, J.L. and Lough, M.F. (2000) Efficient finite-difference model for flow in a reservoir with multiple length-scale fractures, *SPEJ*, 5(3): 268.
- Lee, S.H., Tchelepi, H. and DeChant, L.F. (1999) Implementation of a flux-continuous finite difference method for stratigraphic hexahedron grids, paper SPE 51901 presented at the SPE Reservoir Simulation Symposium, Houston, Feb. 14-17.
- Lee, S.H., Tchelepi, H., Jenny, P. and Dechant, L. (2002) Implementation of a flux-continuous finite-difference method for stratigraphic, hexahedron grids, Society of Petroleum Engineers.
- Long, J.C.S., Aydin, A. and Brown, S.R. (1996) *Rock fractures and fluid flow*,

- Contemporary understanding and applications. National Research Council, National Academy Press, Washington, D.C., 551 pp.
- Long, J.C.S., Remer, S., Wilson, C.R. and Witherspoon, P.A. (1982) Porous media equivalents for network of discontinuous fractures, *Water Resources Research*, 18(3): 645-658.
- Long, J.C.S. and Witherspoon, P.A. (1985) The relationship of the degree of interconnection to permeability in fracture networks. *Journal of geophysical research*, 90(B4): 3087- 3089.
- Lough, M.F., Lee , S.H. and Kamath, J. (1996) A new method to calculate the effective permeability of grid blocks used in the simulation of naturally fractured reservoirs, SPE 36730, 1996 SPE Annual Technical Conference and Exhibition, Society of Petroleum Engineers, Denver, Colorado, U.S.A.
- Lough, M.F., Lee, S.H. and Kamath, J. (1998) An efficient boundary integral formulation for flow through fractured porous media. *Journal of Computational Physics*, 143: 462-483.
- Manwart, C., Aaltosalmi, U., Koponen, A., Hilfer, R. and Timonen, J. (2002) Lattice-Boltzmann and finite-difference simulations for the permeability for three-dimensional porous media, Institute for Physics, University of Mainz, 55099 Mainz, Germany.
- Matheron, G., Beucher, H., Fouquet, C.D., Galli, A., Guerillot, D. and Ravenne, C. (1987) Conditional simulation of the geometry of fluvio-deltaic reservoirs, 62nd Annual Tech. Conf. and Exhibition of the SPE, pp. 591-599.
- Miller, S.M., McWilliams, P.C. and Kerkering, J.C. (1990) Ambiguities in estimating fractal dimensions of rock fracture. In: W. A. Hustrulid and G. A. Johnson (Editor), *Proceedings of the 31st U. S. Symposium on Rock Mechanics*, Rotterdam: A. A. Balkema, pp. 471-478 in *Rock Mechanics Contributions and Challenges*.
- Naff, R.L., Russell, T.F. and Wilson, J.D. (2000) Test functions of three-dimensional control-volume mixed finite-element methods on Irregular grids, *Proceedings of the XIII Conference on Computational Methods in Water Resources*, Calgary (June 2000).
- Naji, H.S. and Kazemi, H. (1996) A fully implicit, three-dimensional, two-phase, control

- volume finite element model for the simulation of naturally fractured reservoirs, 7th Abu Dhabi international Petroleum Exhibition and Conference. Society of Petroleum Engineers, Abu Dhabi, pp. 13.
- Nakashima, T., Arihara, N. and Sato, S.K. (2000) Effective permeability estimation for modelling of naturally fractured reservoirs, SPE 64286, SPE Asia Pacific Oil and Gas Conference and Exhibition, Brisbane, Australia.
- Oda, M. (1985) Permeability tensor for discontinuous rock masses, *Geotechnique*, 35(4): 483-495.
- Ohlberger, M. (1997) Convergence of a mixed finite elements-finite volume method for the two-phase flow in porous media. *East-West J. Numer. Math.*, 5: pp.183 –210.
- Park, Y.C. and Sung, W.M. (2000) Development of FEM reservoir model equipped with the effective permeability tensor and its application to naturally fractured reservoirs, Society of Petroleum Engineering International Oil and Gas Conference and Exhibition in China held in Beijing, China.
- Park, Y.C., Sung, W.M. and Kim, S.J. (2002) Development of FEM reservoir model equipped with an effective permeability tensor and its application to naturally fractured reservoirs, *Energy sources*, 24: 531-542.
- Pickup, G., Ringrose, P.S. and Sorbie, J.L.J. (1994) Permeability tensor for sedimentary structure, *Research Mathematical Geology*, 26(2): 227-250.
- Pinczewski, V. (2001) Reservoir simulation notes, School of Petroleum Engineering, The university of New South Wales, Sydney, Australia.
- Poley, A.D. (1988) Effective permeability and dispersion in locally heterogeneous aquifers, *Water Resources Research*, 24(1): 1921-1926.
- Rasmussen, T.C. (1988) Fluid flow and solute transport through three- dimensional networks of variably saturated discrete fractures, PhD dissertation, University of Arizona.
- Rasmussen, T.C., Jim-Yeh, T.C. and Evans, D.D. (1987) Effect of Variable Fracture Permeability/Matrix Permeability Ratios on Three-Dimensional Fractured Rock Hydraulic Conductivity, *Proceeding of the Conference on Geostatistical, Sensitivity and Uncertainty Methods for Ground Water Flow and Radionuclide Transport*

Modelling, San Francisco.

- Raviart, P.A. and Thomas, J.M. (1977) A mixed finite element method for 2nd order elliptic problems. *Mathematical Aspect of Finite Element Methods* eds. I. Galligani and E. Magnes (Springer, Berlin, 1977): 292-315.
- Reiss, L.H. (1980) *The reservoir engineering aspects of fractured formations*. TECHNIP, Paris.
- Renard, P. and Marsily, G. (1997) Calculating the equivalent permeability: a review: *Advances in Water Resources*, 20(5-6): 253-278.
- Ribeiro, R.F. and Romeu, R.K. (1997) Computing the effective permeability by finite difference, finite elements and mixed-hybrid finite elements, SPE39068, Fifth Latin American and Caribbean Petroleum Engineering Conference and exhibition held in Rio de Janeiro, Brazil, 30 August-3 September.
- Robinson, P.C. (1982). *Connectivity of fracture systems - A percolation theory approach*, Theoretical Physics Division, AERE Harwell, DOE Report No. DOE/RW/81.028.
- Romeu, R.K. and Noetinger, B. (1995) Calculation of internodal transmissivities in finite difference model of flow in heterogeneous porous media. *Water Resources Research*, 31(4): 943.
- Rozon, B. (1989) A generalized finite volume discretisation method for reservoir simulation, *Proceedings of the 10th Society of Petroleum Engineering Symposium on Reservoir Simulation* (Society of Petroleum Engineers, Dallas, pp. 71-84.
- Rudolph, T. and Petersen, V. (1987) *Advances in Engineering Software*. 9, 1: 7 - 28 pp.
- Russell, T.F. (1995). *Rigorous block-centred discretisation on irregular grids: Improved simulation of complex reservoir systems*, Tulsa, OK.
- Russell, T.F. (2000) Relationships among some conservative discretisation methods. In: *Numerical Treatment of Multiphase and Flows in Porous Media*, Z. Chen et. al, ed. *Lecture Notes in Physics 552*, Springer-Verlag (Editors), Berlin.
- Schwartz, F.W. and Smith, L. (1988) A continuum approach for modelling mass transport in fractured media. *Water Resources Research*, 24(8): 1360-1372.
- Smith, L. and Schwartz, F. (1984) An analysis of the influence of fracture geometry on mass transport in fractured media. *Water Resources Research*, 20(9): 1241-1252.

- Snow, D.T. (1965) A Parallel Plate Model of Fractured Permeable Media. PhD dissertation, California University, Berkeley, California.
- Snow, D.T. (1968) Rock fracture spacings, opening and porosities, Soil Mechanics and Foundation Engineering Division, 94: 73-91.
- Snow, D.T. (1969) Anisotropic permeability of fractured media. Water Resources Research, 5(6): 1273-1289.
- Stearns, D.W. and Friedman, M. (1972) Reservoirs in fractured rock in stratigraphic oil and gas fields' classification. Exploration methods and case histories, Am. Assoc. Petroleum Geologists, pp. 82-106.
- Suli, E. (1991) Convergence of finite volume schemes for Poisson's equation on nonuniform meshes. SIAM J. Numer. Anal., 28: pp.1419 –1430.
- Sutopo, Arihara, N. and Sato, K. (2001) Simulation of naturally fractured reservoirs with effective permeability, SPE68705, Society of Petroleum Engineering Asia Pacific Oil and Gas Conference and Exhibition held in Jakarta, Indonesia, 17-19 April 2001.
- Swan, G. (1981) Tribology and the characterization of rock joints, in Proceedings of the 22nd U.S. Symposium on Rock Mechanics, Cambridge: Massachusetts Institute of Technology, pp. 402-407.
- Therrien, R. and Sudicky, E.A. (1996) Three-dimensional analysis of variably- saturated flow and solute transport in discretely- fractured porous media, Journal of Contaminant Hydrology, 23: 1- 44.
- Thomas, J.M. and Trujillo, D. (1995) Analysis of finite volume methods, in: Mathematical Modelling of flow Through Porous Media, eds. A.P. Bourgeat, C. Carasso, S. Luckhaus and A. Mikelic (World Scientific, Singapore, 1995) pp. 203-214.
- Thomas, L.K., Dixon, T.N. and Pierson, R.G. (1983) Fractured reservoir simulation. Society of Petroleum Engineers, pp. 42-54.
- Thomas, T.R. (1982) Rough Surfaces, Longman, New York.
- Tran, N.H. (2004) Characterisation and Modelling of Naturally Fractured Reservoirs, PhD dissertation, The University of New South Wales, Sydney, Australia.
- Tran, N.H., Chen, Z. and Rahman, S.S. (2003a) Characterizing and Modelling of Naturally

- Fractured Reservoirs with the Use of Object-Based Global Optimization, Canadian International Petroleum Conference, Calgary, Alberta, Canada, June 10-12.
- Tran, N.H., Chen, Z. and Rahman, S.S. (2003b) Object-Based Global Optimization in Modelling Discrete-Fracture Network Map: A Case Study. In: Society of Petroleum Engineers (Editor), SPE84456, Society of Petroleum Engineering Annual Technical Conference and Exhibition held in Denver, Colorado, U.S.A., 5-8 October 2003.
- Van Golf-Racht, T.D. (1982) Fundamentals of fractured reservoir engineering. Elsevier Scientific Publishing Company, New York.
- Voss, C.F. and Shotwell, L.R. (1990). An investigation of the mechanical and hydraulic behaviour of tuff fractures under standard conditions, High level Radioactive Waste Management, La Grange park, III.: American Nuclear Society.
- Warren, J.E. and Price, H.S. (1961) Flow in heterogeneous porous media. SPEJ: 153.
- Warren, J.E. and Root, R.J. (1963) The behaviour of naturally fractured reservoirs. Society of Petroleum Engineers: 245-255.
- Weiser, A. and Wheeler, M.F. (1988) On convergence of block-centred finite differences for elliptic problems. SIAM J.Numer.Anal., 25: pp.351 –375.
- Wilson, J.D. (2001) Efficient Solver for Mixed and Control-Volume Mixed Finite Element Methods in Three Dimensions, PhD dissertation, University of Colorado, Denver.
- Witherspoon, P.A., Wang, J.S.Y., Iwai, K. and Gale, J.E. (1980) Validity of cubic law for fluid flow in a deformable rock fracture. Water Resources Research, 16(6): 1016-1024.
- Yang, Y.-k. and Deo, M.D. (2001) Full-tensor multiphase flow simulations with applications to upscaling and discrete-fracture models, SPE66348, Society of Petroleum Engineering Reservoir Simulation Symposium held in Houston, Texas, 11-14 February 2001.
- Zhilentsov, V.N. (1975). Manual for the determination of percolation and suffusive properties of rock beds of hydraulic structures, Energia Publishers, Leningrad.

APPENDIX A

REVIEW OF STEADY STATE FLOW EQUATIONS FOR FLUID FLOW IN POROUS MEDIA

In general, the main processes taking place in a real reservoir are fluid flow and mass transfer. Fluid flow can be defined as simultaneously following up to three phases (oil, water and gas) in a reservoir. Mass transfer may also take place between the phases. A comprehensive model must account the equation for all forces and should also take into account an arbitrary reservoir description with respect to heterogeneity and geometry. Therefore, the main equations are obtained by combining the equation of motion (Darcy's law) with the equation for mass conservation or continuity equation.

Flow of a fluid through a saturated porous media was first studied by Darcy in 19th century. His model, which was supported by experimental and other theoretical considerations, is basically described in theoretical and empirical form by Navier-Stokes equation and Darcy's law, respectively. These two equations are fundamentally similar and one can derive Darcy's law by simplification of Navier-Stokes equation with ignoring the inertia terms and taking the average velocity in very small Reynolds numbers. The applicability of Darcy law is only for the condition that inertial forces can be neglected for the determination of the motion of the fluid.

In fractured porous media, fracture flow is usually considered by applying rigorous Navier-Stokes equation known as cubic law, while Darcy's law is employed for flow through matrix porous media because of its simplicity. In the formulation, fluid flow is assumed as steady state single-phase in the reservoir in which the pore space is saturated with a single fluid. Fluid flow in the media is described in terms of superficial velocity of a flow which is defined as the volumetric flow per unit area normal to the direction of flow. The superficial velocity in Cartesian coordinates (x, y, z) is represented by a vector the superficial velocity vector which has velocity components x, y and z in the coordinate directions,

$$v = (v_x, v_y, v_z) \quad (\text{A.1})$$

Darcy's law can describe the velocity components in differential form as,

$$v_x = -\frac{k_x}{\mathbf{m}} \left(\frac{\partial P}{\partial x} - \mathbf{r} g_x \frac{\partial D}{\partial x} \right) \quad (\text{A.2})$$

$$v_y = -\frac{k_y}{\mathbf{m}} \left(\frac{\partial P}{\partial y} - \mathbf{r} g_y \frac{\partial D}{\partial y} \right) \quad (\text{A.3})$$

$$v_z = -\frac{k_z}{\mathbf{m}} \left(\frac{\partial P}{\partial z} - \mathbf{r} g_z \frac{\partial D}{\partial z} \right) \quad (\text{A.4})$$

where (k_x, k_y, k_z) are permeability values in the coordinate directions, D is an arbitrary function of position (x, y, z) , \mathbf{m} is the fluid viscosity, \mathbf{r} is density of fluid and g is the gravitational acceleration with components of g_x, g_y, g_z .

Defining depth to be the positive in downward direction z , can result $g_x = g_y = 0$ and $g_z = g$. Making a further assumption that the gravitational effect is negligible in all three orthogonal directions, the Darcy's law can be expressed in a more compact vector form as:

$$\bar{v} = -\frac{\bar{k}}{\mathbf{m}} (\nabla P) \quad (\text{A.5})$$

where permeability in the reservoir can be described as permeability tensor, \bar{k} , which is symmetric with diagonal elements corresponding to the permeability in the coordinate directions,

$$\bar{K} = \begin{bmatrix} k_{xx} & k_{xy} & k_{xz} \\ k_{yx} & k_{yy} & k_{yz} \\ k_{zx} & k_{zy} & k_{zz} \end{bmatrix}. \quad (\text{A.6})$$

In the following, the effective permeability K is defined as normalized permeability which is defined as a full tensor that relates the average pressure gradient ∇P to the average fluid velocity V . The conservation of mass for a differential volume element which is the relation between the Darcy's law and continuity equation in steady state condition in the reservoir, may be stated as,

$$\{\text{mass convected in}\} + \{\text{mass injected}\} = \{\text{mass convected out}\} + \{\text{accumulation}\} \quad (\text{A.7})$$

or,

$$\{\text{rate of mass convected (in-out)}\} + \{\text{mass injected}\} = \{\text{mass accumulation}\}. \quad (\text{A.8})$$

This also may be written as,

$$\left[\begin{aligned} &(\mathbf{r}v_x|_x - \mathbf{r}v_x|_{x+\Delta x})\Delta y\Delta z + \\ &(\mathbf{r}v_y|_y - \mathbf{r}v_y|_{y+\Delta y})\Delta x\Delta z + \\ &(\mathbf{r}v_z|_z - \mathbf{r}v_z|_{z+\Delta z})\Delta x\Delta y + \end{aligned} \right] + q\Delta x\Delta y\Delta z = \frac{\partial}{\partial t}(\Delta x\Delta y\Delta z\Phi\mathbf{r}) \quad (\text{A.10})$$

which is the basic material balance over the differential volume element of a reservoir as described in **Figure A. 5-1**.

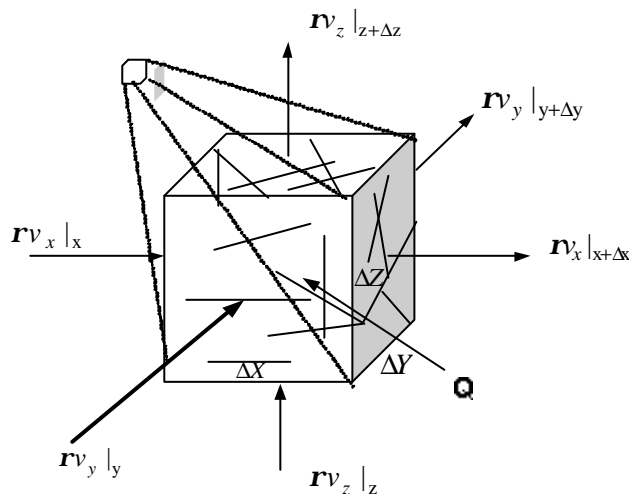


Figure A. 5-1 Differential volume element for flow equilibrium

In naturally fractured porous media the injection rate Q is the source/ sink which is zero for short fractures and non zero for matrix and medium to long fractures. Porosity f is zero in the fractured block. This will simplify the above equation for medium to long fractures and the surrounded matrix to the following equation which is divided by $\Delta x \Delta y \Delta z$:

$$\left[(\mathbf{r}v_x|_x - \mathbf{r}v_x|_{x+\Delta x}) \frac{1}{\Delta x} + (\mathbf{r}v_y|_y - \mathbf{r}v_y|_{y+\Delta y}) \frac{1}{\Delta y} + (\mathbf{r}v_z|_z - \mathbf{r}v_z|_{z+\Delta z}) \frac{1}{\Delta z} \right] + Q = 0 \quad (\text{A.11})$$

where in the limit of $\Delta x \rightarrow 0, \Delta y \rightarrow 0, \Delta z \rightarrow 0$ Equation 3-8 may be written as:

$$-\frac{\partial(\mathbf{r}v_x)}{\partial x} - \frac{\partial(\mathbf{r}v_y)}{\partial y} - \frac{\partial(\mathbf{r}v_z)}{\partial z} + Q = 0 \quad (\text{A.12})$$

or in compact vector form, as

$$-\nabla \cdot (\mathbf{r}v) + Q = 0 \quad (\text{A.13})$$

Note that the gradient of a scalar field, say P , is the vector field, ∇P and can be written as:

$$\nabla P = \bar{i} \frac{\partial P}{\partial x} + \bar{j} \frac{\partial P}{\partial y} + \bar{k} \frac{\partial P}{\partial z} \quad (\text{A.14})$$

where, \bar{i} , \bar{j} and \bar{k} are the co-ordinate unit vectors. Equation 2-13 is the general form of continuity equation which is employed in our both models for calculation of the effective permeability and simulation of flow in naturally fractured reservoirs.

APPENDIX B

COORDINATES OF FRACTURES AND THE RESULTS FOR THE FIELD CASE STUDY PRESENTED IN CHAPTER 4.

**B1 X-Y COORDINATES OF FRACTURES IN CASE STUDY PRESENTED IN
CHAPTER 4 AND PRESENTED IN Figure 4-53:**

Fracture No.	X ₁ (m)	Y ₁ (m)	X ₂ (m)	Y ₂ (m)
1	823	571	751	571
2	811	578	825	531
3	824	550	797	550
4	804	577	686	490
5	753	570	787	532
6	781	528	820	494
7	789	538	775	444
8	818	493	726	424
9	822	519	574	396
10	668	571	759	507
11	760	500	821	492
12	710	577	672	564
13	677	576	666	502
14	636	544	733	511
15	664	577	806	323
16	824	386	571	123
17	497	405	429	38
18	419	205	499	59
19	814	144	775	4
20	825	106	792	82
21	822	54	782	11
22	784	129	815	113
23	811	129	824	126

Fracture No.	X ₁ (m)	Y ₁ (m)	X ₂ (m)	Y ₂ (m)
24	797	151	823	143
25	740	137	730	5
26	757	138	741	15
27	764	140	720	134
28	823	216	681	3
29	715	77	664	4
30	711	91	652	5
31	732	133	655	19
32	688	131	707	5
33	663	67	727	19
34	622	497	544	151
35	527	60	510	3
36	539	93	530	51
37	631	516	639	429
38	509	535	617	516
39	696	494	744	484
40	798	473	825	444
41	799	489	800	421
42	823	510	668	417
43	808	506	670	423
44	791	457	771	314
45	704	575	706	551
46	709	538	726	482
47	741	559	731	391
48	771	528	737	469
49	720	458	683	396
50	740	396	768	375
51	742	382	804	322
52	728	419	609	337
53	824	413	568	284
54	684	360	593	237
55	593	509	688	396
56	637	542	651	480

Fracture No.	X1 (m)	Y1 (m)	X2 (m)	Y2 (m)
57	620	577	651	562
58	629	575	599	548
59	626	563	613	523
60	604	506	577	356
61	740	350	759	331
62	725	358	750	329
63	777	294	804	262
64	551	426	706	277
65	636	397	635	367
66	637	288	637	215
67	651	261	592	260
68	779	445	779	419
69	717	369	707	275
70	697	310	658	300
71	679	298	598	287
72	705	302	721	292
73	714	307	777	251
74	820	314	674	251
75	826	346	810	302
76	825	334	808	325
77	825	310	726	236
78	826	298	534	70
79	795	257	727	163
80	802	256	780	198
81	798	307	751	225
82	763	284	761	267
83	801	224	825	198
84	825	261	815	223
85	826	249	748	217
86	764	214	450	117
87	697	198	480	133
88	500	488	498	429
89	596	558	500	492

Fracture No.	X1 (m)	Y1 (m)	X2 (m)	Y2 (m)
90	593	577	479	405
91	666	517	570	486
92	572	486	526	416
93	824	23	808	7
94	716	75	712	33
95	666	122	692	88
96	632	85	646	18
97	669	122	609	92
98	701	217	645	27
99	655	77	642	38
100	763	163	740	138
101	765	189	761	163
102	784	196	742	180
103	782	180	621	137
104	824	189	691	145
105	710	167	676	156
106	685	155	711	149
107	625	195	710	182
108	665	155	635	117
109	639	130	558	80
110	585	54	559	4
111	595	87	574	54
112	508	92	579	68
113	507	94	449	84
114	593	118	550	106
115	574	144	488	47
116	523	64	461	42
117	532	74	500	64
118	513	203	476	45
119	574	28	611	3
120	528	33	553	5
121	525	16	534	3
122	529	9	512	4

Fracture No.	X ₁ (m)	Y ₁ (m)	X ₂ (m)	Y ₂ (m)
123	674	232	667	201
124	769	268	345	102
125	759	271	151	37
126	731	177	729	142
127	599	159	641	144
128	559	195	597	163
129	494	195	604	176
130	540	300	649	207
131	608	350	514	282
132	528	265	418	205
133	508	261	578	235
134	568	365	550	251
135	559	269	557	252
136	608	376	588	363
137	650	438	540	356
138	573	387	376	264
139	495	329	450	300
140	531	207	589	195
141	473	263	535	211
142	483	275	533	232
143	540	453	514	251
144	559	71	490	3
145	493	25	501	14
146	493	17	482	2
147	429	37	478	14
148	470	89	430	37
149	446	43	383	3
150	432	63	247	1
151	414	76	283	33
152	239	78	306	31
153	288	63	321	38
154	292	89	328	60
155	262	14	230	3

Fracture No.	X1 (m)	Y1 (m)	X2 (m)	Y2 (m)
156	269	45	295	16
157	308	18	324	5
158	385	108	354	39
159	559	144	494	116
160	632	280	643	270
161	584	306	603	294
162	490	400	577	324
163	552	344	545	311
164	725	399	698	312
165	787	578	793	512
166	798	483	823	470
167	522	538	516	514
168	517	531	504	505
169	514	544	508	521
170	540	578	510	555
171	511	561	479	510
172	501	537	406	382
173	386	356	372	339
174	478	390	494	376
175	529	356	556	337
176	408	131	438	86
177	426	139	440	112
178	115	143	430	96
179	377	110	460	109
180	370	123	192	121
181	116	132	228	111
182	279	243	220	67
183	300	280	232	15
184	408	242	343	208
185	270	374	402	292
186	4	117	175	63
187	126	293	40	2
188	10	244	54	15

Fracture No.	X1 (m)	Y1 (m)	X2 (m)	Y2 (m)
189	303	214	212	153
190	216	146	55	28
191	44	32	8	7
192	130	119	35	40
193	74	91	46	1
194	533	323	516	298
195	505	290	457	267
196	511	313	475	277
197	461	282	406	221
198	401	272	460	265
199	339	266	460	258
200	355	223	386	215
201	354	214	372	209
202	424	196	447	190
203	484	183	514	175
204	155	189	7	133
205	56	125	6	124
206	83	107	6	91
207	62	95	27	70
208	130	60	26	1
209	109	34	60	2
210	206	93	74	1
211	139	36	95	0
212	105	77	212	65
213	365	181	176	81
214	142	168	196	164
215	215	161	369	134
216	399	147	362	138
217	450	167	374	150
218	432	176	290	134
219	346	170	412	150
220	384	166	419	152
221	505	185	420	166

Fracture No.	X1 (m)	Y1 (m)	X2 (m)	Y2 (m)
222	401	177	442	152
223	312	140	369	83
224	374	39	354	7
225	387	39	377	6
226	534	163	521	147
227	458	202	433	173
228	323	111	363	71
229	207	273	310	129
230	215	247	288	144
231	305	436	432	318
232	454	9	460	1
233	476	33	483	25
234	212	116	218	4
235	186	54	141	1
236	211	160	114	98
237	244	104	126	104
238	240	143	163	90
239	335	193	276	164
240	342	258	299	200
241	112	60	175	59
242	140	67	112	67
243	205	115	141	113
244	152	135	107	116
245	221	221	88	130
246	102	165	98	135
247	51	306	92	193
248	21	566	51	350
249	62	314	67	290
250	74	266	115	173
251	91	241	16	190
252	41	246	160	243
253	252	317	133	248
254	33	286	44	234

Fracture No.	X1 (m)	Y1 (m)	X2 (m)	Y2 (m)
255	77	302	7	258
256	24	225	6	196
257	42	240	31	222
258	58	279	75	276
259	88	286	60	268
260	29	374	4	231
261	29	323	5	323
262	5	344	39	308
263	10	314	4	297
264	92	344	47	311
265	152	376	65	316
266	23	398	97	327
267	11	433	21	399
268	30	374	37	345
269	12	577	41	356
270	8	579	14	532
271	42	577	2	383
272	243	575	2	433
273	2	425	11	397
274	2	396	20	353
275	74	394	36	354
276	139	467	118	445
277	47	285	19	271
278	16	317	3	272
279	63	130	77	108
280	17	34	9	29
281	12	40	5	35
282	202	44	213	39
283	289	26	267	26
284	270	20	290	12
285	275	8	273	1
286	263	11	263	4
287	332	107	275	106

Fracture No.	X1 (m)	Y1 (m)	X2 (m)	Y2 (m)
288	267	115	216	94
289	463	132	508	123
290	622	125	613	105
291	711	143	695	139
292	387	179	356	162
293	526	364	476	338
294	500	357	476	345
295	521	370	507	341
296	434	381	465	345
297	322	432	426	345
298	329	432	368	400
299	398	383	423	357
300	404	442	460	388
301	393	461	458	407
302	387	576	456	417
303	434	519	461	431
304	421	573	428	496
305	428	577	449	504
306	448	576	450	558
307	458	578	474	557
308	470	579	476	571
309	474	522	462	486
310	476	500	414	463
311	421	471	469	420
312	457	512	401	418
313	427	429	413	415
314	388	432	352	321
315	390	386	307	264
316	403	576	369	466
317	390	576	368	468
318	290	305	328	286
319	287	221	311	218
320	385	484	345	303

Fracture No.	X ₁ (m)	Y ₁ (m)	X ₂ (m)	Y ₂ (m)
321	345	303	265	124
322	403	286	249	214
323	276	372	292	248
324	273	485	276	372
325	287	576	284	480
326	287	469	298	400
327	220	276	240	184
328	289	246	131	202
329	241	231	198	153
330	117	195	91	165
331	144	176	117	165
332	153	207	127	191
333	225	300	142	188
334	204	263	206	131
335	195	260	193	169
336	172	419	195	267
337	178	443	204	280
338	290	350	288	330
339	279	360	302	344
340	263	334	242	319
341	354	363	312	349
342	391	395	299	358
343	326	383	287	364
344	358	412	349	379
345	325	577	359	416
346	333	529	345	402
347	314	551	321	435
348	402	460	293	433
349	307	423	129	205
350	274	371	260	353
351	191	257	139	237
352	108	579	15	484
353	71	578	2	511

Fracture No.	X1 (m)	Y1 (m)	X2 (m)	Y2 (m)
354	58	576	38	558
355	47	575	26	556
356	51	552	124	268
357	124	317	133	260
358	152	362	131	267
359	149	362	137	330
360	188	519	164	414
361	108	541	23	482
362	116	537	71	506
363	74	574	65	510
364	84	576	71	506
365	91	558	63	478
366	53	459	40	437
367	75	472	29	379
368	100	544	77	486
369	100	563	95	547
370	97	576	163	366
371	150	577	96	500
372	118	575	112	548
373	112	573	106	542
374	58	574	65	552
375	102	476	171	246
376	110	453	65	436
377	68	458	109	453
378	113	472	75	456
379	106	486	73	472
380	2	488	32	473
381	157	314	123	289
382	148	277	178	268
383	227	230	179	230
384	213	333	229	294
385	165	342	190	304
386	264	415	138	332

Fracture No.	X ₁ (m)	Y ₁ (m)	X ₂ (m)	Y ₂ (m)
387	229	373	174	338
388	220	414	229	328
389	233	363	236	341
390	270	376	219	360
391	292	435	174	273
392	259	424	202	380
393	340	524	275	425
394	351	577	341	563
395	362	577	359	570
396	329	567	297	562
397	314	576	266	504
398	271	499	159	352
399	261	504	188	408
400	248	501	191	422
401	292	575	271	536
402	241	442	202	437
403	198	486	211	366
404	155	575	195	500
405	151	578	183	429
406	135	575	150	474
407	181	577	167	519
408	165	577	205	510
409	177	577	205	535
410	207	577	194	562
411	182	578	161	564
412	176	426	138	400
413	139	425	162	414
414	222	577	195	530
415	199	559	237	509
416	242	542	249	362
417	254	535	252	523
418	261	533	267	518
419	206	507	214	431

Fracture No.	X ₁ (m)	Y ₁ (m)	X ₂ (m)	Y ₂ (m)
420	253	577	244	562
421	326	468	220	412
422	304	577	283	545
423	348	556	301	523
424	381	577	308	461
425	356	519	379	466
426	342	483	239	347
427	330	405	282	404
428	361	440	292	420
429	266	407	227	381
430	344	506	316	461
431	446	406	425	326
432	431	456	445	408
433	473	577	431	456
434	117	243	110	209
435	240	214	273	171
436	425	25	392	1
437	444	312	413	291
438	234	573	243	562
439	10	530	1	522
440	25	571	28	539
441	77	576	93	562
442	359	465	355	439

B2 THE RESULTS OF EFFECTIVE PERMEABILITY TENSOR IN CASE STUDY PRESENTED IN CHAPTER 4 AND PRESENTED IN Figure 4-54:

Block No.	(Row, Column)	K_{xx}	K_{xy}	K_{yx}	K_{yy}
1	(1, 1)	3.861	0.456	0.456	5.126
2	(1, 2)	4.03	0.681	0.681	3.75
3	(1, 3)	4.257	0	0	1.556
4	(1, 4)	7.269	-1.043	-1.043	8.213
5	(1, 5)	3.797	0.235	0.235	3.277
6	(1, 6)	3.884	0.051	0.051	4.357
7	(1, 7)	4.98	-0.627	-0.627	4.097
8	(1, 8)	5.332	-0.066	-0.066	5.801
9	(1, 9)	1.621	-0.152	-0.152	2.849
10	(1, 10)	5.142	-0.202	-0.202	4.691
11	(1, 11)	2.408	0.057	0.057	3.206
12	(1, 12)	1.45	0.148	0.148	1.498
13	(2, 1)	4.989	-0.92	-0.92	6.357
14	(2, 2)	7.032	1.155	1.155	7.257
15	(2, 3)	7.119	0.711	0.711	10.971
16	(2, 4)	6.862	0.37	0.37	5.818
17	(2, 5)	6.367	0.106	0.106	4.673
18	(2, 6)	7.226	0.17	0.17	8.924
19	(2, 7)	7.9	0.594	0.594	4.916
20	(2, 8)	8.485	-1.689	-1.689	9.849
21	(2, 9)	6.351	1.477	1.477	5.673
22	(2, 10)	8.39	-0.667	-0.667	9.211
23	(2, 11)	3.203	0.849	0.849	4.9
24	(2, 12)	1.657	-0.155	-0.155	1.143
25	(3, 1)	2.018	-0.709	-0.709	4.743
26	(3, 2)	3.691	0.46	0.46	14.299
27	(3, 3)	8.328	-1.224	-1.224	4.401
28	(3, 4)	8.169	0.191	0.191	5.432
29	(3, 5)	7.788	-0.1	-0.1	7.566
30	(3, 6)	5.314	0.006	0.006	6.725
31	(3, 7)	5.083	0.176	0.176	5.622
32	(3, 8)	5.894	0.247	0.247	6.477
33	(3, 9)	7.69	-0.63	-0.63	4.708
34	(3, 10)	8.433	0.27	0.27	6.692
35	(3, 11)	5.983	0.378	0.378	7.629

36	(3,12)	2.547	0.272	0.272	5.277
37	(4, 1)	6.293	-0.018	-0.018	6.313
38	(4, 2)	8.659	-0.807	-0.807	5.394
39	(4, 3)	7.6	-0.367	-0.367	10.989
40	(4, 4)	5.575	-0.79	-0.79	3.802
42	(4, 6)	4.777	0.758	0.758	4.866
43	(4, 7)	6.267	0.701	0.701	3.879
44	(4, 8)	6.76	-0.53	-0.53	3.853
45	(4, 9)	5.652	-0.995	-0.995	4.719
46	(4, 10)	6.939	-1.249	-1.249	5.126
47	(4, 11)	7.769	-0.282	-0.282	8.417
48	(4,12)	2.913	-0.434	-0.434	6.504
49	(5, 1)	5.074	-0.267	-0.267	6.603
50	(5, 2)	9.078	-0.576	-0.576	5.901
51	(5, 3)	7.17	-0.99	-0.99	8.318
52	(5, 4)	4.978	2.553	2.553	4.647
53	(5, 5)	11.571	0.222	0.222	5.556
54	(5, 6)	4.294	-0.762	-0.762	6.398
55	(5, 7)	7.077	-1.268	-1.268	9.533
56	(5, 8)	9.188	-0.268	-0.268	7.253
57	(5, 9)	6.166	0.146	0.146	6.048
58	(5, 10)	6.528	0	0	4.456
59	(5, 11)	4.09	-0.221	-0.221	10.229
60	(5,12)	2.939	-0.088	-0.088	7.589
61	(6, 1)	3.889	-0.785	-0.785	5.648
63	(6, 3)	4.818	0.374	0.374	9.152
64	(6, 4)	10.1	-0.726	-0.726	6.409
65	(6, 5)	8.609	-0.454	-0.454	10.053
66	(6, 6)	8.255	0.975	0.975	7.009
67	(6, 7)	4.209	-0.196	-0.196	6.049
68	(6, 8)	5.736	0.836	0.836	8.011
69	(6, 9)	4.362	-0.849	-0.849	5.198
70	(6, 10)	4.783	0.915	0.915	5.389
71	(6, 11)	4.958	0.466	0.466	5.501
72	(6,12)	2.169	0.513	0.513	4.744
73	(7, 1)	3.242	-0.298	-0.298	6.261
74	(7, 2)	3.915	-0.142	-0.142	2.276
75	(7, 3)	4.979	-0.465	-0.465	4.7

76	(7, 4)	6.908	0.984	0.984	5.001
77	(7, 5)	6.27	0.618	0.618	9.296
78	(7, 6)	8.373	-0.896	-0.896	4.734
79	(7, 7)	11.991	0.368	0.368	6.533
80	(7, 8)	4.852	-0.477	-0.477	3.229
81	(7, 9)	3.29	-0.914	-0.914	5.361
82	(7, 10)	6.133	-0.794	-0.794	5.173
83	(7, 11)	5.061	0.553	0.553	6.135
84	(7,12)	2.915	0.263	0.263	5.556
85	(8, 1)	5.741	-0.311	-0.311	7.537
86	(8, 2)	9.2	0.362	0.362	3.063
87	(8, 3)	6.701	0.724	0.724	3.775
88	(8, 4)	8.017	0.549	0.549	8.737
89	(8, 5)	5.862	0.812	0.812	7.343
90	(8, 6)	1.821	0.101	0.101	3.101
91	(8, 7)	5.384	-0.035	-0.035	8.761
92	(8, 8)	3.074	0.42	0.42	4.221
93	(8, 9)	2.991	-0.091	-0.091	6.806
94	(8, 10)	6.515	-0.404	-0.404	6.265
95	(8, 11)	7.106	-0.391	-0.391	7.592
96	(8,12)	2.589	-0.175	-0.175	11.052
97	(9, 1)	1.802	-0.076	-0.076	4.517
98	(9, 2)	5.206	0.885	0.885	7.646
99	(9, 3)	6.382	1.12	1.12	6.523
100	(9, 4)	6.969	0.005	0.005	3.825
101	(9, 5)	4.106	-0.455	-0.455	6.408
102	(9, 6)	2.847	0.862	0.862	3.571
104	(9, 8)	7.269	0.224	0.224	4.389
105	(9, 9)	2.905	-0.262	-0.262	3.816
106	(9, 10)	5.885	0.227	0.227	5.15
107	(9, 11)	3.827	-0.86	-0.86	4.299
108	(9,12)	2.237	0.311	0.311	5.977
109	(10, 1)	2.407	-0.062	-0.062	4.354
110	(10, 2)	5.222	-0.321	-0.321	4.913
111	(10, 3)	3.932	-0.165	-0.165	4.581
112	(10, 4)	3.726	0.554	0.554	3.03
113	(10, 5)	3.025	-0.044	-0.044	4.287
114	(10, 6)	3.826	0.073	0.073	3.13
115	(10, 7)	5.655	0.311	0.311	3.145

116	(10, 8)	1.82	-0.572	-0.572	3.416
117	(10, 9)	1.715	0.072	0.072	6.615
118	(10, 10)	11.894	-0.395	-0.395	8.311
119	(10, 11)	4.189	1.313	1.313	5.614
120	(10,12)	2.525	-0.424	-0.424	18.766
121	(11, 1)	3.322	0.29	0.29	5.757
122	(11, 2)	4.321	1.456	1.456	7.121
123	(11, 3)	3.179	0.619	0.619	5.664
125	(11, 5)	3.178	0.298	0.298	4.343
126	(11, 6)	2.153	0.303	0.303	3.252
127	(11, 7)	1.631	0.31	0.31	3.895
128	(11, 8)	3.595	0.798	0.798	3.047
129	(11, 9)	3.792	0.545	0.545	4.183
130	(11, 10)	4.559	-0.377	-0.377	5.416
131	(11, 11)	3.222	-0.008	-0.008	2.071
132	(11,12)	2.655	-0.441	-0.441	4.021
133	(12, 1)	2.088	-0.053	-0.053	1.7
134	(12, 2)	3.736	-0.028	-0.028	1.995
135	(12, 3)	2.455	-0.534	-0.534	1.974
136	(12, 4)	2.713	0.065	0.065	1.139
137	(12, 5)	1.022	-0.009	-0.009	1.421
138	(12, 6)	1.181	0.133	0.133	1.428
139	(12, 7)	1.524	0.158	0.158	1.179
140	(12, 8)	2.926	0.416	0.416	1.453
141	(12, 9)	3.223	-0.388	-0.388	1.485
142	(12, 10)	2.029	-0.038	-0.038	1.608
143	(12, 11)	1.069	0.055	0.055	1.085
144	(12, 12)	1.368	0.141	0.141	1.706

**B3 THE RESULTS OF PRESSURE AND VELOCITY DISTRIBUTION IN
CASE STUDY PRESENTED IN CHAPTER 4:**

Block No.	X-centre	Y-centre	Pressure (psi)	Average velocity (ft/sec)
1	35	35	2489	6.569
2	105	35	2317	2.568
3	175	35	2212	1.193
4	245	35	2166	0.978
5	315	35	2135	0.702
6	385	35	2096	0.547
7	455	35	2063	0.476
8	525	35	2050	0.418
9	595	35	2025	0.259
10	665	35	2002	0.193
11	735	35	1994	0.086
12	805	35	1990	0.023
13	35	105	2344	4.001
14	105	105	2254	3.702
15	175	105	2193	2.082
16	245	105	2157	1.567
17	315	105	2122	1.246
18	385	105	2092	0.948
19	455	105	2063	0.883
20	525	105	2042	0.909
21	595	105	2016	0.739
22	665	105	1998	0.592
23	735	105	1989	0.193
24	805	105	1985	0.042

Block No.	X-centre	Y-centre	Pressure (psi)	Average velocity (ft/sec)
25	35	175	2238	1.674
26	105	175	2210	2.234
27	175	175	2168	1.743
28	245	175	2137	1.620
29	315	175	2106	1.469
30	385	175	2084	1.083
31	455	175	2059	0.831
32	525	175	2033	0.746
33	595	175	2009	1.008
34	665	175	1978	2.353
35	735	175	1986	-0.473
36	805	175	1978	0.232
37	35	245	2181	1.276
38	105	245	2164	1.967
39	175	245	2137	1.645
40	245	245	2110	1.278
41	315	245	2086	1.166
42	385	245	2061	0.824
43	455	245	2042	0.738
44	525	245	2027	0.649
45	595	245	2036	-0.808
46	665	245	1950	0.920
47	735	245	1997	1.836
48	805	245	1967	0.570
49	35	315	2152	0.590
50	105	315	2136	1.204
51	175	315	2095	2.689
52	245	315	2074	0.529

Block No.	X-centre	Y-centre	Pressure (psi)	Average velocity (ft/sec)
53	315	315	2057	0.862
54	385	315	2041	0.926
55	455	315	2015	0.724
56	525	315	2004	1.102
57	595	315	1988	1.838
58	665	315	1941	-0.386
59	735	315	1959	0.815
60	805	315	1948	0.814
61	35	385	2135	0.307
62	105	385	2156	-0.752
63	175	385	2121	1.546
64	245	385	2060	0.278
65	315	385	2047	1.149
66	385	385	2031	1.051
67	455	385	2009	0.715
68	525	385	1987	0.905
69	595	385	1960	1.266
70	665	385	1934	0.980
71	735	385	1920	0.792
72	805	385	1911	0.813
73	35	455	2117	0.461
74	105	455	2123	0.394
75	175	455	2114	1.720
76	245	455	2070	0.661
77	315	455	2044	0.744
78	385	455	2013	1.101
79	455	455	1994	1.380
80	525	455	1968	1.127

Block No.	X-centre	Y-centre	Pressure (psi)	Average velocity (ft/sec)
81	595	455	1930	1.220
82	665	455	1901	1.268
83	735	455	1879	1.236
84	805	455	1871	0.847
85	35	525	2099	0.550
86	105	525	2085	0.687
87	175	525	2074	0.821
88	245	525	2056	0.872
89	315	525	2036	0.783
90	385	525	2001	0.384
91	455	525	1967	0.829
92	525	525	1939	0.872
93	595	525	1899	1.124
94	665	525	1866	1.290
95	735	525	1839	2.034
96	805	525	1801	1.607
97	35	595	2069	0.199
98	105	595	2064	0.478
99	175	595	2055	0.419
100	245	595	2042	0.558
101	315	595	2022	0.909
102	385	595	1984	0.535
103	455	595	1944	0.832
104	525	595	1908	1.177
105	595	595	1861	1.480
106	665	595	1808	1.116
107	735	595	1779	1.731
108	805	595	1744	2.115

Block No.	X-centre	Y-centre	Pressure (psi)	Average velocity (ft/sec)
109	35	665	2060	0.117
110	105	665	2057	0.336
111	175	665	2047	0.326
112	245	665	2031	0.314
113	315	665	2008	0.682
114	385	665	1967	0.713
115	455	665	1928	0.776
116	525	665	1883	0.819
117	595	665	1814	1.153
118	665	665	1744	1.491
119	735	665	1715	1.668
120	805	665	1659	2.667
121	35	735	2058	0.090
122	105	735	2054	0.177
123	175	735	2044	0.259
124	245	735	2025	0.295
125	315	735	1999	0.415
126	385	735	1958	0.437
127	455	735	1906	0.650
128	525	735	1846	0.991
129	595	735	1781	1.094
130	665	735	1711	1.995
131	735	735	1594	2.832
132	805	735	1467	4.626
133	35	805	2052	0.046
134	105	805	2048	0.090
135	175	805	2039	0.154
136	245	805	2024	0.153

Block No.	X-centre	Y-centre	Pressure (psi)	Average velocity (ft/sec)
137	315	805	1992	0.179
138	385	805	1938	0.281
139	455	805	1871	0.429
140	525	805	1812	0.646
141	595	805	1759	0.792
142	665	805	1666	1.070
143	735	805	1402	1.944
144	805	805	1000	0.000